

Chapter 5

Physics of Vision in Compound Eyes

ALLAN W. SNYDER, Canberra, Australia

With 36 Figures

Contents

A. Introduction	227
B. Visual Acuity	227
I. Physical Limitation to Spatial Resolving Power	227
1. Receptor Grain (Limitation of the Finite Angular Spacing of Ommatidia)	227
a) Highest Resolvable Spatial Frequency	230
2. Optical Limitations (Diffraction and Finite Rhabdom Diameter)	231
a) Angular Sensitivity Function	231
b) Modulation or Contrast Transfer Functions	234
c) Highest Spatial Frequency Passed by Optics	235
3. Motion (Limitation to Spatial Resolving Power of Finite Integration Time)	236
4. Light Intensity (Limitation of Photon Noise to Contrast Sensitivity)	237
a) Signal-to-Noise Ratio (SNR) of a Sinusoidal Grating at the Retinula Cell Level	238
5. Improvement of Signal to Noise Ratio by Neural Processing	239
II. Minimum Numbers of Photons Necessary for Threshold Resolution of a Sinusoidal Grating	241
III. Design of Compound Eyes	242
1. Angular Rhabdom Diameter for Maximum Contrast Sensitivity at the Sampling Frequency	243
2. Influence of Focal Length on Resolving Power	243
3. Increasing Resolving Power by Isomorphic Scaling	244
4. Degree to which a Compound Eye Takes Advantage of its Potential (Diffraction Limited) Resolving Power	245
5. Aliasing (Effects of Undersampling)	247
6. Determination of Eye Parameter p	247
7. Influence of Angular Motion on Eye Design	250
8. Diurnal Eyes Employing Optical Superposition: Skipper Butterflies	251
9. Summary	252
IV. Strategies for Dark Adaptation	253
1. Eyes without Adaptation Mechanisms	253
2. Increase in Acceptance Angle with Decrease in Luminance	254
3. Neural Pooling	256
4. Comparisons and Discussion	256
V. Neural Processing	257
1. Enhancement of Contrast Sensitivity by Neural Processing	257
2. Transformation of Spatial Information	258
a) Neural Compensations for Optical Blur and Photoreceptor Noise	258
b) Extreme Suprathreshold Conditions (Noiseless Blurred Image)	259
c) Threshold Conditions (Noisy Blurred Image)	259

VI. Spatial Information Capacity of Eyes	261
1. Concept of an Animal's Spatial Information (Picture Reconstructing) Capacity	262
2. Optimum Eye Parameters	263
VII. Comparison of the Compound Eye with the Vertebrate Lens or "Camera Eye"	265
1. Cutoff Frequency of Optics (Theoretic Limit to Resolving Power)	265
2. Anatomic Resolving Power (Photoreceptor Sampling)	265
3. Contrast Sensitivity	266
4. Limitation to Minimum Eye Length	266
5. Change in Resolving Power by Scaling	267
6. Dark Adaptation Mechanisms in the Fovea	267
7. Comparative Advantages of Compound and Camera Eye	268
C. Absolute Sensitivity	268
I. Light-Gathering Capacity of an Ommatidium	269
II. Influence of Length, Diameter, and Shape of Rhabdoms on Absorption	270
III. Influence of Rhabdomeric Dichroism on Absorption	270
1. Open Rhabdoms	271
2. Fused Rhabdoms	273
IV. Dependence of Photon Capture on Chromophore Alignment	273
D. Application of Theory to the Fly <i>Musca</i> : A Neural Superposition Eye	276
I. Basic Principles of Neural Superposition	276
1. Eye Parameter p	277
II. Half Width Acceptance Angle $\Delta\varrho$	278
III. Absolute Sensitivity of Retinula Cells	279
1. Sensitivity of <i>Musca</i> to Extended Sources	279
2. Sensitivity of <i>Musca</i> to Point Sources	279
E. Polarization Sensitivity of Retinula Cells	279
I. Origin of Polarization Sensitivity	280
II. Retinula Cells of Diptera	280
III. Retinula Cells of Crustacean Rhabdoms	280
IV. Retinula Cells in Fused Rhabdoms	281
V. Twisted Fused Rhabdoms	281
F. Optical Properties of Rhabdomeric Membrane	282
I. Review of Photoreceptor Structure	283
1. The Binding of Rhodopsin in Vertebrate Membrane	283
2. Chromophore Orientation in Vertebrate Membrane	283
3. Motion of Rhodopsin Molecules in Vertebrate Membrane	285
II. Dichroic Property of Photoreceptor Membrane	286
1. Vertebrate Disc Membrane Dichroism	286
2. Dichroism of Rhabdomeric Membrane	287
III. Birefringence of Photoreceptor Membrane	290
1. Birefringence of Vertebrate Disc Membrane	290
2. Birefringence of Rhabdomeric Membrane	292
G. Waveguide Properties of Visual Photoreceptors	294
I. Determination of V for Fly Rhabdomeres	295
II. Influence of Waveguide Effects on the Optical Properties of the Rhabdom	299
Appendix A: Influence of Waveguide Effects on Acceptance Angle $\Delta\varrho$	300
Appendix B: Criteria to be a Point or Extended Source	302
Appendix C: Influence of Waveguide Effects on Birefringence of a Rhabdomere	303
1. Solution by Coupled Mode Theory	304
2. Solution by Effective Refractive Index	304
Appendix D: Two-Point Resolution	305
Appendix E: Arbitrary Lattice of Ommatidia	306
Appendix F: Consequences of Parameter p Constant in all Regions of the Eye	307
Appendix G: Polarization Sensitivity of Individual Retinula Cells of a Twisted Fused Rhabdom	307
References	309

A. Introduction

Invertebrates are the class *par excellence* where one finds all manner of variations in the structure and arrangement of photoreceptors and their associated light-gathering and processing structures. We are compelled to search for a physiologic explanation of these unique forms. This article offers a highly personalized view of the physics suited to the task.

Our emphasis is on the more highly evolved compound eyes, i.e., those with the most sophisticated visual apparatus. Consequently, we commence by clarifying how animals with compound eyes reconstruct their environment, as this is presumed to be a primary objective. We learn from the outset that the environmental intensity is a crucial determinate of visual acuity and that an eye must, therefore, optimize the capture of all available photons. Thus, one of the major themes of our development is the appreciation of those adaptations that increase absolute sensitivity.

An apology is due to readers who expect a historical development, for we have instead attempted to present a self-consistent, unifying treatment. Two important topics have been omitted completely, spectral sensitivity and the coding of information by the neurons, but these are expertly dealt with by MENZEL (this volume) and LAUGHLIN (this volume part B), respectively. We recommend the excellent review article by KIRSCHFELD (1969) on the optics of the compound eye to those readers unfamiliar with the subject. In addition, the review article by GOLDSMITH and BERNARD (1974) contains a wealth of material that also serves as a useful background to many topics considered here.

B. Visual Acuity

In this section, we consider the capacity of a compound eye to resolve details of its spatial environment. We begin in Section A by considering the factors that limit an animal's resolving power and then in Section III use them to determine the design of a compound eye. Figure 1 taken in part from KIRSCHFELD (1969), is presented to illustrate the three types of compound eyes referred to in this chapter. The symbols most frequently referred to are summarized in Table 1.

I. Physical Limitations to Spatial Resolving Power

1. Receptor Grain (Limitation of the Finite Angular Spacing of Ommatidia)

Because there is only a finite number of ommatidia, the image at the retina is a quantized version of the object. The smaller the interommatidial angle $\Delta\phi$, the greater the potential of the eye to resolve fine detail. In general, compound eyes are

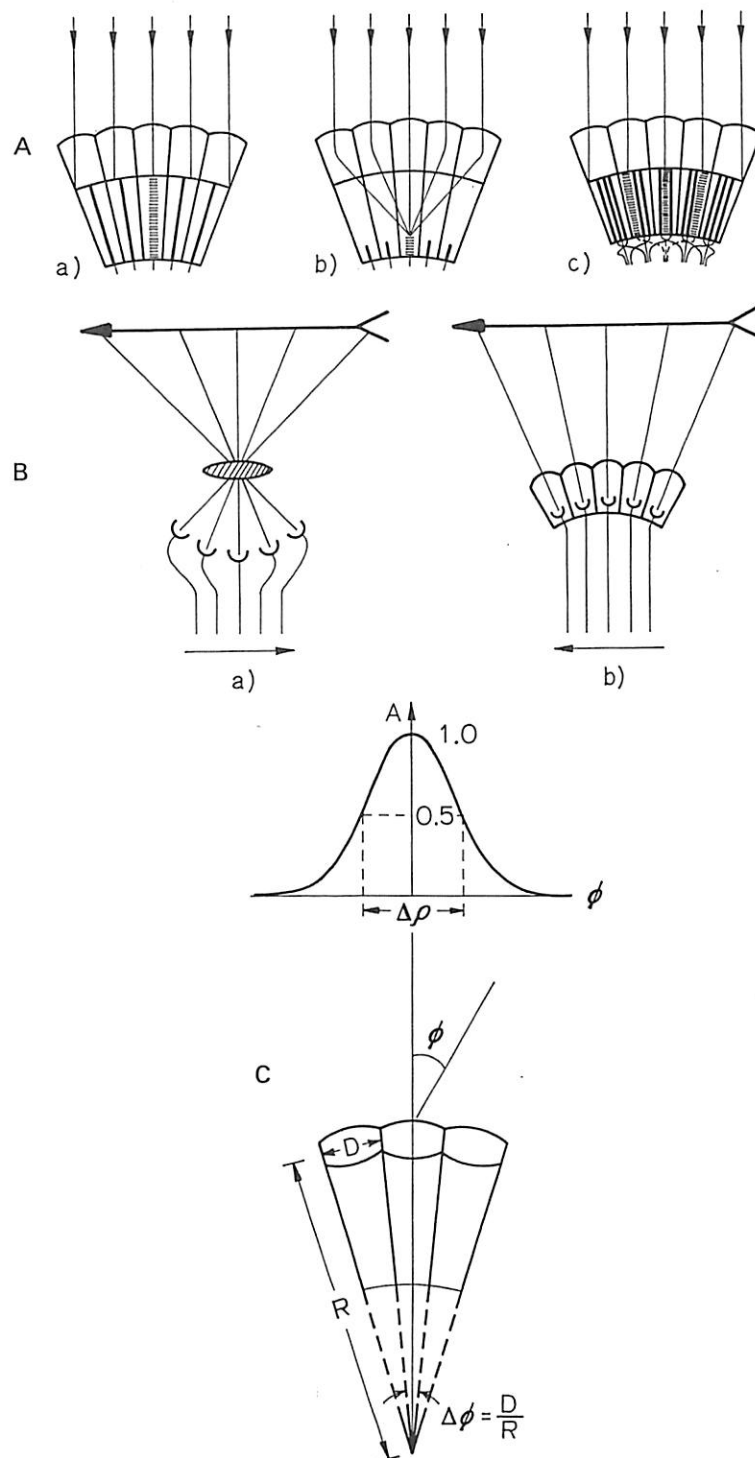


Fig. 1. (A) Schematic representation of three different types of compound eyes: *a* Apposition eye, *b* optical superposition eye, and *c* neural superposition eye. Each eye is illuminated by a distant point source and the illuminated photoreceptor (rhabdom) is indicated by the dashed line. (B) Schematic representation of image formation in the vertebrate lens eye *a* and in the compound eye *b*. (A) and (B) are from KIRSCHFELD (1969). (C) Cross-section of several ommatidia, where D is the facet diameter, R the eye radius, and $\Delta\phi$ the interommatidial angle. The acceptance function of a retinula cell is also shown, where $\Delta\varrho$ is the width of the function at 50% sensitivity and ϕ the inclination to the axis of the ommatidium

Table 1. List of important symbols

p	= eye parameter = $D\Delta\phi = D^2/R = R(\Delta\phi)^2$; [μm]. At the diffraction limit, $p = \lambda/2$ (square lattice); $p = \lambda/\sqrt{3}$ (hexagonal lattice)
$\Delta\phi$	= interommatidial angle = D/R ; [radians] in formulae, [degrees] in figures
D	= facet diameter, assumed to be equal to the entrance pupil diameter; [μm]
R	= (local) eye radius; [μm]
f	= distance from distal tips of rhabdom to posterior nodal point
$\Delta\varrho_1$	= width of lens blur function at 50% height. When diffraction is limited, $\Delta\varrho_1 = \lambda/D$. The angular diameter $\Delta\varrho_A$ of the Airy disc is $\Delta\varrho_A = 2.44\Delta\varrho_1$
λ	= wavelength of light in vacuum
$\Delta\varrho_r$	= effective angular diameter of the rhabdom [radians]. Includes additional light gathering due to crystalline cone, which when not present $\Delta\varrho_r = d_{\text{Rh}}/f$, where d_{Rh} is the rhabdom diameter
$\Delta\varrho$	= width of the angular acceptance function of the photoreceptor retinula cell at 50% sensitivity; [radians]. $\Delta\varrho^2 = (\lambda/D)^2 + (\Delta\varrho_r)^2$
v_s	= sampling frequency, i.e., highest spatial frequency that can be reconstructed by the array of ommatidia; [radians] $v_s = 1/2\Delta\phi$ (square lattice); $v_s = 1/\sqrt{3}\Delta\phi$ (hexagonal lattice)
v_{co}	= cutoff frequency, i.e., highest spatial frequency passed by the optics of an individual ommatidium. $v_{\text{co}} = D/\lambda$, in case of diffraction limit; [radians] ⁻¹
v	= angular velocity; [radians] $[s]^{-1}$
SNR	= signal to noise ratio
m	= modulation (or contrast) of sinusoidal grating
\tilde{m}	= m/SNR
\bar{N}	= mean number of photons absorbed by each photoreceptor of an array, per integration time of the eye, due to a uniform source, infinite in extent
1) \bar{N}	= $\hat{I}(D\Delta\varrho_r)^2$
2) \hat{I}	= intensity parameter = $0.89\varepsilon\Delta t\bar{I}$
3) \bar{I}	= mean number of photons per second entering the entrance pupil per square μm per steradian of field; [$\text{sr}]^{-1} [\mu\text{m}]^{-2} [\text{s}]^{-1}$
4) ε	= quantum efficiency, i.e., the fraction of photons entering the pupil that are counted by the photoreceptors
5) Δt	= integration time (effective shutter time) of the eye; [s]
M_l	= modulation transfer function (MTF) of lens pupil = $[\exp\{-3.56(v\Delta\varrho_1)^2\}]$
M_r	= MTF of rhabdom = $[\exp\{-3.56(v\Delta\varrho_r)^2\}]$; $M = M_l M_r = \exp\{-3.56(v\Delta\varrho)^2\}$

neither spheric nor are they composed of the same size facets (for review, see MAZOKHIN-PORSHNYAKOV, 1969). Consequently, the interommatidial angle $\Delta\phi$ must also depend on the region of the eye. From Fig. 1

$$\Delta\phi = D/R, \quad (B.1)$$

where R is the local eye radius and D the facet diameter. Of these three parameters, R usually displays the greatest variation over one eye as well as between different eyes. Thus, the relatively flat eye regions, where R is large, provide the highest acuity. The size of the head ultimately limits the fraction of total surface area that can be devoted to high resolving power. In many animals (e.g., bee and dragonfly) the interommatidial angles $\Delta\phi$ tend to be smallest in the central (or flatter) region of the eye (PORTILLO, 1933), which has led MAZOKHIN-PORSHNYAKOV (1969),

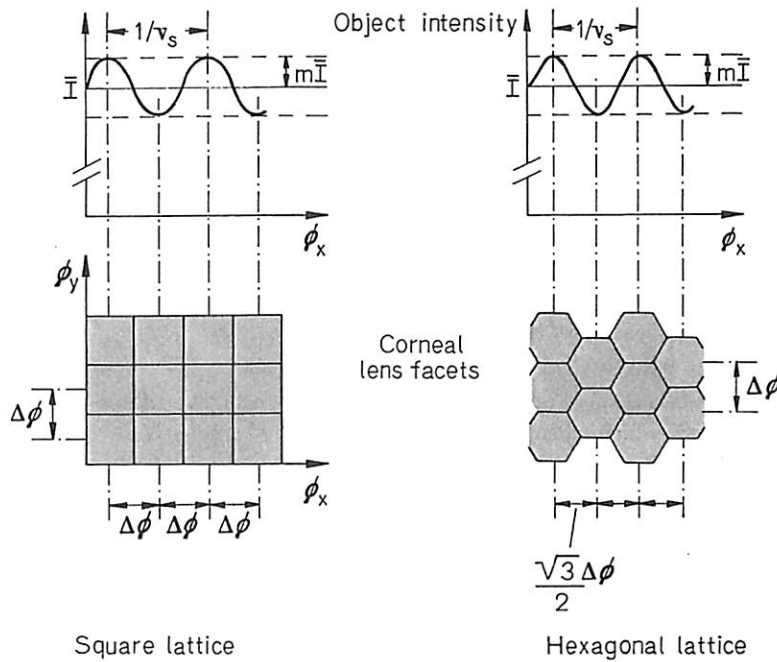


Fig. 2. Highest spatial frequency v_s that can be reconstructed *independent of the grating orientation*, by a square and hexagonal lattice of ommatidia visual axes. Note that there are *special* orientations of the grating for which a larger v can be theoretically reconstructed, e.g., $v = \Delta\phi/\sqrt{2}$ for the square array and $\Delta\phi/2$ for the hexagonal array. A consequence of nonspherical eyes is that facet shape is not in general related to the lattice of visual axes (STAVENGA, 1975). However, for simplicity, we have illustrated the situation for a spherical eye in which the shape of lens facets coincidentally represents the lattice geometry for the visual axes

BARROS-PITA and MALDONADO (1970), and HORRIDGE (1977) to note the analogy with the vertebrate fovea.

The eye parameter p where

$$p = D\Delta\phi = R(\Delta\phi)^2 = D^2/R \quad (\text{B.2})$$

is nearly constant over large portions of many compound eyes, e.g., the honey bee (KUIPER and LEUTSCHER-HAZELHOFF, 1965), the fly *Musca* (STAVENGA, 1975), and other arthropods (HORRIDGE, 1976). Thus, this is a useful parameter to characterize compound eyes.

a) Highest Resolvable Spatial Frequency

The highest angular spatial frequency that can be reconstructed by the array of ommatidia (called the ommatidia sampling frequency v_s) is determined from the geometry of Fig. 2 to be (SNYDER, 1977)

$$v_s = \text{sampling frequency} \quad (\text{B.3a})$$

$$= 1/2 \Delta\phi, \text{ square lattice} \quad (\text{B.3b})$$

$$= 1/\sqrt{3} \Delta\phi, \text{ hexagonal lattice} \quad (\text{B.3c})$$

assuming the array is regular (FRENCH et al., 1977). Both lattice arrangements are found in compound eyes (HORRIDGE, 1976). It is convenient to view v_s as the anatomic resolving power of the compound eye; however, v_s is in general greater than the physiologic resolving power unless certain conditions are satisfied. These conditions include a sufficient luminance and a restricted angular velocity. Furthermore, because of aliasing (Sec. E.III), animals in theory can detect frequencies in excess of $v = v_s$ but they are perceived as lower frequencies.

2. Optical Limitations (Diffraction and Finite Rhabdom Diameter)

Here we consider the limitation to spatial resolving power due to diffraction and the finite diameter of a rhabdom.

a) Angular Sensitivity Function

Because of imperfect dioptrics, ultimately limited by the wave nature of light (pupil diffraction), it is impossible to specify the precise location of a distant point source. This spatial uncertainty is characterized, at the level of the photoreceptor, by the angular sensitivity or acceptance function A of a retinula cell (Fig. 1c) where $\Delta\varrho$ is the width of the function at 50% sensitivity. The minimum $\Delta\varrho$ is set by diffraction (BORN and WOLF, 1970)

$$\Delta\varrho_{\min} \cong \lambda/D, \quad (B.4)$$

where λ is the wavelength in vacuum and D the diameter of the entrance pupil, which is approximately the facet diameter. In practice, a Gaussian function is a good fit to the measured angular sensitivity function of a retinula cell (GOETZ, 1965; TUNSTALL and HORRIDGE, 1967) so that

$$A = e^{-2.77(\phi/\Delta\varrho)^2}, \quad (B.5)$$

where A is normalized to unity (Fig. 1c) at maximum and ϕ is the inclination to the axis of the ommatidia. We next express $\Delta\varrho$ in terms of the physical parameters of the compound eye. Ignoring lens-pupil diffraction and aberrations and assuming that the distal tips of the rhabdomeres are close to the focal plane (as they are in *Drosophila*, *Musca*, and worker bee; for review, see FRANCESCHINI, 1975), $\Delta\varrho$ is simply the angular projection of the rhabdom in object space, i.e.,

$$\Delta\varrho = d_{Rh}/f, \quad (B.6)$$

where d_{Rh} is the diameter of the rhabdom and f is the distance from the distal tips of the rhabdomeres to the posterior nodal point (for review, see STAVENGA, 1975). To account for the possibility of additional light gathering or funnelling by the crystalline cone, we replace d_{Rh}/f by the effective angular diameter of the rhabdom $\Delta\varrho_r$.

We next investigate how imperfections of the lens-pupil modify our geometric optics result that $\Delta\varrho = \Delta\varrho_r$. Because of diffraction (but possibly aberrations in the

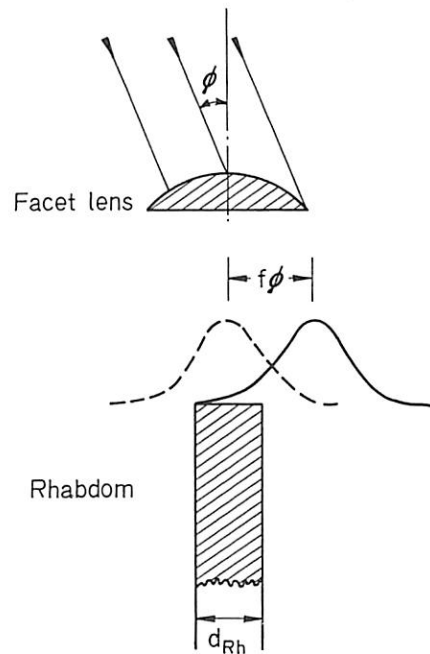


Fig. 3. Displacement of the lens pupil intensity function as a distant point source is moved an angular amount ϕ off axis; f is the distance from the distal tips of the rhabdomeres to the posterior nodal point

optical superposition eyes of nocturnal animals), a distant point source appears as a distribution of light intensity at the distal tips of the rhabdom. Moving the point source a distance ϕ from the axis of the ommatidium as shown in Fig. 3 displaces the center of the distribution by an amount $f\phi$. The angular sensitivity A of a retinula cell is the result of viewing the intensity pattern by a rhabdom of finite width, as the distant point source moves across the animal's visual field. Such a process is described mathematically by convolving (BRACEWELL, 1965) the intensity pattern with the aperture of the rhabdom. The exact analysis first given by KUIPER (1966) for the fly is rather complicated and must be computed numerically. However, approximating both the angular intensity distribution A as well as the rhabdom angular acceptance function A_r by Gaussian functions, we derive a simple result for $\Delta\varrho$ with insignificant error (Fig. 4). The process of convolving the Gaussian function representation of A_1 and A_r results in the angular sensitivity A of a retinula cell, given by Eq. (B.5), of half width (SNYDER, 1977)

$$(\Delta\varrho)^2 = (\Delta\varrho_1)^2 + (\Delta\varrho_r)^2 \quad (B.7a)$$

also shown in Fig. 4, where

$$\Delta\varrho_1 = \lambda/D \quad (B.7b)$$

when the lens pupil is diffraction limited and

$$\Delta\varrho_r = d_{Rh}/f \quad (B.7c)$$

when there is no additional light gathering due to a crystalline cone. Thus, the geometric optics expression $\Delta\varrho = \Delta\varrho_r$ applies, to an accuracy within 10%, when

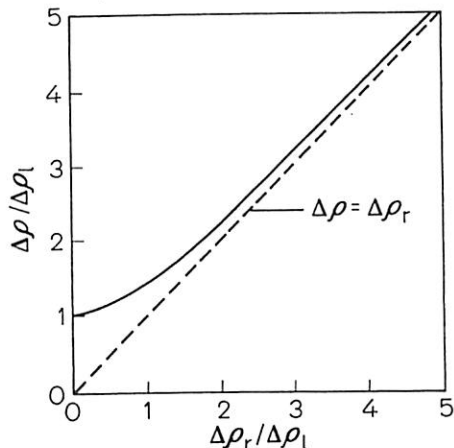
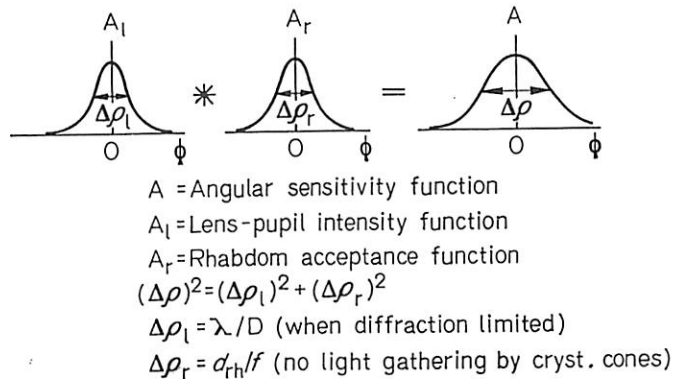


Fig. 4. The angular sensitivity function A of a photoreceptor is determined by convolving the lens pupil function A_l shown in Fig. 3 with the rhabdom acceptance function A_r for the case when both are assumed to be Gaussian functions. The asterisk signifies convolution. For convenience, we note that the angular diameter of the Airy disc $\Delta\rho_{\text{Airy}} = 2.44 \Delta\rho_l$. We have normalized all functions to unity at $\phi=0$, but in general only $A_r=1$ at $\phi=0$. The function A_l at $\phi=0$ is proportional to the pupil area $\pi D^2/4$ times the fraction of photons entering the rhabdom $(\Delta\rho_r/\Delta\rho)^2$. The height of A at $\phi=0$ is found by the process of convolving the two-dimensional Gaussian functions, leading to a constant times $(D\Delta\rho_r/\Delta\rho)^2$ (see SNYDER, 1977)

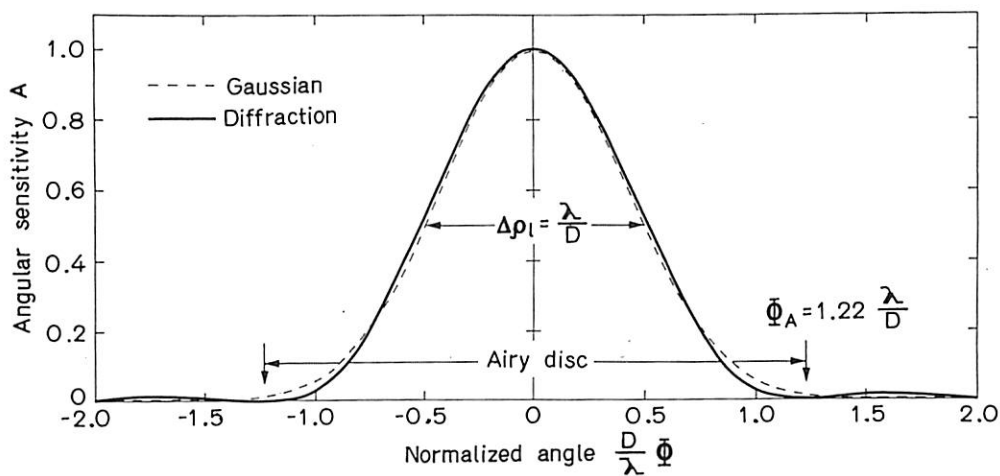


Fig. 5. Angular distribution of intensity pattern A due to diffraction by a circular aperture; ϕ is the inclination of a distant point source to the axis of the ommatidium (see Fig. 1). The angular diameter of the Airy disc is $2.44 \lambda/D$, where λ is the wavelength in vacuum and D the pupil diameter. The dashed line is given by Eq. (B.5) while the solid curve is given by $A = \{2J_1(x)/x\}^2$; $x = \pi v_{co}\phi = \pi D\phi/\lambda$

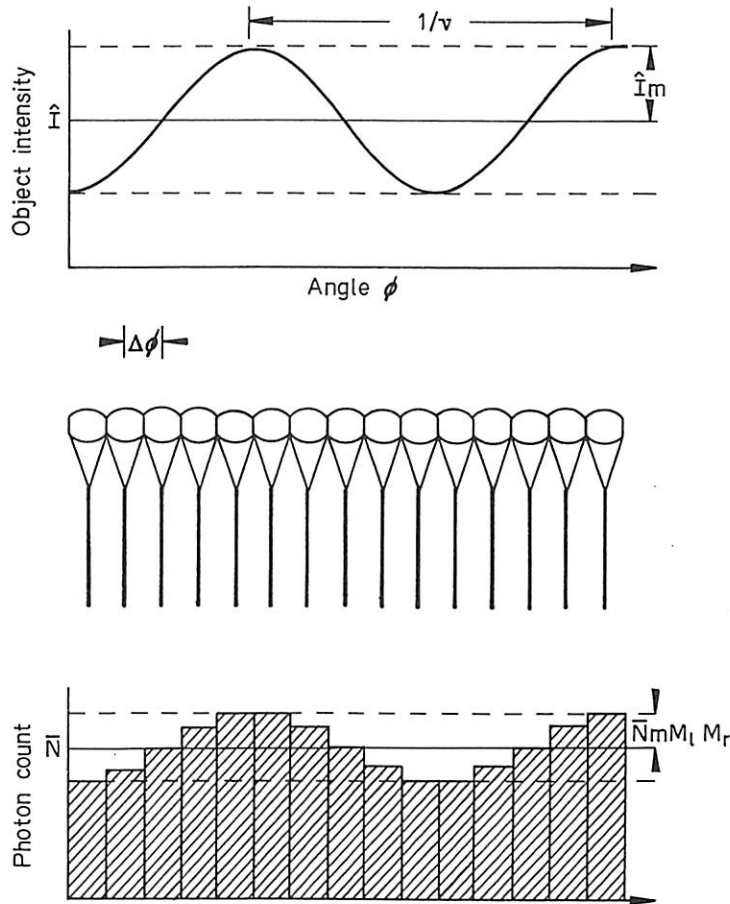


Fig. 6. The effect on object reconstruction of the lens pupil optics and the finite angular diameter of the rhabdom. The object intensity is due to a sinusoidal grating of mean intensity \bar{I} and modulation m . A quantized version of the sinusoid is reconstructed by the array of photoreceptors. The amplitude of the sinusoid is $\bar{N}mM_lM_r = \bar{N}mM$, where \bar{N} is the mean number of absorbed photons in one integration time, M_l and M_r are the modulation transfer functions of the lens pupil and finite rhabdom diameter, respectively

$\Delta\varrho_l < 0.45 \Delta\varrho_r$. For diffraction-limited optics and without light-gathering effects of the crystalline cone, this requires $d_{Rh} > 2.22 \lambda f/D$, i.e., d_{Rh} greater than the Airy disc of the diffraction pattern (Fig. 5). Equation (B.7) together with Eq. (B.5) allow for a very simple description of the angular sensitivity of a retinula cell. Equation (B.7) is not significantly altered by even the most pronounced wave guide effects (see Appendix A) and therefore has general applicability.

b) Modulation or Contrast Transfer Functions (MTF)

The most convenient way to view the effect of spatial uncertainty caused by imperfect optics and a finite rhabdom acceptance angle is via the amount of demodulation that a spatial frequency v experiences when passing through the system (Fig. 6). The modulation transfer function (MTF) at the retinula cell level is obtained by the Fourier transform of the angular sensitivity function, normalized

to unity at zero spatial frequency (GOODMAN, 1968). Fourier transforming Eq. (B.5) leads to

$$M(v) = M_l(v)M_r(v) = e^{-3.56(v\Delta\varrho)^2}, \quad (\text{B.8a})$$

$$M_l(v) = e^{-3.56(v\Delta\varrho_l)^2}, \quad (\text{B.8b})$$

$$M_r(v) = e^{-3.56(v\Delta\varrho_r)^2}, \quad (\text{B.8c})$$

where $\Delta\varrho$ is given by Eq. (B.7).

c) Highest Spatial Frequency Passed by Optics

The highest spatial frequency or *cutoff frequency* v_{co} passed by the optics of an individual ommatidium is defined by

$$M_l(v_{co}) = 0. \quad (\text{B.9a})$$

However, because of our Gaussian representation of M , there is no finite value of v satisfying Eq. (B.9a). An excellent approximation to the cutoff frequency is given by

$$v_{co} = \text{cutoff frequency} \approx 1/\Delta\varrho_l, \quad (\text{B.9b})$$

where $M_l(v_{co}) \approx 0.028$. If the lens pupil is diffraction limited, the cutoff frequency as defined by Eq. (B.9a), is given exactly (GOODMAN, 1968) by

$$v_{co} = D/\lambda \quad (\text{B.9c})$$

as shown in Fig. 7.

If the array of retinula cells is to reconstruct the highest spatial frequency v_{co} passed by the optics, then by Fig. 2 and Eq. (B.3), $v_s \geq v_{co}$, i.e., the interommatidial angle must not be greater than

$$\Delta\phi \approx \Delta\varrho_l/2; \text{ square lattice} \quad (\text{B.10a})$$

$$\approx \Delta\varrho_l/\sqrt{3}; \text{ hexagonal lattice}. \quad (\text{B.10b})$$

Since $\Delta\varrho_{min} = \lambda/D$, there is no advantage in having the interommatidial angle smaller than $\Delta\phi = \lambda/2D$ for resolving the highest spatial frequency passed by the optics.

Optimum $\Delta\phi$ for Diffraction Limited Eye

Assuming diffraction is the only limit to resolving power, what is the optimum interommatidial angle $\Delta\phi$ for a spherical eye? The smaller $\Delta\phi$, the greater the anatomical resolving power or sampling frequency v_s of Eq. (B.3). However, the smaller $\Delta\phi$, the poorer the image quality, i.e. the lower the cutoff frequency $v_{co} = D/\lambda$. This is because the facet diameter D is reduced. The optimum $\Delta\phi$ occurs when the sampling frequency equals the cutoff frequency, i.e. $v_s = v_{co}$ so that $\Delta\phi = \lambda/\sqrt{3}D$ or $p = \lambda/\sqrt{3}$ assuming hexagonally packed ommatidia, where p is the eye parameter of Eq. (B.2). For a spherical eye of radius R , Eq. (B.1) leads to $\Delta\phi = (\lambda/R)\sqrt{3}^{1/2}$. However, as we show in section (B.III.6), only animals that are active in the brightest sunlight and are relatively stationary when examining their prey have a region of their eye fitting this description. To explain $\Delta\phi$ in other animal requires appreciating the limitations to resolving power discussed below.

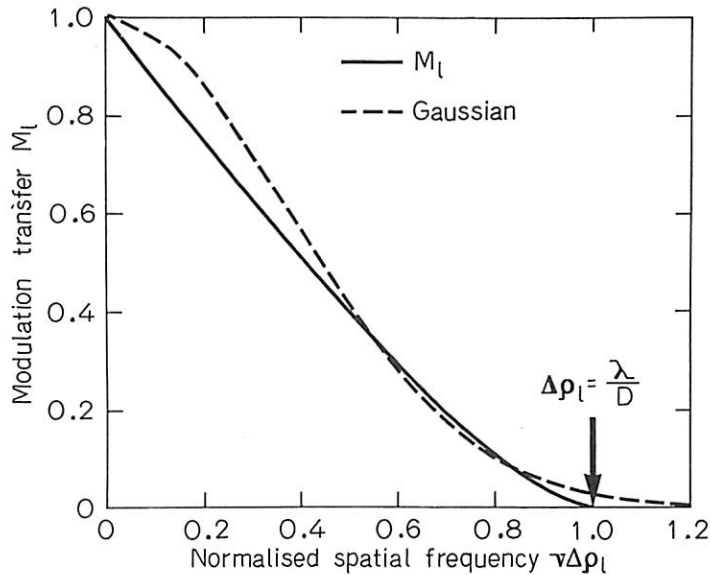


Fig. 7. The modulation transfer function for a circular pupil M_l compared with the Gaussian approximation Eq. (B.8b). The solid curve is given by

$$M_l = \left(\frac{2}{\pi}\right) \{\cos^{-1} x - x(1-x^2)^{1/2}\} \quad \text{for } |x| < 1 \quad \text{where } x = v\Delta\varrho_l = v/v_{co}$$

We have been discussing grating resolution. Wave theory does not set a limit on $\Delta\phi$ for two point resolution, since the image of two distant point sources appears different from one alone. The Rayleigh (1879) criterion arbitrarily sets the minimum at $\Delta\phi = 0.61 \lambda/D$ for diffraction limited optics which is comparable to $\Delta\phi = 0.58 \lambda/D$ we found above for gratings.

3. Motion (Limitation to Spatial Resolving Power of Finite Integration Time)

Because neither transduction nor neural transmission is instantaneous, it is impossible to specify the precise time of an event, just as it is impossible to specify the precise location of a distant point source. Thus, there is a temporal uncertainty of duration Δt in exact analogy with the spatial uncertainty of angular extent $\Delta\varrho$ discussed in Section 2a, where Δt is the integration or exposure time of the eye. If a distant point object moves at an angular velocity v , then it is displaced by an angular distance $v\Delta t$ across the retina in the integration time Δt . Consequently, the effect of movement on spatial resolution is analogous to the process of viewing a stationary scene through a receptor of finite angular diameter. Thus, the additional spatial uncertainty introduced by movement is found by convolving the acceptance function of the retinula cell A with the temporal response function of the retinula cell. If we assume that the temporal response function is Gaussian of half width $v\Delta t$, then the spatial uncertainty function in the presence of movement is characterized by half width $\Delta\varrho$ where (SNYDER, 1977)

$$(\Delta\varrho)^2 = (\Delta\varrho_l)^2 + (\Delta\varrho_r)^2 + (v\Delta t)^2 \quad (B.11)$$

in analogy with Eq. (B.7a). This intuitive approach can be verified by the formalism of SRINIVASAN and BERNARD (1975) who also provide a more complete discussion of the degrading effects of motion on spatial resolving power.

Thus, when there is motion, we must replace $\Delta\varrho$ in the MTF function Eq. (B.8) by $\Delta\varrho$ of Eq. (B.11) so that $M = M_l M_r M_m$ where $M_m = \exp\{-3.56(vv\Delta t)^2\}$. Consequently, the highest frequency passed by the optics is then $v_{co} = 1/\Delta\varrho$ with $\Delta\varrho$ from Eq. (B.11), and there is no advantage in the interommatidial angle $\Delta\phi$ being smaller than

$$\Delta\phi \cong \{(\Delta\varrho_l)^2 + (\Delta\varrho_r)^2 + (v\Delta t)^2\}^{1/2}/2 \quad (B.12)$$

for resolving the highest sinusoidal frequency passed by the optics. The greater the angular velocity v , the greater the spatial uncertainty and the larger we can make $\Delta\phi$. Thus, for an animal that flies predominantly in linear motion, along its longitudinal axis, we might anticipate larger ommatidial angles along the horizontal axis than the vertical axis, as is the case in several species including bees, muscoid flies, dragonflies, and locusts (Review see MAZOKHIN-PORSHNYAKOV, 1969).

4. Light Intensity (Limitation of Photon Noise to Contrast Sensitivity)

If it were not for the presence of noise, ultimately due to the quantum nature of light, there would be no limit to the contrast sensitivity of the compound eye, and the MTF would be sufficient to determine the highest spatial frequency reconstructed by the array of retinula cells. However, because of the random character of photon absorption, a uniform light source appears irregular even to an array of ideal detectors, i.e., those without intrinsic noise (Fig. 8). The standard deviation σ_{noise} in photon counts appearing across an infinite array of photoreceptors is

$$\sigma_{noise} = \sqrt{\bar{N}}, \quad (B.13)$$

where \bar{N} is the mean number of photons captured by the individual photoreceptors per integration time or shutter time of the eye. This result follows from the fact that photon arrival obeys a Poisson distribution (for review, see ROSE, 1973). Because there is an uncertainty of $\sqrt{\bar{N}}$ in the meaning of a photoreceptor count, two light sources can be reliably distinguished only if they differ in intensity sufficiently to exceed $\sqrt{\bar{N}}$ at the photoreceptors. Although the standard deviation in photon counts increases with increasing \bar{N} , its effect on a measurement is relatively less. Thus, *the greater the intensity of light, the greater the contrast sensitivity of ideal photoreceptors*. Since FERMI and REICHARDT (1963) have provided evidence that the photoreceptors of the fly *Musca* are close to ideal, the theory presented here may be more general than simply an upper limit to performance.

From the measurements of LILLYWHITE and LAUGHLIN (1978), we now know that the intrinsic noise of the photoreceptor also obeys (B.13).

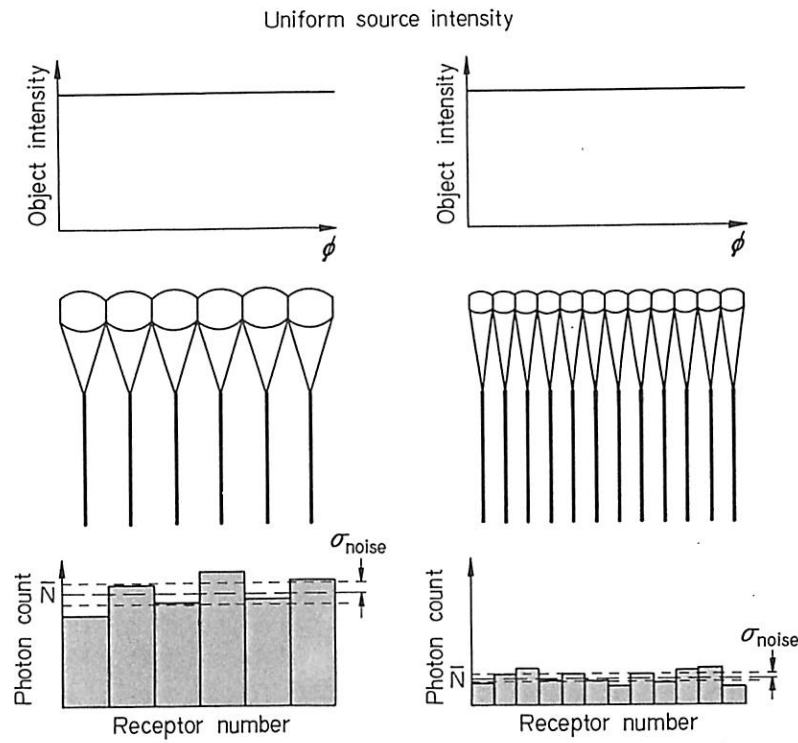


Fig. 8. The fluctuation in photon counts across the photoreceptors (in one integration time) due only to the random arrival of photons (photon noise). The object is a two-dimensional uniform source, infinite in extent. Ommatidia with larger facets accept more photons than those with smaller facets (*assuming nearly equal f/D ratios*) so that their signal-to-noise ratio is greater

a) Signal-to-Noise Ratio (SNR) of a Sinusoidal Grating at the Retinula Cell Level

We now combine the concepts of modulation transfer function with photon fluctuation to determine the SNR of a sinusoidal grating reconstructed by the retinula cells (Fig. 6). The amplitude σ_{sig} of the fluctuation in photon counts about the mean \bar{N} , due to a sinusoidal grating, is shown in Fig. 6 to be

$$\sigma_{\text{sig}} = \bar{N} m M(v) \quad (\text{B.14})$$

if we ignore the fluctuation (photon noise) due to the random arrival of photons. The most likely amplitude in photon noise σ_{noise} is $\sqrt{\bar{N}}$, so that the SNR is

$$\text{SNR} = \sqrt{\bar{N}} m M(v) \quad (\text{B.15})$$

at the retinula cell level.

1) Mean Number \bar{N} of Photons Captured per Integration Time of the Eye Due to a Uniform Source, Infinite in Extent

If we let \bar{I} be the mean number of photons entering the eye per steradian of object field per cm^2 per second, ε the fraction of this number that is absorbed in the rhabdom, Δt the sampling time of the eye, then $N = \bar{I}\varepsilon\Delta t$ times the pupil area

$D^2\pi/4$, multiplied by the solid angle that the rhabdom subtends in object space. We find this solid angle by integrating the assumed Gaussian field of view A_r of the rhabdom as shown in Fig. 4, so that

$$\bar{N} = (\pi/4) D^2 \bar{I} \varepsilon \Delta t \left\{ 2\pi \int_0^{\pi/2} A_r \sin \phi d\theta d\phi \right\} \quad (\text{B.16a})$$

$$\cong (\pi/4) D^2 \bar{I} \varepsilon \Delta t \left\{ 2\pi \int_0^{\infty} \phi A_r d\phi \right\} \quad (\text{B.16b})$$

$$= \hat{I} (D \Delta \varrho_r)^2, \quad (\text{B.16c})$$

where the intensity parameter \hat{I} is defined in Table 1. It is convenient to express the intensity parameter \hat{I} in terms of the field luminance L (in units of candelas [m^{-2}]) (WYSZECKI and STILES, 1967) so that

$$\hat{I} = 1.31 \times 10^3 (\eta \Delta t) L, \quad (\text{B.17})$$

where Δt is in seconds. As a representative example, we take $\varepsilon = 0.5$ and $\Delta t = 20 \text{ ms}$, so that $\hat{I} = 13.1 L$ or

$$\log \hat{I} = 1.1 + \log L. \quad (\text{B.18})$$

The range in $\log L$ of interest is: 3–5 for daylight, 0–3 for inferior lighting, and –4 to –1 for night (LE GRAND, 1968).

2) SNR Expressed in Terms of \hat{I}

It is convenient for later use to express Eq. (B.15) in terms of \hat{I} . From Eqs. (B.8), (B.15), and (B.16b), we have

$$\text{SNR} = D \Delta \varrho_r (m^2 \hat{I})^{1/2} e^{-3.56(v \Delta \varrho)^2}, \quad (\text{B.19})$$

where $\Delta \varrho$ is given by Eq. (B.7).

5. Improvement of Signal to Noise Ratio by Neural Processing

By appropriate neural averaging, the signal to noise ratio (SNR) can in theory be improved at higher levels over that at the level of the photoreceptors. Allowing for parallel processing, this is achieved without rendering the retina more functionally coarse, i.e. without reducing the anatomical resolving power of some higher level from that of the photoreceptor matrix. There are numerous possibilities depending on the plasticity of the brain in adapting to different stimuli. For example, for a repetitive image, like a grating, then the greater the number of photoreceptors participating in the resolution task, the better. This leads to a SNR proportional to $\sqrt{N_s}$ rather than \sqrt{N} , assuming the retina is limited by receptor Poisson noise, where N_s is the summed photon capture of the retina.

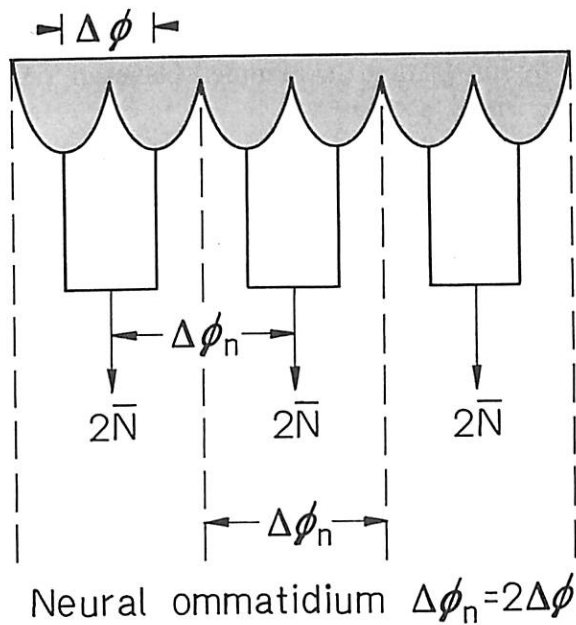


Fig. 9. Example of neural ommatidia

Neural Ommatidia

The example of processing discussed above requires rather sophisticated neural machinery. A less demanding scheme results from a simple combination of ommatidia at higher neural levels and running these summed neurons in parallel with the original receptor neurons. These new functional units are called neural ommatidia and allow the retina to be simultaneously coarse and fine. For example, suppose that ommatidia, with different fields of view, converge to form a neural ommatidium (e.g. Fig. 9) that has an effective facet diameter $D_n = R\Delta\phi_n$, where $\Delta\phi_n$ is the angular separation of adjacent neural ommatidia. The highest spatial frequency that can be constructed by these neural ommatidia is $v_s = 1/\sqrt{3}\Delta\phi_n$. The functional difference between this scheme and the example above is most noticeable at spatial frequencies $v \cong v_s$ for which the present strategy offers no improvement whereas the former gives an improvement proportional to the number of ommatidia involved in the resolution task.

Neural Isolation and the Receptive Field

As we have stressed, neural isolation is not a requisite for preserving the photoreceptor sampling frequency $v_s = 1/\sqrt{3}\Delta\phi$ at higher neural levels. In the presence of lateral interconnectivity, possibly manifested by a center surround receptive field at some higher order neuron as with the ganglion cells of the vertebrate retina, the sampling frequency may still be reconstructed across the array of higher order neurons. For example, consider a hypothetical two-dimensional version of the $\sin x/x$ type of receptive field: $J_1(\psi\phi)/(\psi\phi)$, where $\psi = 2\pi v_s$ and ϕ is the angular displacement in object space from the center of the field. The angular diameter of this receptive field (measured between zero crossings) is $2.1\Delta\phi$, i.e., about two interommatidial angles; nevertheless, by FOURIER transforming this

function, we find that the transfer function of the eye (up to the array of neurons) with this receptive field is *flat* from $v=0$ to v_s and zero for greater values of v . Far from limiting resolving power, neural interconnectivity can *in theory* compensate for optical blur. Whether or not this is advantageous depends on a number of factors discussed in Section B.V.2.

II. Minimum Number of Photons Necessary for Threshold Resolution of a Sinusoidal Grating

To emphasize the need for photon capture in order to unmask the signal from the random fluctuation in photon arrival (photon noise), we determine the minimum, mean number of photons \bar{N} necessary for threshold resolution of a sinusoidal grating by a *hypothetic eye*. The eye is hypothetic not only because of ideal photoreceptors but also because we assume that all ommatidia have equal light capture [i.e., $D\Delta\varrho_r$ is the same for all ommatidia, which is nearly so in *Musca* (STAVENGA, 1975)] and that dark adaptation mechanisms, such as the increase in the acceptance angle $\Delta\varrho$, are inactive. For our example, we assume a square array of lens facets.

To determine the *threshold* frequency v of a *given* eye for a specified mean number \bar{N} of absorbed photons per integration time, we reexpress Eq. (B.19) in the form

$$v\Delta\varrho = 0.57 \{\log \tilde{m}^2 \bar{N}\}^{1/2} \quad (\text{B.20})$$

which is plotted in Fig. 10. The value of $\tilde{m}=m/\text{SNR}$ depends on the grating modulation m and the *threshold* SNR for the animal, which depends on the number of ommatidia that participate in viewing the grating plus the reliability or decision criterion adopted by the animal (ROSE, 1973). It is convenient to take the threshold SNR $\cong 1$ as we have done in our figures.

The $v\Delta\varrho$ scale has a maximum of unity, since the highest frequency v_{co} passed by the optics is shown in Section B.III to be $v_{co} \cong 1/\Delta\varrho$. However, the highest frequency that can be reconstructed by the array of retinula cells is limited by the ommatidial sampling frequency $v_s = 1/2\Delta\phi$ so that $v\Delta\varrho$ can never be greater than $\Delta\varrho/2\Delta\phi$ for any given eye. We have *arbitrarily* selected $\Delta\varrho/2\Delta\phi = 0.66$ for the example of Fig. 10, but one should realize that the position of $\Delta\varrho/2\Delta\phi$ and hence the horizontal portion of the curve can be located anywhere from zero to any position along the dashed curve. We are again reminded that v is the *highest* spatial frequency that can be resolved for a given number of absorbed photons \bar{N} per integration time of the eye.

Several important facts emerge from a perusal of Fig. 10. If an animal is to reconstruct the highest frequency passed by its optics ($v_{co} = v_s$ or $\Delta\varrho/2\Delta\phi = 1$), then from Fig. 10, $\log \tilde{m}^2 \bar{N} = 3.09$, i.e., $\bar{N} = 1230$ photons must be captured per integration time if the grating has unity modulation and assuming the threshold SNR = 1. Taking *Musca* as an example, in which case $\Delta\varrho \cong \Delta\phi$ for retinula cells 1–6 (SNYDER, 1976), it is then necessary to have about $\bar{N} = 6$ photons to reconstruct

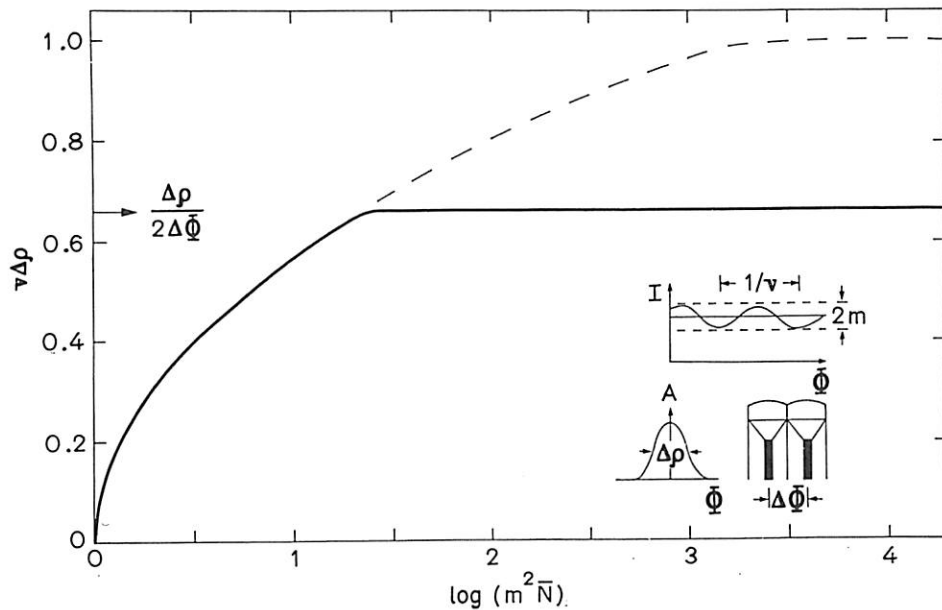


Fig. 10. Highest resolvable spatial frequency for an eye of given $\Delta\phi$ and $\Delta\varrho$. \bar{N} is the mean number of photons absorbed per integration time per receptor cell

the ommatidia sampling frequency ($\Delta\varrho/2\Delta\phi=0.5$). Because of the neural summation in *Musca* (KIRSCHFELD and FRANCESCHINI, 1968), rhabdomeres 1–6 each require only one photon per integration time. If \bar{N} is insufficient to reach the break point of the curve where $v\Delta\varrho=\Delta\varrho/2\Delta\phi$, then the acuity of the eye is less than optimum. In other words, as the light intensity falls below a certain minimum, the acuity also falls as shown in Fig. 10. The fall in acuity is due to photon noise masking the image of the grating at the retinula cell level. We are reminded from Eq. B.11 that $\Delta\varrho$ depends on the angular velocity v of the grating, so that the greater v , the greater $\Delta\varrho$ and hence the lower the spatial frequency v that can be resolved. This is because $v\Delta\varrho$ must be less than or equal to unity.

To compare Fig. 10 with the measured performance of an animal, we must know the conversion from N to intensity (Sec. B.IV) in addition to the threshold SNR of the animal. Thus, there is a margin of error in deciding how well an eye agrees with the hypothetical eye results of Fig. 10. This difficulty can be in part avoided if we determine the slope of acuity fall-off on a $\log v$ vs. \log (intensity) graph, since the slope is independent of the value of SNR at threshold as well as the conversions from N to intensity. Taking the log of Eq. (B.21) and noting that \bar{N} is proportional to intensity, we have $\log v = 1.2 \log$ (intensity). Thus, a slope of about 45° throughout the region of acuity fall-off indicates that the animal is limited only by photon noise and obeys the hypothetical eye criteria discussed at the beginning of this section.

III. Design of Compound Eyes

Having discussed the fundamental limitations to spatial acuity, we now consider the logic behind the design of compound eyes. We assume that the actual resolving power of a diurnal animal is specified by its interommatidial angle $\Delta\phi$. This means, among other limitations discussed above, that the rhabdoms receive

sufficient light for the eye to have adequate contrast sensitivity at the sampling frequency $v=v_s$, where v_s of Eq. (B.3) is the highest spatial frequency that can be faithfully reconstructed by the ommatidia. Thus, *animals with the smallest interommatidial angles have the highest resolving power*. Now it turns out, as we show below, that the principal determinate of high resolving power is the size of the animal's head. High resolving power requires a large head in order to accommodate a long focal length and large facet diameters. We remind the reader that, unless the head is spheric, the radius of curvature R of Fig. 1 is in general independent of head size, e.g., flat portions of the head have $R=\infty$. Because focal length f is defined in Eq. (B.7c) via the angular projection of the rhabdom into object space $\Delta\varrho_r$, we first determine the $\Delta\varrho_r$ necessary for maximum contrast sensitivity at the sampling frequency $v=v_s$.

1. Angular Rhabdom Diameter for Maximum Contrast Sensitivity at the Sampling Frequency $v=v_s$

By Eq. (B.16c), the greater the angular rhabdom diameter $\Delta\varrho_r$, the greater the photon capture and hence the greater the potential for higher contrast sensitivity. However, by Eq. (B.8c), the greater $\Delta\varrho_r$, the smaller the modulation of the image at the level of the photoreceptors and hence the smaller the potential contrast sensitivity. Thus, there is an optimum $\Delta\varrho_r$ for maximum contrast sensitivity. Assuming the eye is limited by Poisson noise at the photoreceptor level, the optimum $\Delta\varrho_r$ is determined by maximizing the SNR [Eq. (B.19)] leading to $\Delta\varrho_r=0.375/v$. But the highest spatial frequency that the animal can faithfully reconstruct is the sampling frequency $v=v_s$, where v_s is defined by Eq. (B.3). Consequently, the angular rhabdom diameter for maximum contrast sensitivity at the animal's sampling frequency is

$$\Delta\varrho_r = 0.87 \Delta\phi = d_r/f \quad (B.21)$$

for ommatidia packed in a hexagonal array and $\Delta\varrho_r=0.75\Delta\phi$ for a square array, where d_r is the rhabdom diameter and f the focal length of the optics. In other words, the acceptance angle of the rhabdom $\Delta\varrho_r$ is slightly less than the interommatidial angle $\Delta\phi$. This assumes the eye is adapted to bright light. As a consequence of Eq. (B.21) we see from Eq. (B.16c) that the number of photons absorbed per rhabdom is proportional to p^2 , where p is the eye parameter defined by Eq. (B.2).

2. Influence of Focal Length on Resolving Power

Here we determine the focal length of the optics f , which is approximately the distance from the distal tips of the rhabdomeres to the corneal facets. This gives an indication of the axial length of an ommatidium. From Eq. (B.21) we observe that f is proportional to the animal's resolving power $(\Delta\phi)^{-1}$ and thus proportional to v_s . Therefore, the greater the animal's resolving power, the greater the axial length of ommatidium and hence the larger the animal's head. Since it is obviously

advantageous for the eye to be as small as possible, particularly for flying insects, we now consider the limitations of having a smaller focal length f while retaining the animal's resolving power $(\Delta\phi)^{-1}$. From Eq. (B.21), f can be reduced arbitrarily provided the rhabdom diameter d_r is also reduced equivalently. However, because of wave effects which are discussed in Section VII, when the diameter of a rhabdom of fixed length is reduced it becomes a poorer absorber of light, and below about $0.5 \mu\text{m}$ it fails to act as an efficient absorber of photons. For open rhabdoms, e.g., *Musca*, there is the additional possibility of optical cross-talk, which reduces contrast sensitivity to a negligible amount for a rhabdomere center to center spacing less than $1 \mu\text{m}$. Thus, the *minimum* focal length possible is seen from Eq. (B.21) to occur when $f \approx (\Delta\phi)^{-1} \mu\text{m}$, with $\Delta\phi$ in radians. For example, $f \approx 57 \mu\text{m}$ when $\Delta\phi = 1^\circ$ and about $115 \mu\text{m}$ when $\Delta\phi = 0.5^\circ$. In practice, as expected, the rhabdom diameter is greater than the minimum value so that f is larger than $(\Delta\phi)^{-1}$ and can be determined from Eq. (B.21). Another advantage of a longer focal length is a greater depth of focus because focal depth depends on f/D . In conclusion, for a fixed sending power the minimum focal length, and hence head size is limited by restrictions on the rhabdom diameter.

By equating $\Delta\phi$ of Eqs. (B.21) and (B.1), we obtain the relation between facet diameter, local eye radius R , rhabdom diameter d_r and focal length f (Fig. 1) for a given interommatidial angle $\Delta\phi$

$$Rd_r = 0.87Df. \quad (\text{B.22})$$

This can also be expressed in terms of the eye parameter p of Eq. (B.2) and the F number f/D as

$$p = 1.15 \frac{d_r}{F}. \quad (\text{B.23})$$

These relations hold approximately in many compound eyes adapted to diurnal conditions.

3. Increasing Resolving Power by Isomorphic Scaling

In Fig. 11 we show how the resolving power of the compound eye is doubled by isomorphic scaling. In particular, the facet diameter D must be doubled to double the highest spatial frequency [v_{eo} of Eq. (B.9c)] passed by the optics while the interommatidial angle $\Delta\phi$ must be halved to sample this higher frequency. If large and small eyes are to have equal SNRs at the photoreceptor level, then the angular rhabdom diameter $\Delta\varrho_r$ must be halved. This is because $M_r(v_s)$ of Eq. (B.8c) depends on the ratio $\Delta\varrho_r/\Delta\phi$. If we assume the small eye is designed with the smallest focal length f possible, i.e., smallest rhabdom diameter possible, then to halve $\Delta\varrho_r$ we must double f . Because the eye parameter $D\Delta\phi$ is equal in both eyes, $\Delta\phi^{-1}$ is proportional to \sqrt{R} . Accordingly, the focal eye curvature must be four times larger to double the resolving power. By doubling resolving power, there are four times as many ommatidia per field of view. Furthermore, because $D\Delta\phi$ is the same in both eyes, they both have the same depth of focus and the rhabdoms of each have equal photon capture. These scaling laws should apply when comparing

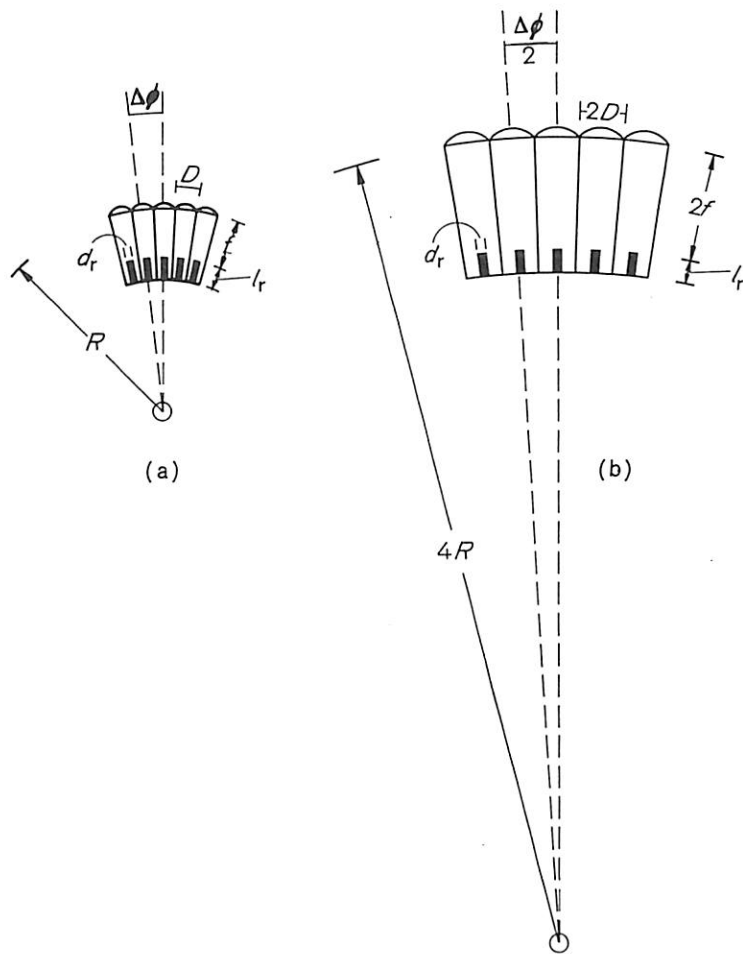


Fig. 11a and b. Doubling resolving power of an eye by isomorphic scaling. R is the radius of curvature and only equals the radius of the animal's head for a spherical compound eye. The eye in (b) has twice the resolving power of (a)

animals with similar life styles and employing identical optical and neural strategies.

Larger eyes have a potential for enhanced contrast sensitivity because of their greater photon capture. This assumes the appropriate neural processing (section B.5). It could also be that larger eyes can afford more space to specialized regions, e.g. a larger fovea.

4. Degree to Which a Compound Eye Takes Advantage of its Potential (Diffraction-Limited) Resolving Power

Here we distinguish between the actual resolving power of an animal as specified by the interommatidial angle $\Delta\phi$ (or equivalently by the sampling frequency v_s) on one hand and the degree to which an animal realizes its potential resolving power $v=v_{co}$ as set by the pupil diameter on the other hand. In other words, is the interommatidial angle sufficiently small to sample the highest spatial frequency $v_{co}=D/\lambda$ passed by the optics, i.e., is $v_s=v_{co}$ [see Eqs. (B.3) and (B.9c)]?

When the eye does take advantage of all spatial frequencies passed by the optics, the interommatidial angle is

$$\Delta\phi = 1/v_{co} \sqrt{3} = \lambda/D \sqrt{3} \quad (B.24)$$

for hexagonal packing, which is the smallest value needed to reconstruct all frequencies $v \leq v_{co}$. It is convenient to express the degree to which eyes utilize their full diffraction-limited potential by the eye parameter p of Eq. (B.2). When diffraction limited

$$p = D\Delta\phi = \lambda/\sqrt{3}. \quad (B.25)$$

To take an example, $p = 0.29 \mu\text{m}$ in diffraction-limited eyes at $\lambda = 500 \text{ nm}$. The legitimate application of Eq. (B.25) presumes knowledge of the wavelength at which the animal desires its highest resolving power.

Eyes that satisfy $v_s = v_{co}$ or equivalently Eq. (B.25) have two interesting properties. Firstly, from Eqs. (B.16c) and (B.21), the number of photons captured by a rhabdom N is proportional to p^2 and by Eq. (B.25) is independent of any physical eye parameter such as pupil diameter or head size. Furthermore, from Eqs. (B.21) and (B.25), the F number f/D of an eye obeys the simple relation $F \approx 2d_r/\lambda$.

Although no known compound eye has an eye parameter p as small as $0.29 \mu\text{m}$, many foveas of bright-light locusts, dragonflies, and wasps closely approach it, i.e., animals that are active in brilliant sunlight and are nearly stationary while examining their prey. For example, in the central fovea of the Australian sand wasp *Bembix*, $p \approx 0.31 \mu\text{m}$ (HORRIDGE, 1977) which satisfies Eq. (B.25) exactly at $\lambda \approx 540 \text{ nm}$, while $p \approx 0.42 \mu\text{m}$ in the fovea of hoverfly (COLLETT and LAND, 1975).

These eyes are rather exceptional. The minimum p values for many diurnal animals is greater than $0.5 \mu\text{m}$, e.g., mantids (HORRIDGE, 1977). In other words, the interommatidial angle $\Delta\phi$ is too large to sample all available information passed by the optics. Why is it that so many eyes undersample, i.e., have $v_s < v_{co}$? SNYDER (1977) and SNYDER et al. (1977) have provided an explanation. Since the modulation transfer function of the optics $M_1(v)$ of Fig. 7 is zero at $v = v_{co}$, the contrast sensitivity of the animal is zero at $v = v_{co}$. Furthermore, unless the animal is in the brightest light and stationary relative to its prey, it has nearly negligible contrast sensitivity for high frequencies near $v \approx v_{co}$. This is because, from Fig. 7, $M_1 \ll 1$. Thus, unless the animal can receive sufficient light (within the integration time of the eye) to have adequate contrast sensitivity at high spatial frequencies, it need not sample at the diffraction limit. This means the ommatidia can be shorter (f shorter) and the eye less flat in the region of high acuity or the facet diameter can be larger allowing for greater light capture per ommatidia. The greater portion of most eyes have $0.5 \mu\text{m} < p < 1 \mu\text{m}$ except in the small locally flat region of certain bright-light animals where p approaches $0.3 \mu\text{m}$. Eyes that must be spheric, e.g., for image formation reasons as in the skipper optical superposition eyes, must therefore be comparatively large to accommodate low p values.

We extend our discussion of eyes with p greater than the diffraction limit in Section B.III.6 after noting an interesting consequence of undersampling.

5. Aliasing (Effects of Undersampling)

Eyes with $p > \lambda/\sqrt{3}$ undersample, i.e., the highest spatial frequency they can faithfully reconstruct v_s is less than v_{co} . However, spatial frequencies in the range $v_s \leq v \leq v_{co}$ appear as lower spatial frequencies to the animal (BRACEWELL, 1965, p. 197):

$$v_{app} = v_s - (v - v_s) = 2v_s - v, \quad (B.26)$$

where v_{app} is the apparent spatial frequency. In other words, the animal can *detect* frequencies higher than v_s up to v_{co} but these frequencies appear lower than $v = v_s$ to the animal. GOETZ (1965) has shown that *Drosophila* has aliasing effects by measuring the turning response above $v = v_s$. One would expect that under normal environmental conditions for an animal that aliasing is a small effect; otherwise, the animal could have made use of its diffraction-limited optics.

Lastly, we note that this deleterious effect of undersampling at the retinular cell level can be removed at a higher level by a neural filter mechanism producing a flat transfer function up to $v = v_s$ where it then cuts off. Such a neuron would have a $\sin x/x$ type of receptive field of the form $2J_1(\pi v_s \psi)/\pi v_s \psi$ where ψ is the angular distance from the center of the receptive field.

6. Determination of Eye Parameter p

We noted in Section B.IV.4 that only those animals that are active in the brightest sunlight and remain relatively stationary while examining their prey have an eye parameter p near that given by Eq. (B.25), i.e., have interommatidial angles $\Delta\phi$ small enough to sample the highest spatial frequency passed by the pupil. These animals receive sufficient light (within the integration time of the eye) to have adequate contrast sensitivity near the sampling frequency $v_s = v_{co}$ where $M_1(v_{co}) = 0$. All other animals have increased $\Delta\phi$ and hence p to some minimum value necessary for adequate contrast sensitivity at their sampling frequency. In this Section, we follow the analysis of SNYDER (1977) to determine this minimum p value assuming that the visual system is limited only by Poisson noise at the photoreceptor level.

Here we consider the SNR across the array of photoreceptors in which case increasing p increases the SNR. If we assume no further neural processing, then this SNR is proportional to the perceived contrast sensitivity of the animal. Other possibilities, discussed in section B.1.5 render SNR independent of individual receptor noise but this is not considered in the following analysis. We instead assume that the noise \sqrt{N} of the individual photoreceptor is limiting.

Contrast Sensitivity. The contrast sensitivity (CS) of an animal is the reciprocal of the minimum grating modulation m necessary for threshold detection of a grating at frequency v . If it were not for noise in the visual pathways, m^{-1} would be infinite. However, because of photoreceptor noise, the CS at the photoreceptor level is found from Eq. (B.15) to be

$$CS(v) = m^{-1}(v) = \sqrt{NM(v)}, \quad (B.27)$$

where \bar{N} from Eq. (B.16) is the number of photons captured per rhabdom and from Eq. (B.8) M is the modulation transfer function of the optics and rhabdom, assuming threshold detection occurs when the ratio SNR is unity. The greater the spatial frequency v , the lower the animal's contrast sensitivity reaching a minimum value of zero at $v = v_{co}$. It is observed from Eq. (B.15) that the contrast sensitivity of an array of photoreceptors is closely related to the SNR of fluctuations across the array.

Our purpose is to determine the eye parameter p of Eq. (B.2) and the angular rhabdom diameter $\Delta\varrho_r$ of Eq. (B.7c) that maximize the contrast sensitivity at the sampling frequency v_s of the ommatidia as defined by Eq. (B.3). We have already shown in Section II.C.1 above that $\Delta\varrho_r = 0.87\Delta\phi$ maximizes the contrast sensitivity. Now we determine the value of p that will provide adequate contrast sensitivity at the highest spatial frequency sampled by the ommatidia $v = v_s$ assuming the animal is in the brightest light of its usual environment.

From Eqs. (B.16c), (B.21), (B.8a), (B.3b), and (B.11), we can rewrite the expression for contrast sensitivity Eq. (B.27) at the sampling frequency

$$CS(v_s) = 0.45p \sqrt{\bar{I}} e^{-0.89 \left[\left(\frac{\lambda}{p} \right)^2 + \left(\frac{v \Delta t}{\Delta \phi} \right)^2 \right]} \quad (B.28)$$

for square packing. For hexagonal packing, we replace $\Delta\phi$ by $\sqrt{3}\Delta\phi/2$ so that p in Eq. (B.28) equals $D\sqrt{3}\Delta\phi/2$.

We begin by assuming the animal and object are stationary, relative to one another so that $v=0$ in Eq. (B.28). From Eq. (B.28), it is clear that the greater p , the greater the contrast sensitivity $CS(v_s)$ at the sampling frequency. Of course, the greater p , the more inefficient the animal is in sampling its diffraction-limited optics. Therefore, we want the minimum value of p that provides a tolerable contrast sensitivity for the animal in its brightest environment. Let's suppose that the minimum value is $CS=2$ so that the animal can detect gratings at $v=v_s$ of 50% contrast or greater. Since in nature, contrasts above 50% are rare, $CS=2$ is a reasonable minimum value for tolerable contrast sensitivity.

In Fig. 12 we show the optimum eye parameter p vs. log luminance (upper scale) for $\lambda=500$ nm and a minimum contrast sensitivity of $CS=2$. The results are found from Eq. (B.28) with $v=0$. The luminance scale is taken from the example of Section II.D with $(\Delta\varrho/\Delta\phi)^2 = (\lambda/p)^2 + 0.56$. It is clear from this figure that the appropriate eye parameter p depends on the luminance, assumed to be the largest value in the animal's typical environment. In particular, from Fig. 12 for hexagonal packing, the diffraction-limited eye with $p=0.29 \mu\text{m}$ requires the brightest natural light for the barely adequate contrast sensitivity of $CS=2$. In Appendix E, we show that $\log m^2 \bar{I} \geq 5$ for a diffraction-limited eye to be the optimum design independent of the packing geometry.

For those animals that are *not* active in the brightest light, there is no loss in having p greater than the diffraction limit and in fact there is a gain because the focal length can be shorter, the eye less flat, or photon capture increased by increasing D . Note from Fig. 12 that p need only be slightly larger than the diffraction-limited value to be optimum for an environment 2–3 log units less than the brightest sunlight. For example, an eye with a hexagonal lattice of ommatidia

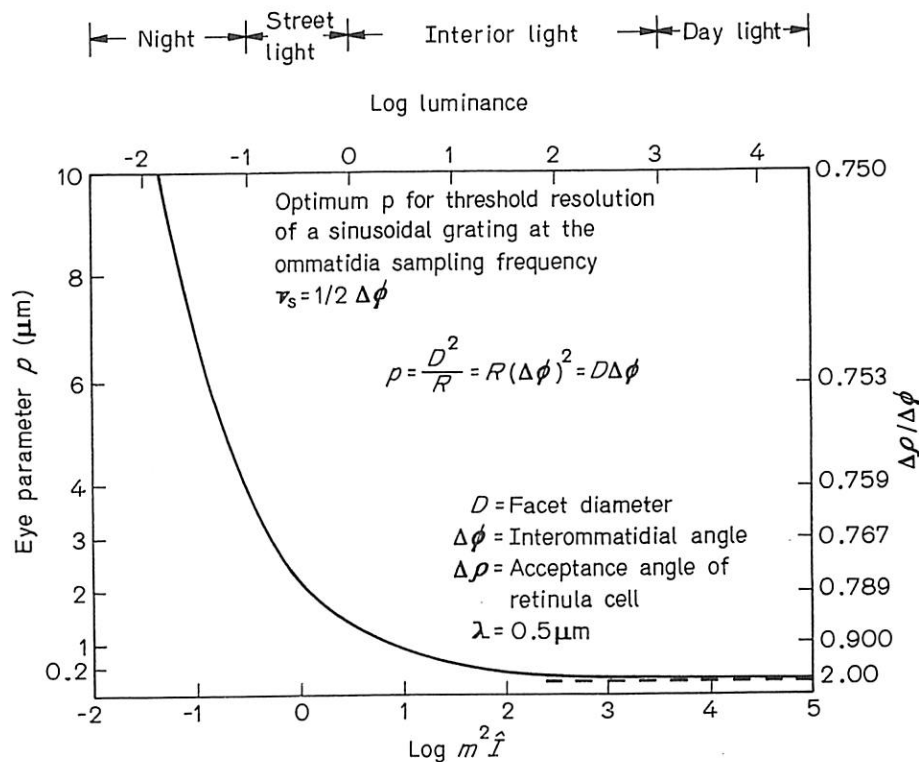


Fig. 12. Optimum eye parameter p for a given intensity parameter \hat{I} and contrast or modulation m . The luminance scale is in candelas per square meter for the case of $m=0.5$. The results are for square facets. For hexagonal facets, we replace $p=D\Delta\phi$ by $p=D\sqrt{3}\Delta\phi/2$. In both cases, the dashed line is the asymptote $p=0.25 \mu\text{m}$

and $p=0.5 \mu\text{m}$ is the optimum design for an environment 3 log units less intense than necessary for the diffraction-limited eye where $p=0.29 \mu\text{m}$. To use Fig. 12 for an hexagonal lattice, define p as $D\Delta\phi(\sqrt{3}/2)$. In Fig. 12 we also show the ratio $\Delta\rho/\Delta\phi$ corresponding to each p value, where $\Delta\rho$ is the acceptance angle of a retinular cell and $\Delta\phi$ the interommatidial angle.

Comparison with Measured p Values. HORRIDGE (1977) has compared the predicted p values of Fig. 11 to those measured in various animals. The foveas of bright-light locusts, dragonflies, and wasps have p between $0.31 \mu\text{m}$ and about $0.45 \mu\text{m}$. The foveas of mantids and a large portion of the eye of bright-light insects have $0.45 \leq p \leq 1$; eye edge of many diurnal insects, $1 \leq p \leq 2$; eye of nocturnal dragonfly, $2 \leq p \leq 3$; eyes of deep-sea crustacean, $3 \leq p \leq 6$. The trend is clear. The dimmer the animal's environment, the less it takes advantage of its diffraction-limited optics.

Since there is an optimum eye parameter p for each intensity, the compound eye ideally would have a range of values for p across its head if it is to perform optimally over a range of values for intensity. For example, if p varies from 0.3 to $0.5 \mu\text{m}$ (representative of the dragonfly *Hemicordula*, HORRIDGE, 1976), this allows for a range of 3 log units in luminance for which the eye design is optimum. If p

varies from 0.3 to 1 μm , then the eye can accommodate 4 log units change in luminance while remaining at optimum.

Despite the apparent advantage of having a substantial range in p across the eye, in many animals p appears rather constant, e.g., as in *Musca* (STAVENGA, 1975). It remains possible that, because of neural summation, p of the neural ommatidia vary significantly. For example, because of convergence in the human peripheral retina, there is an enormous variation in the receptor spacing at the neural level while there is none at the rod photoreceptor level (SNYDER et al., 1977). Furthermore, the variation follows a curve like that of Fig. 12. Thus, although the facet topology may not display large values of p , the neural ommatidia quite possibly do (Sec. V).

While there would appear to be no alternative strategies for optimizing to different contrast levels, there are other possibilities for dealing with reductions in intensity. One is by the method of optical superposition, which effectively increases the light-gathering aperture for a rhabdom (HORRIDGE, 1975; KIRSCHFELD, 1975). The other is to increase the acceptance angle $\Delta\phi$ during dark adaptation (Sec. IV).

Although the theory presented here suggests why many animals have p above the diffraction limit, it does not answer why some animals have comparatively large p values even though they are in bright light. For example, *Musca* has $p \approx 1.3 \mu\text{m}$ (STAVENGA, 1975), i.e., about 4.5 times greater than the diffraction limit. One possible explanation is that such animals have a high angular velocity. We consider this possibility next.

7. Influence of Angular Motion on Eye Design

It is apparent from Eq. (B.28) that, when the animal is undergoing angular velocity v , the effect is equivalent to a reduction in intensity from \hat{I} to \hat{I}_t , where

$$\hat{I}_t = \hat{I} e^{-1.78 \left(\frac{v \Delta t}{\Delta \phi} \right)^2} \quad (\text{B.29})$$

so that, to include angular motion in Fig. 12, we simply replace $\log \hat{I}$ by $\log (\hat{I}) - 0.78(v \Delta t / \Delta \phi)^2$. The quantity $v \Delta t$ is the amount the animal turns in one integration time. We see, for example, that the effect of $v \Delta t = 2 \Delta \phi$ is equivalent to a reduction in 3 log units of intensity. Taking $v \Delta t = 3^\circ$, $\Delta \phi = 1.5^\circ$, $\Delta t = 20 \text{ ms}$, we find that $v \Delta t = 2 \Delta \phi$ is equivalent to the animal turning $180^\circ/\text{s}$. This is less than the average chasing behavior of the housefly (COLLETT and LAND, 1974). Thus, if an animal, like *Musca*, is active in the midrange of daylight (say, log luminance ≈ 3.5) but, say, typically turns at 180° in 1 s, Fig. 11 shows that $D \Delta \phi = 1$ as in *Musca* rather than $D \Delta \phi \approx 0.33$, when $v = 0$.

From the above logic, it is also easy to understand the advantage of increasing $\Delta \phi$ from the center of the eye to the side (along the horizontal axis) of an animal with a direct flight pattern, because increasing v is compensated for by increasing $\Delta \phi$ in the ratio $v \Delta t / \Delta \phi$ discussed above. Assuming that $D \Delta \phi$ is constant around the eye, this is consistent with an eye having its greatest eye radius in front and smallest on the side (PORTILLO, 1936; MAZOKHIN-PORSHNYAKOV, 1969).

8. Diurnal Eyes Employing Optical Superposition: Skipper Butterflies

Our discussions so far have been primarily for apposition eyes, although they apply fairly generally to neural superposition eyes as well. However, animals employing optical superposition require special consideration. Here we study the skipper eye which provides a unique example of a diurnal animal with high resolving power while employing optical superposition. Optical superposition is a strategy generally restricted to the eyes of nocturnal moths. Neural superposition eyes are discussed in Section D (see Fig. 1).

The skipper eye is hemispheric (DØVING and MILLER, 1969; HORRIDGE et al., 1972), probably as a consequence of its image formation by optical superposition. Accordingly, facet diameter D and interommatidial angle $\Delta\phi$ are interrelated by the radius R of the animal's head: $D = R\Delta\phi$. Furthermore, D , $\Delta\phi$, and hence the eye parameter p are constant everywhere on the skipper eye. By virtue of the image-forming characteristic of superposition optics, $\Delta\phi$ is also related to the center-to-center distance d_{cc} between rhabdoms: $d_{cc} = f\Delta\phi$, where f is the focal length (or posterior nodal distance) of an individual lens facet. Because the eye is spheric, f is also the distance from the center of the eye to the distal tips of the rhabdoms. By equating our two expressions for $\Delta\phi$, we have a fundamental relation for optical superposition eyes

$$Rd_{cc} = fD \quad (B.30)$$

which also holds for neural superposition eyes (Sec. D) and is quite likely at least approximately valid for apposition eyes.

The light-gathering capacity of a rhabdom is given by Eq. (B.16) for superposition and neural superposition eyes. For optical superposition, many facets are recruited in the task of gathering light for one rhabdom. From the work of HORRIDGE et al. (1972), it appears that the angular diameter of the summed participating facets $\phi_\Sigma \approx 30^\circ$, independent of the animal's size or the diameter of the individual facets. For angles ϕ_Σ greater than 30° , it is probably difficult for a crystalline cone to sufficiently bend the light rays for accurate image formation. The mean number of photons counted by a rhabdom due to a uniform extended source \bar{N} is proportional to $(R\phi_\Sigma \Delta\varrho_r)^2$ where $\Delta\varrho_r$ is the angular rhabdom diameter. Since the rhabdoms are surrounded by tracheal walls that in turn are closely packed with their neighbors (HORRIDGE et al., 1972), and assuming that all light falling within the tracheal walls is absorbed, we then have $\Delta\varrho_r \approx \Delta\phi$. Consequently, each rhabdom captures an amount of light proportional to $(D\phi_\Sigma)^2$ due to a uniform source infinite in extent. Assuming that the angular diameter of the participating facets is nearly constant in all animals ($\phi_\Sigma = \text{constant} \approx 30^\circ$), then the *photon capture of each rhabdom depends only on the diameter of the individual facet D* . The optical superposition eye thus has high contrast sensitivity, i.e., an amount $(\phi_\Sigma/\Delta\phi)^2$ greater than an apposition eye of the same size.

The image quality is limited by the diffraction of the *individual* facet diameter D ; however, we cannot exclude the possibility of some aberrations due to the superposition optics. Nevertheless, intracellular measurements of the acceptance

angle in *Epargyreus clarus* by DØVING and MILLER (1969) indicate that aberrations are not very significant. In particular, they find that $\Delta\varrho \approx 2^\circ$ (see Fig. 1C for nomenclature). To see how this compares with the theoretic expression for $\Delta\varrho$ when only diffraction is limiting, we use the theory of Section B.2.a. From DØVING and MILLER (1969), $D = 27 \mu\text{m}$, $\Delta\phi = 1.5^\circ$, and $\lambda \approx 520 \text{ nm}$. Recalling from our discussion above that $\Delta\varrho_r = \Delta\phi = 1.5^\circ$ together with $\Delta\varrho_l = (\lambda/D) = 1.11^\circ$, then from Eq. (B.7) $\Delta\varrho \approx 1.9^\circ$. This is sufficiently close to the measured value $\Delta\varrho \approx 2^\circ$ to show that the optical quality of skipper is nearly diffraction limited even though many facets participate in the image formation.

Recall our discussion of Section B.III.4 where we showed that the eye parameter $p = D\Delta\phi$ gives the efficiency of the animal in sampling the highest frequency passed by the optics. For *Epargyreus clarus*, $p \approx 0.7 \mu\text{m}$, which according to the logic of Fig. 12 is the correct design for an animal not normally in the brightest sunlight. However, skippers usually favor bright conditions and we are compelled to explain the discrepancy. There are two possibilities. Skippers have a rapid chasing behavior and accordingly, like *Musca*, receive only a small amount of light per integration time of the eye (Sec. 3 above). Since skipper eyes are unable to be locally flat, only those animals with large heads can have comparatively small p .

Because there are many skipper eyes with D nearly independent of head size R , it follows in these animals that resolving power is proportional to R , i.e., $\Delta\phi$ and hence p are proportional to R^{-1} . Remember also that the light capture of a rhabdom is proportional to $(\phi_\Sigma)^2$ for extended sources and thus, in this instance, the same for large and small eyes. For point sources, the greater ϕ_Σ the better. This observation is consistent with the second explanation above, i.e., only big eyes can accommodate small $\Delta\phi$ and have large absolute resolving power.

One question remains unanswered. Because skipper undersamples, (varying between 0.5 and 1.2 μm depending on eye size), why should it not increase light capture (i.e., increase ϕ_Σ) an additional amount until aberrations limit the highest spatial frequency passed to the sampling frequency $v_s = 1/\sqrt{3} \Delta\phi$? Perhaps the superposition image deteriorates rapidly beyond 30° or possibly the animal can make use of its comparatively good image quality in movement detection by aliasing.

9. Summary

We have considered the physical factors that influence the performance and design of compound eyes. In this section, eye design is characterized by the facet topology through the parameter $p = D\Delta\phi$ (facet diameter multiplied by the interommatidial angle) and by the acceptance angle $\Delta\varrho$ of the ommatidium. The most suitable value of these parameters is shown to depend critically on the intensity of light as well as on the angular velocity of the animal. This assumes that pupil diffraction and Poisson noise of the individual rhabdomeres are limiting. For example, it is advantageous for an animal to have its commatidia spaced at the limit set by pupil diffraction, i.e., $p \approx 0.3 \mu\text{m}$, only if it is active in bright light and relatively stationary while examining objects, otherwise p should be larger (Fig. 11).

Since an increase in the angular velocity of an animal was shown to be equivalent to a decrease in light intensity, the design of *Musca* ($p \cong 1 \mu\text{m}$) is consistent with an animal performing high-speed aerial acrobatics at high light intensities (LAND and COLLETT, 1974).

The *absolute* (or anatomic) resolving power of an animal with compound eyes is set by the interommatidial angle $\Delta\phi$ and not by p , e.g., when comparing eyes with foveas that are designed at the limit set by lens diffraction ($p \cong 0.58\lambda$), we typically find that the larger eyes have the smaller $\Delta\phi$. In this regard, we note that the highest resolving power achieved in vertebrate eyes (say three times that of man), e.g., eagles and falcons (FOX et al., 1976), is about 100-fold that in those compound eyes with the highest anatomic resolving power, e.g., the dragonfly *Aeschna palmata* with $\Delta\phi = 0.24^\circ$ (SHERK, 1976). The biologic reason for this significant difference is probably embodied in the concept of subjective resolution (KIRSCHFELD, 1976).

Finally, it is necessary to mention that our investigation was limited to extended objects as the acuity task. An insect that is contrasted by the clear sky is a good example of a nonextended object (e.g., two *Musca* separated by more than 70 cm appear like distant point sources to each other; SNYDER, 1977). Further discussions on resolution of isolated points are given in Appendix D.

IV. Strategies for Dark Adaptation

In this Section, we examine various strategies for design that allow an animal to have sufficient resolving power over a range of contrast and intensity when the eye parameter $p = D\Delta\phi$ is constant over the eye. Except when stated otherwise, the eye is assumed to be spheric with ommatidia that have identical facet diameters D and interommatidial angles $\Delta\phi$. The theoretic calculations are given by SNYDER (1977).

1. Eyes Without Adaptation Mechanisms

In Section II we showed that, because of photon noise, the resolving power of an eye decreases as the luminance decreases. The highest spatial frequency v that can be resolved at a particular luminance is given by Curve 1 of Fig. 13. This figure depicts a Curve 1 for two different eyes, one with $p = 0.25 \mu\text{m}$ (p at the minimum value set by diffraction), the other with $p = 1.0 \mu\text{m}$. It is convenient to plot $v\Delta\phi$ rather than v because the curves then apply to an eye of arbitrary interommatidial angle $\Delta\phi$. The results are found from Eq. (B.19) by determining the threshold v at each intensity, assuming $\text{SNR} = 1$.

The results of Fig. 13 assume that Poisson noise of *individual* rhabdomeres is limiting. However, by the appropriate neural averaging discussed in section 1.5, the SNR can be greatly enhanced at higher levels over that at the photoreceptor array. This is because of the repetitive or coherent nature of the grating stimulus. Consequently, if say 100 ommatidia are involved in the resolution task, then the luminance scale for curve 1 of Fig. 18 is shifted to the right by two log units, i.e. the animal performs as if the environment were two log units brighter.

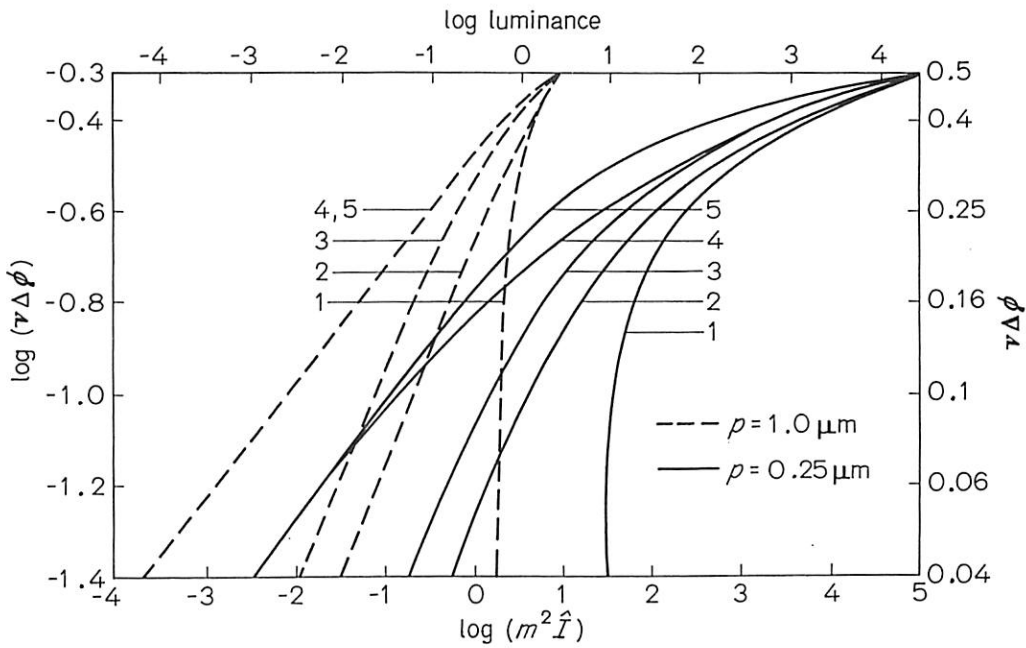


Fig. 13. The highest resolvable (or threshold) spatial frequency v vs. luminance in candelas per square meter for various strategies of dark adaptation. The luminance scale is for a sinusoidal grating of 50% modulation m or contrast (the mean of all possible contrasts 0 to 1) and $\lambda = 500 \text{ nm}$. Two different eyes are considered, both spheric, one with $p = 1.0 \mu\text{m}$ and the other with $p = 0.25 \mu\text{m}$. Curve 1 is for an eye with no dark adaptation mechanism, Curve 2 for widening the acceptance angle, Curve 3 for neural pooling, Curve 4 for neural pooling together with widening the acceptance angle, and Curve 5 for a range in facet diameters over the eye. Simple expressions for these curves can be easily found for the low intensity limit from Eq. (B.19) because $v \ll v_{eo}$ so that $M_1 = 1$. Accordingly, for Curve 1: $v\Delta\phi = 0.5$ provided $m^2\hat{I} \geq 1.8p^{-2}$; for Curve 2: $v\Delta\phi = 0.23p(m^2\hat{I})^{1/2}$; for Curve 3: $v\Delta\phi = 0.38p(m^2\hat{I})^{1/2}$; and for Curves 4 and 5: $v\Delta\phi = 0.34p^{1/2}(m^2\hat{I})^{1/4}$. Curve 2 is less than Curve 3 because $M_r = 0.61$ instead of unity

2. Increase in Acceptance Angle with Decrease in Luminance

Suppose that the acceptance angle $\Delta\varrho$ of the ommatidia increases as the luminance decreases. This occurs in a number of animals (for review, see WALCOTT, 1975). The advantage of increasing $\Delta\varrho$ has been given qualitatively by LAUGHLIN (1975). As the luminance decreases, the contrast sensitivity at the high spatial frequencies becomes inadequate. By increasing $\Delta\varrho$ the contrast sensitivity of these high spatial frequencies is further reduced but that of lower spatial frequencies is enhanced. Since the highest potential resolving power is irretrievably reduced, the slight loss to acuity by increasing $\Delta\varrho$ a certain amount can be offset by the gain in photon capture allowing for resolution of lower spatial frequencies.

Figure 14 demonstrates that there is an optimum acceptance angle $\Delta\varrho$ at each luminance. When the eye is designed at optimum ($\Delta\varrho_r = 0.75\Delta\phi$) shown as the dashed line, we see that the sampling $v_s = 1/2\Delta\phi$ can be resolved but only if $\log m^2\hat{I} \cong 5$. However, as $\log m^2\hat{I}$ decreases below 1, not even extended uniform objects ($v \cong 0$) can be seen reliably. Had we taken $\Delta\varrho_r = 2\Delta\phi$, the eye would be unable to resolve the sampling frequency $v_s = 1/2\Delta\phi$, but it would be able to resolve low frequencies at luminances when the eye with $\Delta\varrho_r = 0.75\Delta\phi$ is unable to resolve anything. In other words, the greater $\Delta\varrho_r$, the better the detection of low frequency

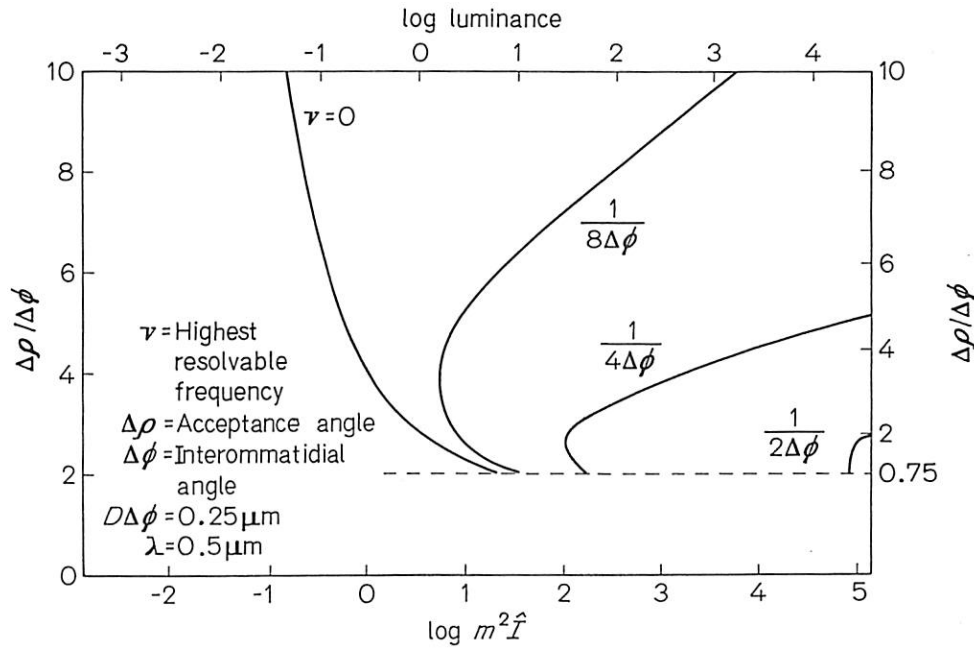


Fig. 14. Highest resolvable frequency for an animal with a given $\Delta\phi$ and $\Delta\varrho$. The luminance scale is in candelas per square meter for the case of 50% object modulation

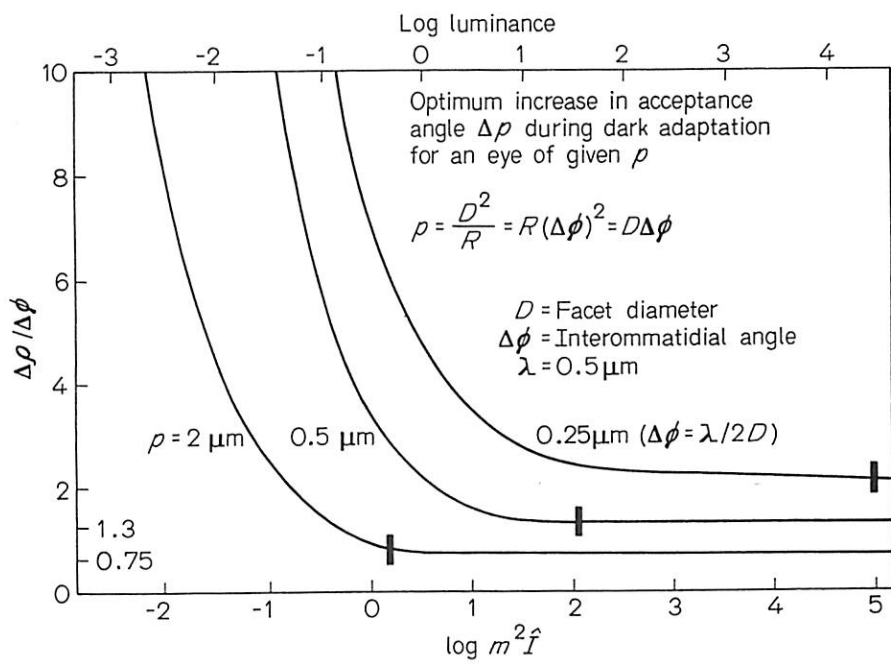


Fig. 15. Optimum acceptance angle $\Delta\varrho$ for each intensity during dark adaptation for an eye of given $\Delta\phi$ and p . The luminance scale is in candelas per square meter for 50% object modulation

gratings at low luminances. At each value of $m^2 \hat{I}$, there is an optimum value of $\Delta\varrho_r$ given by the turning points on Fig. 14, e.g., $\Delta\varrho_r = 1.5\Delta\phi = 0.375/\nu$ when $\log m^2 \hat{I} \cong 2$. This optimum $\Delta\varrho$ is shown in Fig. 15 for three different eyes with $p = 2 \mu\text{m}$, $0.5 \mu\text{m}$, and $0.25 \mu\text{m}$, respectively. By plotting $\Delta\varrho/\Delta\phi$, we have generalized our curve to an eye of arbitrary interommatidial angle. It should be noted that a comparatively

small change in $\Delta\varrho$ is required to accommodate large changes in luminance. WALCOTT (1975) has described anatomic changes during light adaptation that can easily accommodate the theoretic optimum suggested here, e.g., $\Delta\varrho$ of *Lethocerus* changes from 3.5° to greater than 9° when dark adapted. Curve 2 of Fig. 13 shows the highest spatial frequency v vs. luminance for an eye that increases its acceptance angle in the optimum manner discussed above. Because there can be a range in environmental contrasts at each intensity, it is theoretically advantageous to have a range in $\Delta\varrho$ across the eye.

3. Neural Pooling

If the luminance is reduced below that necessary for sufficient contrast sensitivity at the sampling frequency, it is advantageous to form a larger neural ommatidium by neural convergence and gain in contrast sensitivity at low spatial frequencies. This neural convergence could be hard wired, i.e., exist in parallel with through running neurons or it could depend on intensity. In both cases, the effect is to form an effective larger ommatidium. The results of this strategy are shown in Fig. 13, Curve 3.

Now suppose, together with neural pooling, that the acceptance angle $\Delta\varrho$ changes such that $\Delta\varrho_r$ is proportional to the neural interommatidial angle $\Delta\phi_n$ so that $D\Delta\phi_n = D_n\Delta\phi_n$, where D_n is the effective pupil diameter of the neural ommatidium. The gain in contrast sensitivity at lower spatial frequencies equals $p_n(I)/p$, where $p_n(I)$ is the neural eye parameter $D_n\Delta\phi_n$ and is set according to Fig. 12 while $p = D\Delta\phi$. The highest spatial frequency resolved at any given luminance I equals the neural sampling frequency $v_{ns}(I) = \{p/p_n(I)\}^{1/2}v_s$. The result of this strategy is given in Fig. 13, Curve 4.

4. Comparisons and Discussion

It is clear from Fig. 13 that all of the strategies considered offer an improvement in spatial resolution at low intensities compared to that of Curve 1 for no adaptation mechanism. DVORAK and SNYDER (1978) have measured the variation in grating resolving power by monitoring the extracellular response of direction-sensitive, motion-detecting neurons and find that the results indicate a dark adaptation strategy similar to that of Curve 4 in Fig. 13.

It is of interest to compare these results to a *spheric* eye where the facet diameter D changes (i.e., p changes) over the animal's head, but the eye radius remains as in the above examples. We show in Appendix B that Curve 5 of Fig. 13 applies, where $\Delta\phi$ and p now refer to the minimum values on the eye. Although an eye with a range in D is theoretically better than one with neural pooling (large facet diameters have less pupil diffraction), this assumes the radius is sufficiently large to accommodate a substantial number of facets with a large range of diameters. In comparison, an eye with versatile neural pooling can function nearly as well and yet be considerably smaller, because in theory the whole head can act as one neural facet at low intensities while at high intensities the individual

ommatidia do the sampling. Moreover, for eyes with a range in the parameter p , each portion of the head is best suited to a different contrast luminance level which need not be the case for a neural pooling strategy. Obviously, it is advantageous to combine neural pooling with an eye that has a range in p . Lastly, we stress that only apposition eyes have been considered. Optical superposition eyes (for review, see HORRIDGE, 1975; KIRSCHFELD, 1975) can theoretically maintain their highest potential acuity for a change of $\log q$ units in luminance, where q is the number of recruited facets making up the superposition image. See Section III.8.

V. Neural Processing

In this section, we consider the role of neural processing in regard to spatial information as well as possible strategies to achieve this role. We begin by considering two important tasks that may involve neural processing: 1) the improvement of contrast sensitivity and 2) the transformation of spatial information from one form to another.

1. Enhancement of Contrast Sensitivity by Neural Processing

In the above section, we showed that photon noise of an individual photoreceptor limited the contrast sensitivity or equivalently the SNR across the photoreceptor array. Now it should be rather obvious that, by appropriate weighted averaging and correlating of the individual photoreceptor signals, the SNR appearing across an array of higher order neurons can be improved upon that appearing across the receptor array assuming the averaging procedure itself is noise-free. The most elementary example is for a uniform extended source that has an SNR proportional to $\sqrt{\bar{N}}$ at the photoreceptor level but a potential SNR of $\sqrt{i\bar{N}}$ at some higher level, where \bar{N} is the mean number of photons captured by an individual photoreceptor and i is the number of photoreceptors. This result holds more generally with slight modification. In particular, the SNR or contrast sensitivity to sinusoidal gratings of frequency v is $\sqrt{i\bar{N}}M(v)$, where i is the number of photoreceptors per angular area participating in the resolution measurement and M is the modulation transfer function of the optics and rhabdom. *With this form of processing, the contrast sensitivity is independent of the diameter of an individual photoreceptor (except weakly through M), and depends instead upon the total angular retinal area $i(\Delta\theta_r)^2$ devoted to the detection process.* Thus, the gain in contrast sensitivity is proportional to \sqrt{i} . Whether or not the nervous system has such versatility remains unknown. The great advantage in contrast sensitivity discussed above is due mostly to the coherent or repe nature of the signal, i.e., a sinusoidal grating. For the incoherent type of object world that occurs naturally, there is no corresponding increase in spatial discrimination by the weighted, correlated averaging discussed above. Recall that improving contrast sensitivity for gratings at each frequency, e.g., by parallel Fourier channels, need not improve spatial

discrimination of broad spectrum signals, even if the system is linear. This is because, due to noise, the subtle fluctuations of the image in the frequency domain are no easier to detect than subtle fluctuations in the space domain, in addition to the added problem of phase correlation. Thus, there may be no compelling reason for the nervous system to adopt such a strategy. However, if the animal had one or several preferred acuity tasks, e.g., the recognition of a characteristic pattern, then the nervous system could be designed to respond only to this pattern with an enormous contrast sensitivity. Furthermore, the pooling of ommatidia as discussed in Section BI.5 and IV would appear advantageous to the animal as luminance decreases.

2. Transformation of Spatial Information

The ommatidia provide a two-dimensional sampled version of the object world, which the nervous system must subsequently analyze. We can view each level in the visual pathway as a generalized transform of the visual input. Each transformation results in a form more convenient for decoding. For example, one direct transformation is via a pointwise measure of visual intensity (ROBSON, 1975). Another is by a spatial frequency transform. For example, if the nervous system had the capability of performing a Fourier transformation, e.g., as manifested by parallel Fourier channels of narrow band width, then the contrast sensitivity to *sinusoidal gratings* is proportional to $D^2 M^2(v)/(\Delta v)^2$, where D is the pupil diameter, M the modulation transfer function of the optics and rhabdom, and Δv the band width of each channel, assuming only photon noise at the photoreceptor level is limiting. The minimum bandwidth $(\Delta v)^2$ is proportional to the inverse angular area of the eye devoted to the resolving task. Thus, maximum contrast sensitivity is proportional to the number of photons captured within the angular region devoted to the resolution task, as mentioned in Section 1 above. However, the evidence for effective Fourier channels in the nervous system is lacking (ROBSON, 1975, p. 112).

a) Neural Compensations for Optical Blur and Photoreceptor Noise

SNYDER and SRINIVASAN (1979) have suggested a transformation for the visual pathways in the human retina that may also have some relevance for compound eyes. They propose that neural processing compensates for both optical degradation as well as noise contamination at the photoreceptor level—a hypothesis consistent with many psychophysical measurements. We now present the argument as originally applied to the human retina.

It is clearly impossible for neural processing to restore those high frequencies already lost at the photoreceptor level, nor can it filter the noise from the image without simultaneously filtering out some of the object information as well. In other words, subsequent neural processing is unable to recover object information that is already lost at the photoreceptor level, but it can transform this information from one form to another analogous to translating from one language to another. We now determine the transfer properties of the neural processing, assuming its only task is to transform the image at the photoreceptor level to a cortical image that

looks like the object. This requires that the nervous system compensates for optical blur as well as for noise contamination. Our discussion commences with the limiting case of extreme suprathreshold conditions.

b) Extreme Suprathreshold Conditions (Noiseless Blurred Image)

When the photoreceptor image is comparatively free of noise, presumed to be the case in extreme suprathreshold conditions, then theoretically all photoreceptor image distortion is due only to the blurring effect of the eyes' optics, i.e., due only to the nonuniform properties of the transfer function for the dioptrics M_l . The neural image will then appear most like the object when the transfer function of the neural apparatus M_n is the inverse of the optical transfer of M_l , i.e.,

$$M_n = M_l^{-1}. \quad (\text{B.32})$$

Taking the data of CAMPBELL and GUBISCH (1966) for the human dioptrics shown in Fig. 16a, then M_n becomes that shown in Fig. 16b. The product of the two curves gives Fig. 16c. In other words, because of this neural compensation for optical blur, the overall transfer function of the visual system M is uniform with spatial frequency as shown in Fig. 16c. Deblurring is made physically realizable by having the nervous system increase its sensitivity (gain) at those spatial frequencies that are attenuated most by the optics, i.e., neural processing amplifies the high spatial frequencies relative to the lows as shown in Fig. 16b.

One significant consequence of a uniform transfer function M for the entire visual system is that gratings of equal contrast are perceived to have identical contrast, independent of their spatial frequency. Indeed, brightness-matching measurements show this to be approximately true, in photopic conditions, provided the grating contrast is sufficiently high (WATANABE et al., 1968; BLAKEMORE et al., 1973; GEORGESON and SULLIVAN, 1975). Consequently, contrast constancy at suprathreshold conditions is consistent with the hypothesis that the neural system transforms the photoreceptor image to a cortical image more nearly resembling the object. The receptive field of a hypothetic neuron at the site of this cortical image would have the center surround form discussed in Section B.II.5 above, i.e., by FOURIER transforming Fig. 16c.

c) Threshold Conditions (Noisy Blurred Image)

Now we consider the other extreme when, in addition to optical blur, the image at the photoreceptor level suffers from significant noise contamination. This situation is most dramatic at threshold conditions. What properties must then be manifested by neural processing for the neural image to look most like the object? When photoreceptor noise is significant, amplifying the signal also amplifies the noise. Furthermore, high frequencies are comparatively noisier than lower spatial frequencies because of the modulation transfer function of the optics shown in Fig. 17a. It is intuitive that the neural image will then appear more like the object if the nervous system is less sensitive to these noisy or unreliable frequencies compared to the more reliable ones. Frequencies which are 100% reliable (i.e., $v=0$) should be reproduced in their entirety (i.e., transmitted without any attenuation or amplifi-

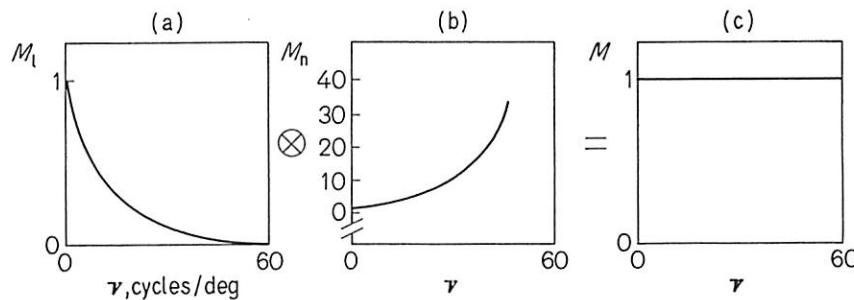


Fig. 16. The modulation function for the visual system $M(v)$ determined as a product (denoted by the symbol \otimes) of the optical transfer function $M_l(v)$ with the neural transfer function $M_n(v)$. The case of extreme suprathreshold conditions is shown when the neural modulation transfer function equals the inverse of the optical transfer function, i.e., $M_n = M_l^{-1}$. The optical modulation transfer function M_l is for a pupil diameter of about 3 mm and is found by interpolating the data of CAMPBELL and GUBISCH (1966) for the human eye

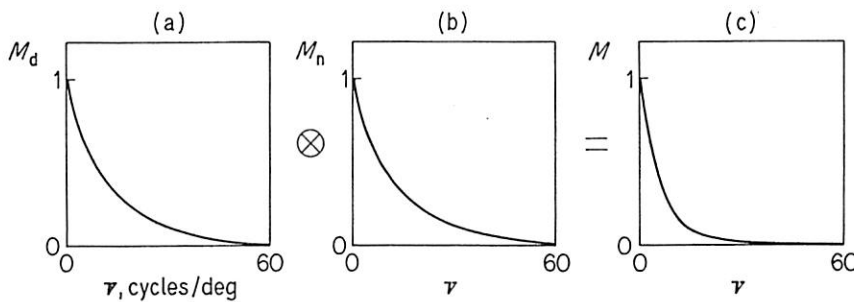


Fig. 17a and b. The same as for Fig. 16 but now for threshold conditions. (a) is the same as Fig. 16a but (b) is given by $M_n = M_1$ so that $M = M_1^2$

cation). On the other hand, frequencies that are 0% reliable, i.e., frequencies which contain only noise and no signal like $v=60$ cpd in Fig. 17a should be completely excluded because they contain no object information and will only contaminate the image with noise. Frequencies that are partially reliable should be attenuated to an extent that depends upon their reliability. At threshold, the reliability of the image is proportional to M_1^2 . Consequently, the neural compensatory mechanism must fulfill two competing roles: deblurring on the one hand, characterized by $M_n = M_1$. It turns out that (SNYDER and SRINIVASAN, 1979) the transfer function of the neural apparatus M_n is given by the product of these two competing effects

$$M_n = M_1^{-1} M_1^2 = M_1 \quad (B.33)$$

i.e., when the nervous system deblurs the image in a weighted manner, comparatively suppressing the relatively noisier frequencies. The transfer function of the entire visual system, $M = M_1 M_n$, then becomes

$$M = M_1^2. \quad (B.34)$$

In other words, if the neural image is to look like the object in contrast threshold conditions, then the transfer function for the visual system depends only upon the

square of the transfer function of the optics. Taking the data of CAMPBELL and GUBISCH (1966) for the transfer function of the human dioptrics as shown in Fig. 17a and multiplying it by the transfer function for the nervous system $M_n = M_1$ shown in Fig. 17b leads to the transfer function of the visual system $M = M_1^2$ shown by Fig. 17c. Indeed, above about three cycles per degree, the shape of the well-known human threshold contrast sensitivity function (e.g., CAMPBELL and ROBSON, 1968) is nearly identical to that of Fig. 17c when plotted on a linear frequency scale as we show here. Thus, the threshold contrast sensitivity function (above three cycles per degree) as well as the extreme suprathreshold sensitivity function are consistent with the hypothesis that neural processing transforms the photoreceptor image to a neural image that better resembles the object. The receptive field of a hypothetic neuron at the site of the cortical image at threshold looks like that at suprathreshold but without the surround.

In summary then, the essential concept for noise compensation is that the neural network must be least sensitive to those spatial frequencies that are comparatively unreliable, i.e., those spatial frequencies with a low SNR appearing across the photoreceptor array. Because of attenuation by the optics, the high spatial frequencies are more unreliable so the neural network is comparatively insensitive to them. The essential concept for optical compensation is that the neural networks must be most sensitive at those spatial frequencies attenuated most by the optics. In extreme suprathreshold conditions, a wide range of spatial frequencies are reliable so that only optical compensation is necessary. At threshold conditions, all spatial frequencies are comparatively unreliable so that both optical and noise compensation is necessary.

by the
case of
als the
 M_1 is
UBISCH

6a but

which
letely
te the
to an
age is
must
 $= M_1$
neural

B.33)

para-
of the

B.34)

should
in the

VI. Spatial Information Capacity of Eyes

In this Section we derive a measure of an animal's capacity for spatial acuity. We begin with a strictly mathematic definition of the spatial information capacity of an eye H and then show how H can be interpreted as an animal's picture-making ability. We assume that the eye is limited by photoreceptor noise. From information theory (e.g., GOLDMAN, 1953), the information capacity of an eye per visual angle is

$$H = \int_0^{v_s} v dv \ln \{1 + \sigma_s^2(v)/\sigma_n^2(v)\}, \quad (B.34)$$

where $v_s = 1/\sqrt{3A\phi}$ is the sampling frequency of the photoreceptors, Eq. (B.3), σ_s^2 , σ_n^2 the power spectra (BRACEWELL, 1965) of the signal and noise at the level of the photoreceptor, respectively.

The power spectrum σ is related to the total power P by the integral

$$P = 2\pi \int_0^\infty \sigma^2 v dv, \quad (B.35)$$

where P is the variance for a random process. The noise power is \bar{N} assuming photon shot noise while an example of signal power is $N^2 M^2(v)$ for an object spectrum of a single frequency, i.e., a delta function.

This definition aids in specifying σ_n^2 and σ_s^2 . For example, since the noise of the photoreceptors is statistically independent, the noise power spectrum is approximately flat up to the sampling frequency so that from the above equation

$$N = 2\pi \sigma_n^2 \int_0^{v_s} v dv \quad (B.36)$$

and $\sigma_n^2 = \bar{N}/\pi v_s^2$. This is the noise power spectrum due to a uniform extended object.

Since all spatial frequencies are equally likely within the object world and because the eye is assumed to have no prior knowledge of the visual scene, we assume the object world has objects of random size and shape or equivalently the power spectrum of the object world is flat. Therefore σ_s^2 is proportional to $\{\hat{I}D^2(\Delta\varrho_r)^2\}^2(CM)^2$ where all qualities are defined in Table 2 while C is the mean contrast of the object world. Assuming C is small, then the noise power spectrum σ_n^2 is proportional to $\hat{I}D^2(\Delta\varrho_r)^2(\Delta\phi)^2$ so that

$$\frac{\sigma_s^2(v)}{\sigma_n^2(v)} = k\hat{I}(CD)^2 \left(\frac{\Delta\varrho_r}{\Delta\phi} \right)^2 M^2(v), \quad (B.37)$$

where $k=1$, with units $(\Delta\phi)^2$. Replacing this equation into the integral expression for H gives the information capacity of the eye from which the optimum eye parameters can be determined. In the limit of low luminance ($\hat{I} \rightarrow 0$), using the fact that $\ln(1+\epsilon) \approx \epsilon$ when $\epsilon \ll 1$, Eq. (B.34) can be expressed by a simple analytic form. We then find that for an eye of fixed facet diameter, the ratio $\Delta\varrho_r/\Delta\phi$ should be as large as possible. However, our primary concern is for the high intensity limit because nocturnal animals generally employ optical superposition (Sec. B.III.8 above). When $\sigma_s \gg \sigma_n$, Eq. (B.34) has the asymptotic solution (SNYDER et al., 1977).

$$H \approx (v_s^2/4) \left\{ \ln 1 + k\hat{I}(CD)^2 \left(\frac{\Delta\varrho_r}{\Delta\phi} \right)^2 M(v_s) \right\}^{1/2} \quad (B.38)$$

assuming that M can be approximated by a Gaussian as given by Eq. (B.8), i.e., $M(v_s) = \exp\{-3.56(v_s\Delta\varrho)^2\}$. Equation (B.1) is accurate over a wide range of intensities but becomes inaccurate as $\hat{I} \rightarrow 0$. Furthermore, Eq. (B.38) can be shown to equal the number of different pictures an eye can reconstruct (SNYDER et al., 1977).

1. Concept of an Animal's Spatial Information (Picture-Reconstructing) Capacity

An eye must reconstruct its spatial environment from an array of intensity measurements, each measurement provided by an individual ommatidium. It is convenient to view this spatial quantization as a two-dimensional mosaic or checkerboard, i.e., a picture constructed from many smaller elements. Thus, the number of ommatidia, per field of view, sets the capacity of the eye for fine detail.

The fine detail of a picture is lost if there is inadequate contrast between the various elements. Accordingly, the capacity of the eye for contrast sensitivity is determined by the number of *different* intensity levels that can be discriminated by an array of ommatidia. At first, it might be thought that an infinite number of different intensity levels can be distinguished; however, photon noise sets a lower limit to the number that are reliable. The more photons captured by the ommatidia, the greater the number of intensity levels and thus the greater the contrast sensitivity of the animal. In other words, both space and intensity are quantized by the eye.

Now it is clear that for a spheric eye, as the number of ommatidia per field of view increases, the potential of the eye for resolving fine detail also increases, but there must be fewer photons available for each of the ommatidia and hence a smaller number of recognizable intensity levels. Because of this unavoidable competition between the capacity of the eye for fine detail on the one hand and the capacity for contrast sensitivity on the other, what is the most appropriate number of ommatidia per field of view? The answer clearly depends on the number of available photons, but some measure of acuity performance is required. A natural metric is the number of *different* pictures that can be reconstructed by the mosaic of ommatidia, i.e., by the many elements that make up each picture. Assuming that there are n_p ommatidia per field of view, each one with *one* of n_i possible intensity levels, the *maximum* number of

ors is
cy so

B.36)

pictures that can be reconstructed by the ommatidia is $n_i^{(np)}$. Now it follows from the classic arguments of information theory (GOLDMAN, 1953; PIERCE, 1961) that the logarithm of the *maximum* number of *different* pictures that can be reconstructed, per field of view, by the ommatidia is the *spatial information capacity of the eye*, denoted here as H .

$$H = \ln n_i^{(np)} = n_p \ln n_i \quad (B.39)$$

Spatial Information Capacity = (No. of Ommatidia per Field of View) \otimes ln (No. of Different Intensity Levels),

where ln is to the base e. By using the logarithm of the number of pictures, we preserve the intuitive notion that doubling the number of ommatidia per field of view n_p doubles the spatial information capacity H of an eye. Having established the essential concept, we next relate n_p and n_i to the physical parameters of the compound eye. The number of ommatidia per square radian of object space n_p is proportional to $(\Delta\phi)^{-2}$ which in turn is proportional to v_s^2 . The number of intensity levels n_i that can be reliably distinguished by the ommatidia is limited by noise, ultimately due to the quantum nature of light, i.e., photon noise, and by imperfect optics; ultimately due to the wave nature of light, i.e., by diffraction.

Because of the random nature of photon absorption, a uniform light source (infinite in extent) appears nonuniform to an array of ommatidia and σ_n is the standard deviation in photon counts across an infinite array of ommatidia. Because of this σ_n degree of uncertainty in the interpretation of a photon count, there is only a finite number of intensity levels that can be distinguished with certainty by the ommatidia.

We suppose here that the intensity levels need be separated by $2\sigma_n$ intervals to be reliably discriminated, i.e., the standard deviation of one level just meets the standard deviation of the neighboring level. This is the usual reliability criterion for communication systems (e.g., CARLSON, 1975) and is analogous to assuming that the threshold SNR is unity (see SNYDER et al., 1977). Thus, n_i is found by determining the number of intervals of width $2\sigma_n$ that can fit into a given range of mean object intensity. This intuitive procedure gives the maximum number of intensity levels that can be reliably distinguished (CARLSON, 1975).

We are reminded that our expression for spatial information capacity H , given by Eq. (B.34), equals the *maximum* number of pictures that ommatidia can reconstruct. It is convenient to know what distribution of object intensities would produce this maximum. From information theory (e.g., PIERCE, 1961), we learn that a random scene fulfills the requirement, i.e., a scene containing objects of random contrast and random size (or identical size at random distances from the eye). Such a scene is the epitome of the unexpected since every spatial frequency has equal importance. The spatial information capacity H of an eye is, therefore, equivalent to the amount of information that it can extract from a random scene. Accordingly, we determine the number of possible contrast levels that exist when the object intensity is random.

In the absence of noise, the standard deviation in photon counts, due to the random scene is σ_s . In the presence of noise, twice the standard deviation in photon counts is given by $2(\sigma_{sig}^2 + \sigma_{noise}^2)^{1/2}$, remembering that variances and not standard deviations must be summed (GOLDMAN, 1953). Dividing this expression by $2\sigma_n$ gives the number n_i of possible intensity levels

$$n_i = \{1 + \sigma_s^2 / \sigma_n^2\}^{1/2}. \quad (B.40)$$

From our discussion, it is clear that Eq. (B.38) has the form of Eq. (B.39) (with an effective σ_s/σ_n) so that the asymptotic form for H can be associated with the picture-making capacity of the ommatidia.

2. Optimum Eye Parameters

We now determine those eye parameters that maximize the information capacity of the eye. From Eq. (B.38), H is maximized when $\Delta\varrho_r = 1.06\Delta\phi$ so that Eq. (B.38) becomes

$$H = (v_s^2/4) \ln \{1 + 0.26 k \hat{I}(CD)^2 M_1(v_s)\}^{1/2}. \quad (B.41)$$

Recalling that v_s is proportional to $\Delta\phi^{-1}$ and that $M_1(v_s)$ depends only on the eye parameter $D\Delta\phi$, we see that for a given facet diameter H is maximized when the eye samples at the diffraction limit $p = D\Delta\phi = \lambda/\sqrt{3}$ or equivalently when $v_s = v_{co}$. Furthermore, there is no loss by oversampling, i.e., v_s can exceed v_{co} without lowering H . In other words, if the eye can be flat in some small region, then according to information theory, it pays to have $\Delta\phi$ at the diffraction limit.

Now, if we consider the optimum eye parameter p for an eye of fixed radius R , then an entirely different result emerges. In this case $D = R\Delta\phi$ so that image quality and photon capture must be sacrificed by decreasing $\Delta\phi$. Consequently, there exists a trade-off between fine detail and contrast for which information theory via Eq. (B.41) gives an optimum p . The diffraction-limited eye is the optimum design only when the luminance \hat{I} is sufficient. From Eq. (B.41) this luminance is determined by the equation

$$\ln \{0.26k\hat{I}RC^2p e^{-2.67(\lambda/p)^2}\} = 1 \quad (\text{B.42})$$

with $p = \lambda/\sqrt{3}$. Thus, at $\lambda = 500$ nm, $\log(C^2R\hat{I}) \approx 5$ with R in units μm and \hat{I} in the units of Table 2. The greater the eye radius R , the smaller the luminance necessary for the animal to utilize its diffraction-limited optics. For example, with $R = 10^3 \mu\text{m}$, $\log C^2\hat{I} = 2$, which from Fig. 12 is seen to require moderate inferior lighting if a diffraction-limited eye is to resolve a grating of 50% contrast.

Summary. If we design an eye to maximize its information capacity, then $\Delta\varrho_r \approx \Delta\phi$ and, for a given facet diameter, the $\Delta\phi$ should be at the diffraction limit $\Delta\phi = \lambda/\sqrt{3}D$ provided the eye can be locally flat. If on the other hand, the eye is spheric and limited to radius R , then a minimum luminance is required for the diffraction limit to be the design that maximizes information capacity. The greater the head size, the smaller the required luminance. Or stated differently, larger eyes can make more efficient use of their optics.

These conclusions differ from those of Section C.III.6, where we determined eye design by finding the minimum parameter p necessary for adequate contrast sensitivity across the photoreceptor array at the ommatidial sampling frequency $v = v_s = 1/\sqrt{3}\Delta\phi$. The results of Section C.III.6 maximize the SNR across the rhabdoms. In contrast, the results of information theory are in general independent on the SNR at the photoreceptor level because it is implicitly assumed that weighted averaging can be performed neurally to achieve the high SNR of Eq. (B.37) at some higher level. The equivalent expression for signal to noise power at the photoreceptor level is proportional to $\bar{N}M^2(v)$. In other words, information theory assumes the theoretically best neural processing possible and therefore the amount of light captured per ommatidium is deemphasized.

Eyes that can be locally flat do not in general have their ommatidial angles at the diffraction limit, just as in the vertebrate lens eye cones are not in general set by the diffraction limit. Consequently, the prediction of information theory is not confirmed in either case, while that of Section III seems rather broadly applicable.

The results of the original presentation on information theory by SNYDER et al. (1977a) and SNYDER et al. (1977b) differ from those presented here due to an error in their expression for the ratio of the signal to noise power spectrum. The correct expression is presented in Eq. (B.38) which also applies to the vertebrate eye when $\Delta\varrho_r$ is set equal to $\Delta\phi$.

VII. Comparison of the Compound Eye with the Vertebrate Lens or "Camera Eye"

We are now in a position to consider differences between the compound and camera eye. This is presented by way of a brief review of the vertebrate eye.

1. Cutoff Frequency of Optics (Theoretic Limit to Resolving Power)

For all practical purposes, the *highest* spatial frequency passed by the vertebrate optics v_{co} is given by diffraction theory

$$v_{co} = D/\lambda \quad (B.43)$$

in cycles per radian, where D is the average entrance or apparent pupil diameter in bright light (e.g., about 2.3 mm in man; CRAWFORD, 1936) and λ the wavelength at peak photopic sensitivity (about 555 nm in man; LEGRAND, 1968, p. 84). Thus, at $\lambda = 555$ nm, $v_{co} \approx 10\pi D$ cycles per degree, where D is in mm, so that $v_{co} \approx 72$ cpd in man.

While it is true that Eq. (B.34) also applies in dimmer light when D is larger and hence so is v_{co} , nevertheless because of aberrations, the modulation transfer function of the optics is extremely small at frequencies significantly less than v_{co} (CAMPBELL and GUBISCH, 1966). Consequently, due to the noise of any measuring device, the highest observable spatial frequency passed by the optics rarely exceeds that predicted by Eq. (B.1) with D in bright light.

Because the theoretic limit to resolving power is given by v_{co} , the ratio of a single facet diameter of a compound eye to the pupil diameter of a vertebrate in bright light gives the relative potential resolving power of the two animals. For example, the smallest humming birds have a resolving power more than ten times greater than the largest dragonflies. The larger an eye, the greater its diurnal pupil diameter D , and hence the greater its capacity for high resolving power. However, the realization of this capacity demands a sufficient number of photoreceptors per visual angle as we discuss next.

2. Anatomic Resolving Power (Photoreceptor Sampling)

The cutoff frequency v_{co} sets the limit to resolving power as imposed by pupil diffraction. However, the highest spatial frequency that can be faithfully reconstructed by the retina, or anatomic sampling frequency v_s , is limited by the angular center-to-center spacing of photoreceptor $\Delta\phi$ (SNYDER and MILLER, 1977).

$$v_s = 1/\Delta\phi \sqrt{3} \quad (B.44)$$

for hexagonal packing. Only when $v_s = v_{co}$ can the photoreceptor reconstruct frequencies up to v_{co} , requiring a *maximum* angular photoreceptor spacing of $\Delta\phi = 1/v_{co} \sqrt{3}$ necessary for $v_s = v_{co}$.

Note that it is possible to oversample in a vertebrate retina of fixed size by reducing the diameter of photoreceptors. However, in a compound eye of fixed size and shape, reducing $D\Delta\phi$ also reduces D so that the resolving power is lowered.

The logic for selecting $D\Delta\phi$ is the same as for selecting the optimum compound eye parameter $p=D\Delta\phi$ discussed in Section B.III.4. In particular, $D\Delta\phi$ is the minimum value for sufficient contrast sensitivity at the sampling frequency $v=v_s$ at the highest luminance of the animal's environment. Thus, those animals that are active in the brightest light and are comparatively stationary relative to their prey are expected to have the smallest $D\Delta\phi$ values. These animals can take the greatest advantage of their potential optics. Curiously, desert hawks, eagles, and probably man take significantly less advantage of their potential optics ($D\Delta\phi \approx 0.5 \mu\text{m}$) (see MILLER, this volume) than wasps and dragonflies ($D\Delta\phi \approx 0.31 \mu\text{m}$). One possible explanation for this pronounced undersampling is that the modulation transfer function for vertebrate optics is significantly smaller near $v=v_{eo}$ than for the compound eye. In other words, the compound eye, with a pupil diameter 10^{-2} that of birds, is more nearly diffraction limited. Furthermore, because of their small diameter, the cones in the eagle may be inefficient light absorbers and, because of their close packing, not optically well isolated. Both of these effects cause reduced contrast sensitivity so that it would be advantageous for $D\Delta\phi$ in the eagle to be comparatively large for adequate contrast sensitivity at the anatomic sampling frequency $v=v_s$.

As in the compound eye (Sec. B.III.5), because of aliasing, an animal with $v_s < v_{eo}$ can detect spatial frequencies within the interval $v_s < v < v_{eo}$, but these appear to the animal as frequencies lower than $v=v_s$. We expect that aliasing is difficult to observe under natural environmental conditions; otherwise, the animal would gain more information with a smaller $D\Delta\phi$, i.e., a larger v_s .

3. Contrast Sensitivity

The contrast sensitivity of the photoreceptor array is given by Eq. (B.27). From this expression, we can determine the angular photoreceptor diameter $\Delta\varrho_r$ and eye parameter $D\Delta\phi$ that maximize the contrast sensitivity at $v=v_s$ in the highest luminance of the animal's natural environment. The photoreceptor inner segments should touch $\Delta\varrho_r = \Delta\phi$ for maximum contrast sensitivity (SNYDER and MILLER, 1977). Thus, the photon capture of a photoreceptor is proportional to $(D\Delta\phi)^2$ and is consequently independent of eye size and absolute resolving power when comparing eyes with the same $D\Delta\phi$.

4. Limitation to Minimum Eye Length

One would imagine that it is advantageous to have the shortest eye possible. Weighing against this are decided disadvantages. The shorter the eye, the greater the possibility for chromatic aberration, the smaller the depth of focus and the more narrow the photoreceptors necessary for holding $\Delta\phi$ constant. A short depth of focus is correctable by a rapid accommodation response while chromatic aberration is counteracted by having monochromatic vision in the retina region for highest resolving power. Consequently, the minimum photoreceptor diameter limits the axial length of the eye. The smaller the photoreceptor diameter, the more poorly it absorbs light and the more it becomes optically coupled to its neighbors. This effect is intolerable for a photoreceptor center-to-center spacing d_{cc} of less than $1 \mu\text{m}$.

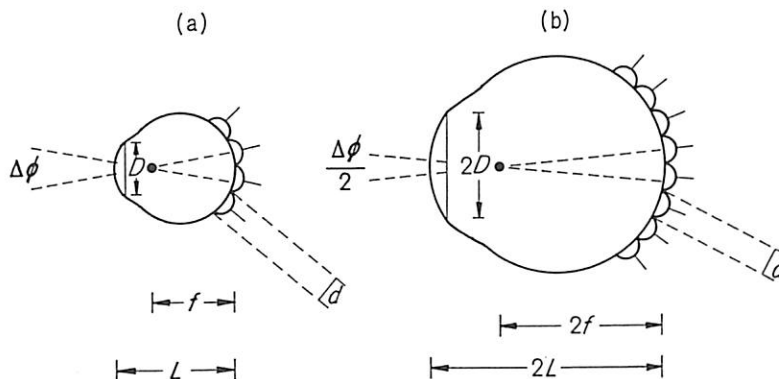


Fig. 18a and b. Doubling resolving power by isomorphic scaling. The resolving power of eye (a) is half that of (b), but the center-to-center cone spacing is the same in both cases

because the contrast sensitivity at $v = v_s$ is negligible. Since $\Delta\phi = d_{cc}/f$, where f is the focal length or more accurately the posterior nodal distance (about 16.7 mm in man), $f = v_s d_{cc} \sqrt{3}$ and the minimum focal length possible must certainly exceed $f = v_s \sqrt{3} \mu\text{m}$.

5. Change in Resolving Power by Scaling

It is reasonable to suppose that the axial length of an eye is as small as possible or equivalent that the density of photoreceptors is at the maximum tolerable following the logic of the above arguments. Consequently, within any one strategy, say birds of prey, resolving power is determined by head size. In other words, both pupil diameter D and focal length are linearly proportional to the axial length of the eye. In such cases, the resolving power of the eye is doubled by doubling the eye size. This isomorphic scaling procedure is shown in Fig. 18. Note that the F number f/D , the photon capture per receptor $(D\Delta\phi)^2$, and d_{cc} are unchanged by isomorphic scaling, but four times as many photoreceptors are necessary. However, allowing for appropriate neural processing (Section 1.5) larger eyes have potentially greater contrast sensitivity because they capture more photons.

The strategy of Fig. 16 applies to birds of prey (see MILLER, this volume) and is analogous to that discussed for the compound eye in Section B.III.3. In these birds, $f \approx 0.66L$ while $D \approx 0.25L$, where L is the axial eye length. In the centermost region of the deep fovea, f may even exceed L due to the negative lens action of the foveal pit (SNYDER and MILLER, 1978).

6. Dark Adaptation Mechanisms in the Fovea

While it is theoretically possible for each rhabdom to open its acceptance angle to 180° and capture all light entering the ommatidium, each cone is limited to an acceptance angle of $\Delta\phi$. Cones like rhabdoms can be pooled neurally to form larger receptive units as intensity diminishes. Thus, in theory, the gain in contrast sensitivity by neural pooling is the same for vertebrate and compound eyes. However, the highest resolvable frequency at any given luminance is $v_s p/p_n(I)$ for the vertebrate instead of $v_s \{p/p_n(I)\}^{1/2}$ as for the compound eye, where $p = D\Delta\phi$, $p_n = D_n\Delta\phi_n$ for compound eye, $D\Delta\phi_n$ for vertebrate eye with the subscript indicating

neural quantities. *In other words, comparing a compound eye with a vertebrate eye of the same p value, the vertebrate eye suffers a greater loss in its high frequency resolving power for a given decrease in luminance*, i.e., the vertebrate eye must sacrifice more by neural pooling than the compound eye. This is a consequence of an adjustable rhabdom acceptance angle ($0 < \Delta\varrho < 180^\circ$).

7. Comparative Advantages of Compound and Camera Eye

In this section, we compare the lens and compound eyes with the same resolving power. *For a given resolving power*, the pupil diameter equals the facet diameter while the focal length of the ommatidium and vertebrate eye must be approximately equal. Thus, the depth of both eyes is approximately the same, assuming photoreceptors of equal length. However, the compound eye covers a significantly greater surface area and consequently occupies a significantly greater volume. The increase in surface area of the eye has the potential advantage of a greater field of view in addition to a higher photon capture for the eye. This additional photon capture, together with the advantage of a changeable acceptance angle and the possibility of optical superposition confer an enormous advantage in contrast sensitivity on the compound eye, particularly at spatial frequencies lower than the anatomic sampling frequency $v_s = 1/\sqrt{3} \Delta\phi$. However, if the animal can cover its head with ommatidia, it could equally cover its head with many lens eyes or several with large pupil diameters, each with the same axial length as an ommatidium. Such a visual system lacks the advantages of a variable acceptance angle at the photoreceptor level, and so at best remains slightly inferior in contrast sensitivity to the theoretic best compound eye design. *Thus, in theory, an animal with a compound eye is better in contrast sensitivity than one with many vertebrate lens eyes each having the same axial length as an ommatidium.* However, the lens eye has a greater number of receptors per 180° of visual angle and thus the advantage of specialized regions of the retina. If man were to have a compound eye with as many facets as cones, he would require an enormous head (KIRSCHFELD, 1976). Many compound eyes only occupy a small region of the head, e.g., mantids, which could be better replaced by two lens eyes of equal size. The smallest hummingbirds have a head size equal to the head of large dragonflies, but their resolving power is ten times greater. Such observations make one wonder if the option for camera eyes was available to these animals. Finally, some invertebrates have lens eyes, e.g., spiders.

C. Absolute Sensitivity

In this section, we are concerned with adaptations that maximize the capture and absorption of light. Because of the inherent particle nature of electromagnetic radiation, light arrives at the eye in irregular bursts of energy or photons. Consequently, all visual information must be extracted from photons, so that a rhabdom is ideally a photon counter.

We have already emphasized (Sec. B.I.4) that the random arrival of photons introduces a fundamental uncertainty in the interpretation of an array of photon counts and that the greater the number of absorbed photons the better the reliability. It is also true that the more sophisticated the animal's visual system, the greater the need for efficient photon capture. For example, the finer the animal measures space and time, the more accurately it can determine position and movement. However, an accurate assessment of motion precludes protracted integration in time, just as a precise determination of position precludes extended integrations in space (BARLOW, 1964). Consequently, the animal is forced to optimize its often meagre allocation of photons. We can now begin to appreciate that animals are starved for light, no matter how bright the environmental intensity, and can anticipate many adaptations for maximizing photon capture. Our intent in this section is to provide the theoretic basis for evaluating the absolute sensitivity of an ommatidium. In Section B we considered the effects of optical and neural superposition on absolute sensitivity, so they are not mentioned again here.

I. Light-Gathering Capacity of an Ommatidium

In this section, we consider the capacity of an ommatidium to collect light from a uniform source of angular diameter $\Delta\psi$. The number N of photons absorbed by a rhabdom in the integration time of the eye is easily derived (Appendix B) leading to

$$N = \bar{N} \{1 - e^{-0.69(\Delta\psi/\Delta\varrho)^2}\}, \quad (C.1)$$

where \bar{N} is the number of photons when the source is infinite in extent (Sec. B.I.4) and $\Delta\varrho$ is the width of the acceptance angle at 50% sensitivity

$$\bar{N} = \hat{I}(D\Delta\varrho_r)^2, \quad (C.2)$$

$$(\Delta\varrho)^2 = (\lambda/D)^2 + (\Delta\varrho_r)^2. \quad (C.3)$$

All symbols are defined in Table 1 and described in Section B. We find that, to an accuracy of 90%, the source appears infinite in extent to a photoreceptor when its angular diameter has a value $\Delta\psi > 1.8 \Delta\varrho$, i.e., $N \approx \bar{N}$, and appears like a distant point source when $\Delta\psi < 0.4 \Delta\varrho$, i.e., $N \approx 0.69 \bar{N}(\Delta\psi/\Delta\varrho)^2$.

RODIECK (1973) and KIRSCHFELD (1974) have noted that the pupil diameter D of a human is of the order 10^5 greater than most ommatidia but that the F numbers (f/D) of ommatidia can be equal or greater than the human eye. They concluded that compound eyes do worse than human eyes for detecting distant point sources but as good or better for detecting extended sources. To see this, we neglect any additional light gathering of the crystalline cone, so that $\Delta\varrho_r = d_{Rh}/f$, where d_{Rh} is the diameter of the rhabdom. Thus, N for extended sources is proportional to $(d_{Rh}/F)^2$.

For nonextended sources (Appendix B), i.e., those with $\Delta\psi < 0.4 \Delta\varrho$, the light-gathering capacity is proportional to $(d_{Rh}/F\Delta\varrho)^2$. Two extreme cases now emerge.

When the acceptance angle is limited by diffraction, $\Delta\varrho \approx \lambda/D$, the light-gathering capacity of the ommatidia is proportional to $(d_{Rh}/F)^2$. Whereas, when $\Delta\varrho \approx d_{Rh}/f$, as it is for *Musca* rhabdomeres 1–6, then the light gathering is proportional to D^2 . Allowing for appropriate neural processing, however the greater the summed photon capture of an eye, the greater its potential for detecting both point and extended source. Consequently larger eyes are theoretically superior.

II. Influence of Length, Diameter, and Shape of Rhabdoms on Absorption

The intensity parameter \hat{I} in Eq. (C.2) is proportional to the efficiency ε of photons captured by the rhabdom (SNYDER and PASK, 1973) (see Eq. B.16)

$$\varepsilon = \varepsilon_0 (1 - e^{-\eta\alpha l}), \quad (C.4)$$

where ε_0 is the fraction of photons that have not been diverted by scattering or absorption prior to the rhabdom, α is the length of the rhabdom, l is the absorption coefficient (specific optical density of the visual pigment), and η the fraction of the light that travels inside the rhabdom (SNYDER, 1975 and Sec. G).

If we ignore waveguide effects, $\eta=1$ and ε is independent of the diameter or shape of the rhabdom. [The diameter d_{Rh} of the rhabdom appears directly in Eq. (C.2)]. Thus, for economy of photopigment, the rhabdom could taper without loss in absorption. Note that absorption increases the longer the rhabdom or the more densely packed the membrane (larger α).

Waveguide effects become important when both $(l/d_{Rh}) \gg 1$ and the waveguide parameter V is less than 2, where (SNYDER, 1975)

$$V = \pi d_{Rh} (n_{Rh}^2 - n_s^2)^{1/2} / \lambda. \quad (C.5)$$

n_{Rh} and n_s are the refractive indexes of the rhabdom and its surround, respectively. In Fig. 19, we present η for both a uniform and atapered rhabdom. KIRSCHFELD and SNYDER (1975) have shown that rhabdomeres 7 and 8 of *Musca* have $1 < V < 2$ for $600 \text{ nm} < \lambda < 300 \text{ nm}$. Rhabdomeres 1–6 have twice these V values but, unlike 7 and 8, they are tapered with $d_{Rh}/d_0 = 2$.

III. Influence of Rhabdomeric Dichroism on Absorption

Rhabdomeric (microvilli) membrane is dichroic, i.e., its absorption depends on the direction of the electric vector \mathbf{E} of linearly polarized light (MOODY, 1964; BORN and WOLF, 1970). Measurements of dichroism indicate the degree to which the absorbing dipoles (chromophore group) are aligned within the visual membrane. In Section F this subject is discussed more fully. Our purpose here is to modify Eq. (C.4) for rhabdomeric photoreceptors, i.e., to provide a *macroscopic* description of the effect of dipole alignment within the visual membrane.

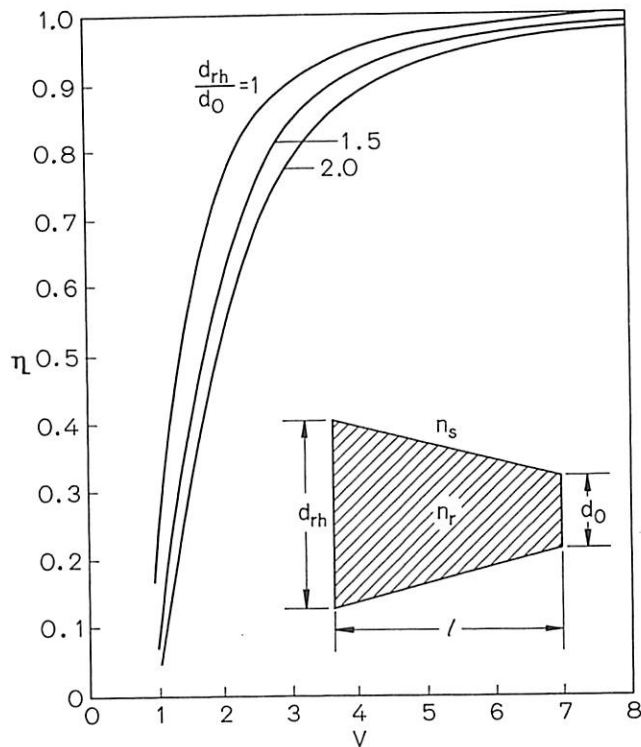


Fig. 19. The fraction η of light power within a photoreceptor of length l

At first sight, it would appear that the only importance of dichroism is to provide a photoreceptor with the potential for polarization sensitivity. This is misleading. Our analysis of dipole alignment within microvilli membrane in Section IV reveals that dichroism is in fact an important determinate of the *absolute* sensitivity of a photoreceptor to *unpolarized light*. However, we must first present the macroscopic description before we can appreciate this last fact.

The dichroic ratio δ of an infinitesimal section of microvilli membrane is defined as

$$\delta = \alpha^x / \alpha^y \quad (C.6)$$

where α^x is the absorption coefficient for E parallel to the microvilli membrane and α is the absorption coefficient for E perpendicular to the microvilli membrane.

1. Open Rhabdoms

Taking account of dichroism for the rhabdomeres of Fig. 20, Eq. (C.4) becomes (SNYDER, 1975)

$$\varepsilon = \varepsilon_0 \left\{ 1 - \frac{(e^{-\eta \alpha^x l} + e^{-\eta \alpha^y l})}{2} \right\} \quad (C.7)^1$$

for *unpolarized light*.

¹ Transcription errors appear in Eqs. (20)–(22) of SNYDER (1975) which are corrected by replacing $\eta/2$ by η and noting a necessary sign change within the brackets of Eq. (C.21) to conform with the result given here.

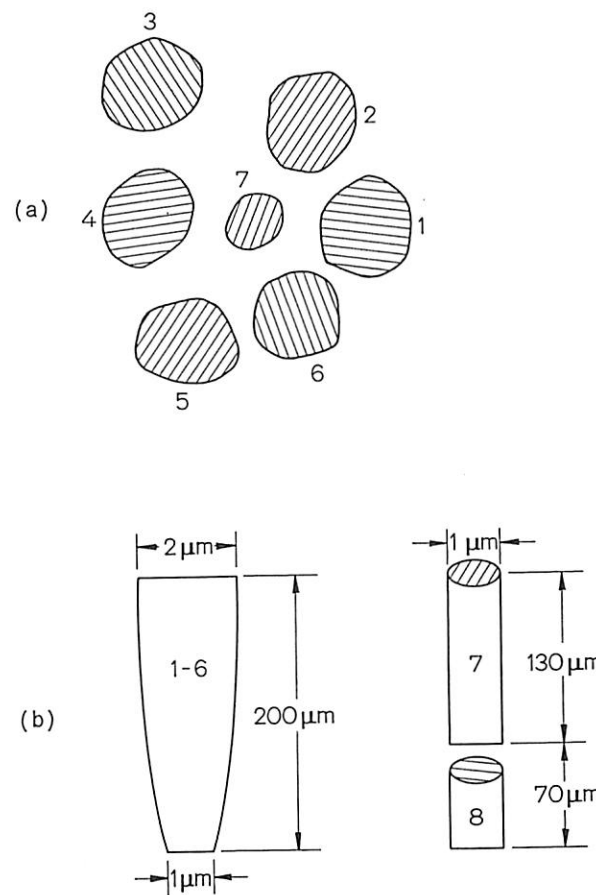


Fig. 20a and b. Rhabdomeres of fly *Musca* eye. (a) is a schema of a cross-section in the distal end. The parallel dark lines represent the microvilli. (b) represents a schema of the rhabdomeres in a longitudinal section. Rhabdomeres 1-6 are tapered with the largest diameter at the distal end. The drawings are from the electron micrographs of MELAMED and TRUJILLO-CENÓZ (1968) and BOSCHEK (1972)

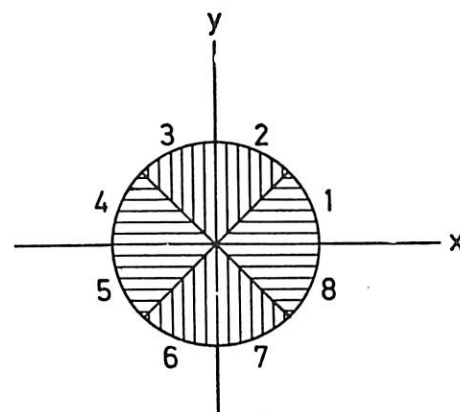


Fig. 21. Hypothetic fused rhabdom, with eight rhabdomeres each with equal cross-sectional area. The dark lines represent the microvilli, which are either parallel or perpendicular to the x and y axes

2. Fused Rhabdoms

The most common photoreceptors of those animals with compound eyes have all rhabdomeres fused into a cylindric light guide called a fused rhabdom (Fig. 21). The participating rhabdomeres are optically (and possibly electrically) coupled to each other and share the total light accepted by the rhabdom. A full treatment of the fused rhabdom is presented by SNYDER (1973) and SNYDER et al. (1973) so that we need only borrow some of their results for the remaining discussion.

For simplicity, we limit our discussion to rhabdoms with the special property that the summed light adsorbed by all rhabdomeres is independent of the direction of \mathbf{E} (SNYDER, 1973). This is exactly fulfilled by crustacean rhabdoms but is approximated by the rhabdoms of many animals (see also Appendix G). Then Eq. (C.4), for rhabdomere i , becomes

$$\varepsilon_i = \varepsilon_0 \left(\frac{A_i}{A} \right) \left(\frac{\alpha_i^x + \alpha_i^y}{2\alpha} \right) (1 - e^{-\eta\alpha l}) \quad (\text{C.8a})$$

for *unpolarized light*, where α_i is the absorption coefficient and A_i the area in cross-section of rhabdomere i

$$\alpha = (\alpha_1^x A_1 + \alpha_2^x A_2 \dots \alpha_8^x A_8)/A \quad (\text{C.8b})$$

$$= (\alpha_1^y A_1 + \alpha_2^y A_2 \dots \alpha_8^y A_8)/A, \quad (\text{C.8c})$$

$$A = A_1 + A_2 + A_3 \dots A_8. \quad (\text{C.8d})$$

The superscripts x and y are for \mathbf{E} parallel and perpendicular to the microvilli of rhabdomere i , respectively. The general situation is discussed by SNYDER and SAMMUT (1973).

If we want the number of photons absorbed by the entire rhabdom, i.e., the summed absorption of all rhabdomeres, Eq. (C.4) becomes

$$\varepsilon = \varepsilon_0 (1 - e^{-\eta\alpha l}), \quad (\text{C.9})$$

where α is given by Eq. (C.8b). For the special case of a symmetric rhabdom, with eight rhabdomeres, all with equal area and perpendicular microvilli $\alpha = (\alpha^x + \alpha^y)/2$ with α^x and α^y defined as in Eq. (C.6).

IV. Dependence of Photon Capture on Chromophore Alignment

The light-absorbing molecule, the chromophore group retinal, is a dipole and absorbs maximally when \mathbf{E} is parallel to the π -electron cloud of its conjugated double bonds. Retinal is embedded in the protein molecule (opsin) such that the dipole is parallel to the membrane surface (LIEBMAN, 1975; TÄUBER, 1975).

Now it is well-known from dichroic measurements that the dipoles are arranged differently in the photoreceptor membrane of various animals. For example, the dipoles are arranged at random within the plane of the vertebrate outer segment disc membrane (SCHMIDT, 1938; LIEBMAN, 1975). They are also arranged at random within the plane of the microvillus membrane of fly rhabdomeres 1–6 (KIRSCHFELD and SNYDER, 1975). In sharp contrast, the dipoles appear to be highly aligned along the axis of the microvillus membrane in the crustacean rhabdom (SNYDER, 1973; MOTE, 1974; GOLDSMITH, 1975) and relatively highly aligned in the central rhabdome of the fly (KIRSCHFELD and FRANCESCHINI, 1976). We are compelled to search for a functional basis to explain the diversity in dipole orientation. Why is the visual membrane of one animal more dichroic than that of another? SNYDER and LAUGHLIN (1975) have provided a possible answer to this question. Only a précis of their argument is given here, since an intuitive interpretation of their mathematics is also available (LAUGHLIN et al., 1975).

As is usual in physics, it is advantageous to simplify the problem, preserving only features that contain the essential physics. SNYDER and LAUGHLIN (1976) accomplished this by approximating the cylindric microvillus with a square microvillus. The results are nearly identical to those obtained by the relatively complicated mathematics necessary for an exact analysis of a microvillus (ISRAELACHVILI et al., 1976). However, the square microvillus model provides the intuitive insight helpful for solving the problem (see also Sec. VI).

For simplicity, we neglect the form dichroism and assume perfect dipoles all lying parallel to the microvillus membrane. Such dipoles have no absorption when \mathbf{E} is perpendicular to their axis. Our conclusions do not require these assumptions, but the necessary mathematics and intuition is simplified. It is rather obvious from Fig. 22 that dipoles should be oriented at random in the plane of the vertebrate disc membrane to have maximal absorption to unpolarized light. In rhabdomeres also, absorption depends on the degree to which the dipoles are aligned with the microvillus axis. Taking this into account, the absorption coefficients for a fly rhabdomere have the form (SNYDER and LAUGHLIN, 1975)

$$\alpha^x = 4\alpha_{||} \cos^2 \phi, \quad (C.10a)$$

$$\alpha^y = 2\alpha_{||} \sin^2 \phi, \quad (C.10b)$$

where ϕ is the inclination of the dipole axis with the microvillus axis and $\alpha_{||}$ is the absorption of a dipole when \mathbf{E} is parallel to its axis. Substituting this result into Eq. (C.7) we can calculate the alignment angle ϕ necessary for maximum absorption for any given length absorption ratio $\alpha_{||}l$. The results are shown in Fig. 22.

It is clear that long and short fly rhabdomeres should have their dipoles oriented differently for optimum absorption of unpolarized light. Long rhabdomeres like 1–6 should have $\phi \cong 45^\circ$ which is mathematically equivalent to a random orientation in the membrane. Short photoreceptors like rhabdomere 7 and particularly rhabdomere 8 should have dipoles comparatively more aligned. The membrane dichroic ratio Δ associated with these values of ϕ is also determined by SNYDER and LAUGHLIN (1975). Rhabdomeres 1–6 should have a Δ slightly less than 2:1 whereas rhabdomere 8 could be larger than 8:2 (Fig. 7 of SNYDER and LAUGHLIN, 1975).

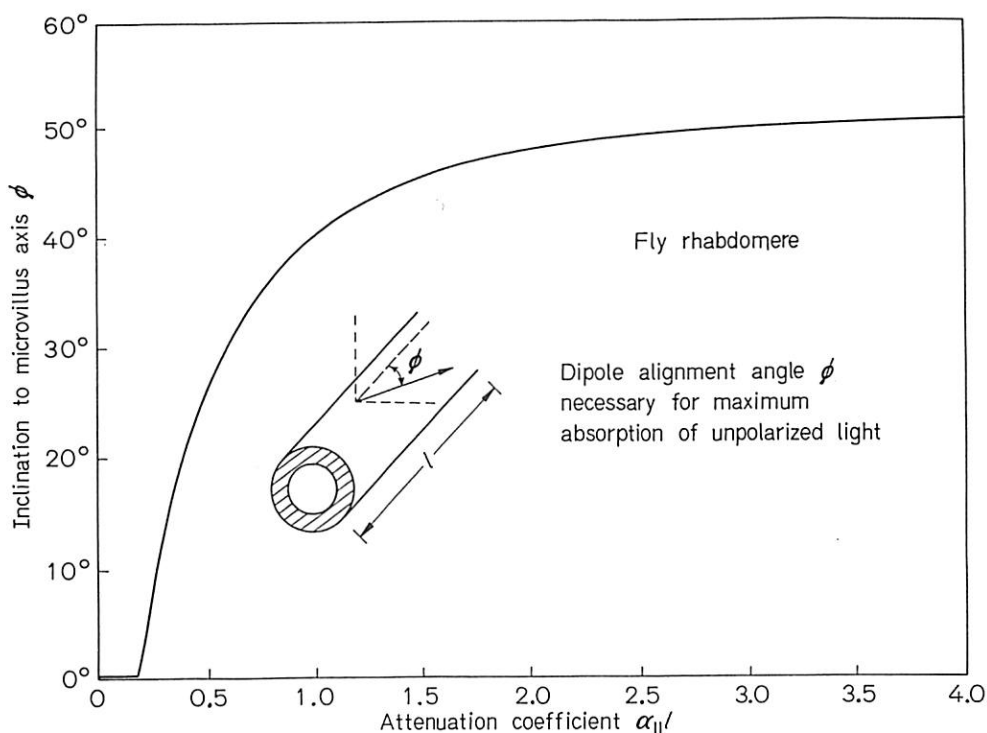


Fig. 22. The dipole alignment angle ϕ necessary for maximum absorption of unpolarized light. $\alpha_{||}$ is the absorption coefficient for E parallel to the axis of the microvilli of Fig. 20

The physical principle required to understand Fig. 22 is that, in a long receptor, dipoles at the top act as filters in front of those at the bottom. If all dipoles are perpendicular to the direction of incident light and parallel to each other when unpolarized light is introduced, only the component with E parallel to the microvilli is absorbed. The perpendicular component passes through unabsoed (perfect dipoles). The dipoles at the top absorb most of the light while the dipoles at the bottom are ineffective because they are illuminated by light with E perpendicular to the dipoles. Thus, if the rhabdomere is long enough, it is advantageous to randomize dipole orientation.

To determine the dipole alignment necessary for optimum photon capture in fused rhabdoms, we substitute Eq. (C.10) into Eq. (C.9), where $\alpha = \alpha^x + \alpha^y$. When α is maximum, photon capture is maximum. This occurs when $\phi = 0^\circ$ independent of the length of the fused rhabdom. Thus, in fused rhabdoms of arbitrary length, like in crustacea, the dipoles need be highly aligned for optimum photon absorption when the light is unpolarized. The dichroic ratio δ was shown by SNYDER and LAUGHLIN (1975) to be theoretically as high as 20 which is not unrealistically large.

In conclusion, the above theory and its consistency with dichroic measurements provide strong evidence for the view that *dipoles are oriented in the plane of visual membrane to provide photoreceptors with the maximum absorption to unpolarized light*. This is consistent with the view that a photoreceptor's primary objective is to maximize the effectiveness of every available rhodopsin molecule and that membrane dichroism is only a secondary consequence of this primary objective.

The physical basis for the high dichroic ratio of only certain rhabdomeric membranes is still open, but recent studies by KIRSCHFELD and FRANCESCHINI (1976) suggest that the presence of a photostable pigment, possibly a carotene, may change the fluidity of the microvillus membrane in some of the No. 7 rhabdomeres of *Musca* and hence affect the alignment of dipoles.

D. Application of Theory to the Fly *Musca*: A Neural Superposition Eye

Having considered the physical limitations to resolving power in addition to the absolute sensitivity of eyes, we now apply our concepts to a real compound eye. This requires *precise* knowledge of $\Delta\phi$, D , and $\Delta\varrho_r$ in the various regions of the eye. Of all compound eyes, only the neural superposition variety has been investigated sufficiently for an in-depth theoretic interpretation. Accordingly, much of our knowledge is derived from the brilliant studies of KIRSCHFELD (1967), KIRSCHFELD and FRANCESCHINI (1968, 1969), FRANCESCHINI and KIRSCHFELD (1971a, b), FRANCESCHINI (1975), and STAVENGA (1975).

I. Basic Principles of Neural Superposition

Musca has an open rhabdom (Fig. 20), i.e., geometrically isolated rhabdomeres with separate fields of view (AUTRUM and WIEDEMANN, 1962; BOSCHEK, 1971). Only rhabdomeres 7 and 8 view the world centered along the axis of their ommatidium. Each of the other six rhabdomeres look in the direction of one of the neighboring ommatidia (KIRSCHFELD, 1967; FRANCESCHINI, 1975; STAVENGA, 1975). Consequently, the interommatidial angles $\Delta\phi$ equal the angular spacing of rhabdomeres, i.e., the center to center spacing d_{cc} between the neighboring rhabdomeres of Fig. 23 obeys the relation

$$\frac{d_{cc}}{f} = \frac{D}{R} = \Delta\phi, \quad (\text{D.1})$$

where f is the distance from the distal tips of the rhabdomeres to the posterior nodal point (KIRSCHFELD and FRANCESCHINI, 1968; STAVENGA, 1975). Although the values of f and $\Delta\phi$ depend on the region of the eye (the range of f and $\Delta\phi$ is given in Table 2), the quantity f/D or F number of the ommatidia is nearly the same in all regions of *Musca* studied by STAVENGA (1975) and BEERSMA et al. (1975)

$$F = f/D \cong 1.9, \quad (\text{D.2})$$

where D is the diameter of the entrance pupil.

Table 2. Anatomy and theory for *Musca*

D	= diameter of the entrance pupil which is approximately the facet diameter	$\Delta\varphi$ for retinula cells 1-6
f	= distance from the distal tips of the rhabdomeres to the posterior nodal point which is approximately the focal length of the lens	$\Delta\varphi \cong 0.9 \Delta\phi$ $4.6^\circ > \Delta\varphi > 2.3^\circ$
λ	= wavelength in vacuum	$\frac{\Delta\varphi_r}{\Delta\phi} = \frac{d_{Rh}}{d_{cc}} = 0.8$
$\Delta\varphi$	= width of retinula cell acceptance function at 50% sensitivity	$\Delta\varphi$ for retinula cells 7 and 8
$\Delta\varphi_r$	= angular diameter of rhabdomere (d_{Rh}/f)	$\Delta\varphi \cong \{0.59 \lambda^2 + 0.64\}^{1/2} \Delta\phi$ $2.6^\circ > \Delta\varphi > 1.3^\circ$; ($\lambda = 0.49 \mu\text{m}$) $2.4^\circ > \Delta\varphi > 1.2^\circ$; ($\lambda = 0.36 \mu\text{m}$)
<i>Rhabdomere diameter (distal end)</i>		<i>Angular diameter of airy disc $\Delta\varphi_A$</i>
$d_{Rh} \cong 2 \mu\text{m}$; (R1-6)	$\cong 1 \mu\text{m}$; (R7 and 8)	$4.3^\circ > \Delta\varphi_A > 2.2^\circ$; ($\lambda = 0.49 \mu\text{m}$) $3.2^\circ > \Delta\varphi_A > 1.6^\circ$; ($\lambda = 0.36 \mu\text{m}$)
<i>Center to center spacing of rhabdomeres</i>		<i>Eye parameter p</i>
$d_{cc} \cong 2.5 \mu\text{m}$		$p = D\Delta\phi = \frac{D^2}{R} = \frac{d_{cc}}{F}$ $\cong 1.3 \mu\text{m}$
F number = $f/D \cong 1.9$		
$16 \mu\text{m} < D < 32 \mu\text{m}$		
$30 \mu\text{m} < f < 61 \mu\text{m}$		
<i>Interommatidial angle</i>		
$\Delta\phi = d_{cc}/f$		
$4.8^\circ > \Delta\phi > 2.4^\circ$		
<i>Eye radius</i>		
$R = D/\Delta\phi$		
$189 \mu\text{m} < R < 781 \mu\text{m}$		

The values used in this table are taken from BOSCHEK (1971), FRANCESCHINI (1975), and STAVENGA (1975).

If $\Delta\phi$ depends on the region of the eye, so must the eye radius R . Since $D = R\Delta\phi$, from Eqs. (D.1) and (D.2), $R = f^2/Fd_{cc}$, i.e., R is a constant times f^2 . Assuming d_{cc} is constant in all regions of the eye, Table 2 shows that R changes by about a factor of 4 in *Musca*.

Depth of Focus

It is necessary for the rhabdomeres of *Musca* to function as light guides if they are to be optically isolated. This is because the depth of focus $\delta f \cong 2\lambda F^2 \cong 4 \mu\text{m}$ at $\lambda = 500 \text{ nm}$ is significantly less than the rhabdomere length. However, the focal depth of fly optics is sufficient to neglect the defocus caused by chromatic aberrations, which have been measured by MCINTIRE and KIRSCHFELD (1978) to be about $3.3 \mu\text{m}$ from $\lambda = 300 \text{ nm}$ to 580 nm .

1. Eye Parameter p

From these anatomic facts, we can determine that the eye parameter $p = D\Delta\phi$ given by Eq. (B.2) is nearly constant over the eye and that

$$p = D\Delta\phi = d_{cc}/F \cong 1.3 \mu\text{m} \quad (\text{D.3})$$

since $d_{cc} \cong 2.5 \mu\text{m}$ (e.g., BOSCHEK, 1971). Thus, the sampling frequency v_s of *Musca* is 5.2 times greater than that necessary to reconstruct the highest frequency $v_{co} = \lambda/D$,

passed by the lens pupil, assuming $\lambda=500 \text{ nm}$ and square facets or about 4.5 times greater for hexagonal facets (see Sec. B.I).

The theoretic results of Sections B.II and B.IV suggest that $p \cong 1.3 \mu\text{m}$ is optimum for an animal most active in the late afternoon or at dusk. However, when we account for the high angular motion of *Musca*, which conservatively is 180° turn per second (LAND and COLLETT, 1974), the reasoning of Section B.I.3 shows that this is equivalent to a reduction of about 3 log units in intensity. Thus, although *Musca* is active in daylight, its high angular velocity requires the same eye design as an animal in a darker environment.

II. Half Width Acceptance Angle $\Delta\varrho$

Since there is no additional light gathering due to a crystalline cone in *Musca*, the acceptance angle $\Delta\varrho_r$ is simply the angular diameter of the rhabdomeres,

$$\Delta\varrho_r = d_{Rh}/f, \quad (\text{D.4})$$

where d_{Rh} is the diameter of the rhabdomeres. Thus, the acceptance angle of the fly is taken directly from Eq. (B.7) or Fig. 2.4 for the diffraction-limited lens pupil. Using Eq. (D.1), we can express $\Delta\varrho_r$ given by Eq. (4.4) as $\Delta\varrho_r = d_{Rh} \Delta\phi / d_{cc}$.

We showed in Section B.II that the optimum $\Delta\varrho_r$ is $0.75 \Delta\phi$. Taking $d_{Rh} \cong 2 \mu\text{m}$ for rhabdomeres 1–6 (BOSCHEK, 1971), we find that $\Delta\varrho_r \cong 0.8 \Delta\phi$ in *Musca* which is very close to the theoretic prediction. For rhabdomeres 7 and 8, $\Delta\varrho_r \cong 0.4 \Delta\phi$, which is far from optimum.

From Eq. (B.7) we find that the half width acceptance angle $\Delta\varrho$ of *retinula cells* 1–6 is

$$\Delta\varrho = \{0.59 \lambda^2 + 0.64\}^{1/2} \Delta\phi, \quad (\text{D.5})$$

and is virtually insensitive to changes in λ , between 350–650 nm, having an average value of about $\Delta\varrho \cong 0.9 \Delta\phi$. Thus, $\Delta\varrho$ depends on the region of the eye, ranging between $4.6^\circ > \Delta\varrho > 2.3^\circ$ (Table 2). We note that HORRIDGE et al. (1976) found that $\Delta\varrho$ for cells 1–6 in *Calliphora* is independent of λ .

From Eq. (B.7) we find that the half width acceptance angle $\Delta\varrho$ of *retinula cells* 7 and 8 is

$$\Delta\varrho = \{0.59 \lambda^2 + 0.15\}^{1/2} \Delta\phi, \quad (\text{D.6})$$

which is also rather insensitive to changes in λ (Table 2).

Finally, we have shown in Appendix A that the presence of the pronounced waveguide effects in rhabdomeres 7 and 8 (KIRSCHFELD and SNYDER, 1976) does not significantly alter $\Delta\varrho$, but the shape of the angular sensitivity function is more Gaussian than in cells 1–6.

III. Absolute Sensitivity of Retinula Cells

In this section, we consider the absolute sensitivity of *Musca* retinula cells to extended and point sources. Before beginning, it is necessary to clarify the criterion to be a point or an extended source. It is shown in Appendix B that, as far as one ommatidium is concerned, an extended source is one with an angular diameter that exceeds $1.8 \Delta\varrho$, while a point source is one with an angular diameter less than $0.4 \Delta\varrho$. To make these numbers more meaningful, we calculate the separation between two *Musca* necessary for one to appear as an extended or point source to the other. The value of $\Delta\varrho$ depends on the region of the eye and is different for rhabdomeres 7 and 8 and 1–6 (Table 2). We take $\Delta\varrho = 3^\circ$ as a representative value and the length of *Musca* to be 1 cm. Thus, *to appear like extended sources to each other, two Musca must be separated by less than 25 cm, while a separation of more than 100 cm is necessary to appear like point sources to each other.*

1. Sensitivity of *Musca* to Extended Sources

From Section C we know that the absolute sensitivity of a rhabdomere to an extended source is proportional to $(D\Delta\varrho_r)^2$, which in *Musca* is proportional to p^2 . Thus, each ommatidium of *Musca* is equally sensitive to an extended source.

2. Sensitivity of *Musca* to Point Sources

From Section C and Appendix B, we learn that the absolute sensitivity of a rhabdomere to a point source is proportional to $D^2(\Delta\varrho_r/\Delta\varrho)^2$. The ratio $\Delta\varrho_r/\Delta\varrho$ depends only on the parameters p and λ . Thus, the sensitivity to point sources depends on D^2 . Since the facet diameter D changes by a factor of two over the eye, a point source appears four times brighter in the region of the eye with highest acuity (smallest $\Delta\phi$) than in the region of poorest acuity (largest $\Delta\phi$).

E. Polarization Sensitivity of Retinula Cells

The sensitivity of a retinula cell to the direction of the electric vector \mathbf{E} of linear polarized light depends not only on the dichroism of the microvilli but also on the gross morphology of the rhabdom in addition to the optical properties of cells above it. Since polarization sensitivity is fully treated by WATERMAN (Part B, this volume), we only consider some of the more theoretic concepts necessary for a quantitative analysis.

I. Origin of Polarization Sensitivity

Nearly all retinula cells show some sensitivity to the direction of \mathbf{E} . The origin of this polarization sensitivity is the dichroic property of the individual microvillus membrane as discussed in Section F. Nevertheless, evidence is accumulating in favor of the view that in most cases the dichroism of a microvillus is only a by-product of an adaptation to maximize the *absolute* sensitivity of the cell to *unpolarized* light (see Secs. C.IV and F). Recent evidence has in fact shown that the potentially high polarization sensitivity of retinula cells is often deliberately decreased by a twisting of the rhabdom (MENZEL, 1975; SNYDER and MCINTYRE, 1975; WEHNER et al., 1975).

When a retinula cell does show a high polarization sensitivity, its rhabdomere is usually associated with a very specialized arrangement or structure. The best known examples include the crustacean rhabdom with interdigitating orthogonal microvilli and the ninth cell of the bee which is quite short and proximal to the other eight retinula cells (SNYDER, 1973; MENZEL and SNYDER, 1974). Here we give a brief account of polarization sensitivity in several rhabdom types and discuss the effect of twisting.

II. Retinula Cells of Diptera

SHAW (1969b) and SNYDER (1973) have shown that, because of self-screening, the longer a dipteran rhabdomere or the greater the concentration of photopigment within it, the lower its sensitivity to polarized light. The measured polarization sensitivity ratio (PS) of cells 1–6 is between 1 and 2 (KIRSCHFELD and SNYDER, 1975) which is consistent with the view that the dipoles are aligned to optimize absorption of *unpolarized* light. To see this we assume that the absorption coefficient of fly microvilli is between 0.5 and 1.0% per μm and find from Fig. 22 that the dipoles should lie near 45° (or at random) with the microvillus axis.

Because rhabdomeres 7 and 8 are shorter (Fig. 20), they have less self-screening and therefore potentially greater polarization sensitivity. Furthermore, since rhabdom 8 lies beneath rhabdomere 7 and because their microvilli are perpendicular, the polarization sensitivity of cell 8 can be amplified (SNYDER, 1973; GRIBAKIN and GOVARDOVSKII, 1975). Lastly, we note from Fig. 22 that it is advantageous from the point of view of absolute sensitivity to *unpolarized* light for the microvillus dichroism to be greater (higher alignment of dipoles with microvillus axis) in short than long cells. All of these facts taken together lead to the theoretic possibility of a high polarization sensitivity in cell 8. Most of this argument can also be applied to the ninth cell of the bee (SNYDER, 1973; MENZEL and SNYDER, 1974).

III. Retinula Cells of Crustacean Rhabdoms

A theoretic analysis of crustacean rhabdoms shows that the polarization sensitivity of each retinula cell is independent of its absolute sensitivity and exactly equal to the dichroic ratio of the microvilli (SNYDER, 1973). The high polarization

sensitivity measured intracellularly (e.g., SHAW, 1969b; GOLDSMITH, 1975) demonstrates that the dichroism of crustacean microvilli is also high. This is an advantage both for polarization sensitivity and absolute sensitivity to unpolarized light, since, for optimum absolute sensitivity, dipoles should be highly aligned in fused rhabdom structures (Sec. C.IV).

IV. Retinula Cells in Fused Rhabdoms

A simple analysis for determining polarization sensitivity of retinula cells that form a fused rhabdom is given by SNYDER (1973). It should be noted that the direction of \mathbf{E} for maximum retinula cell response need not in general be parallel or perpendicular to the microvilli of the cell (SNYDER and SAMMUT, 1973). When the absorption of the *entire* rhabdom, i.e., the summed absorption of all rhabdomeres, is independent of the direction of \mathbf{E} , the polarization sensitivity of each retinula cell equals that of its microvilli dichroism (SNYDER, 1973).

Symmetric Fused Rhabdoms

There is a class of fused rhabdoms that is particularly simple to analyze and also have an important physical property. In these rhabdoms, the summed number of photons absorbed by all of the rhabdomeres is independent of the direction of \mathbf{E} , i.e., the *whole* or macroscopic structure is isotropic (see Appendix G) and *the polarization sensitivity ratio of each retinula cell equals that of the dichroic ratio of the microvilli* (SNYDER, 1973). Many fused rhabdoms approximate this situation. An example of this type of rhabdom is one that has eight rhabdomeres, each with an equal cross-sectional area, equal microvilli dichroism, and equal absorption where four of the rhabdomeres have microvilli oriented perpendicular to the direction of the microvilli of the other four rhabdomeres (Fig. 21).

V. Twisted Fused Rhabdoms

The fused rhabdoms of a number of hymenopterans have a significant structural twist (MENZEL, 1975; WEHNER et al., 1975; MENZEL and BLAKERS, 1976; WEHNER, 1976). As first shown by SNYDER and MCINTYRE (1975), the twist reduces the polarization sensitivity (PS) of the retinula cells. The greater the amount of twist, the greater the reduction in PS. For example, taking a twist of 180° as found by WEHNER et al. (1975) in the worker bee, the analysis of SNYDER and MCINTYRE (1975) shows that the PS is negligible, independent of the amount of microvilli dichroism or birefringence. WEHNER (1976) gives a particularly lucid account of the functional role of twisted rhabdoms in the worker bee.

In Appendix G, we derive a simple analytic expression for the polarization sensitivity ratio PS of a retinula cell within a twisted fused rhabdom. The results are shown in Fig. 23 for a total twist angle of 52° , assuming the rhabdom undergoes a uniform twist rate throughout its length L . The results are for $\alpha_{\parallel}L=2$, e.g., a 1% absorption per μm and $L=200\mu\text{m}$, but they are changed insignificantly for values

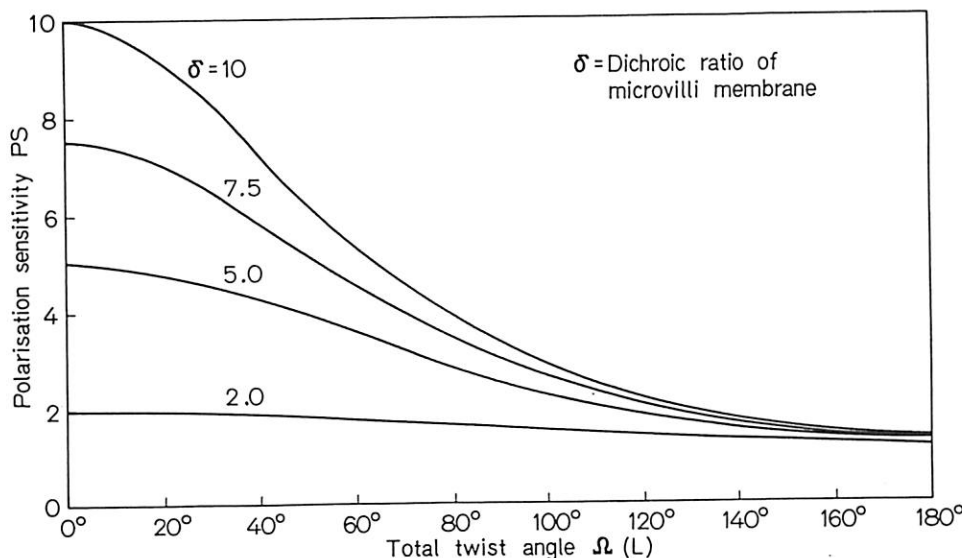


Fig. 23. The polarization sensitivity ratio PS for a retinula cell of a fused rhabdom that is twisted an amount $\Omega(L)$ degrees in its total length L . The twist rate is uniform along the length of the rhabdom. We have taken $\alpha_{||}L = 2$, where $\alpha_{||}$ is the absorption coefficient of the rhabdomeric membrane when E is perpendicular to the microvilli, but the results are changed insignificantly for values of $\alpha_{||}L$ between 1 and 3

between $\alpha_{||}L$ equal to 1 and 3, corresponding to 40 and 78 % total absorption by the whole rhabdom. It is clear from the figure that 180° twist obliterates PS. This result is intuitive when one realizes that for a 180° twist, an average of half of the length of the rhabdom has microvilli that are perpendicular to the other half. Thus, unless the absorption is so large as to take place principally in the top half, the effect is like crossed polarized lenses.

F. Optical Properties of Rhabdomeric Membrane

The optical properties of a material arise from the various ways that electromagnetic energy interacts with its atoms or molecules. Since every structure is distinguished by a unique arrangement of molecules, its optical properties represent a characteristic "fingerprint", i.e., a positive means of identification. We are concerned here mainly with birefringence and dichroism. Birefringence is the dependence of the refractive index on the direction of the electric vector E of linearly polarized light. It indicates the degree of alignment of the membrane substructure, i.e., its crystallinity. Dichroism is the dependence of absorption on the direction of E and indicates the degree of alignment of the absorbing dipoles within the membrane. Our purpose in this section is to show how measurements of birefringence and dichroism provide specific information on the properties of visual

membrane. Because we must introduce some simplifications in our model of visual membranes, it is advisable to remind ourselves of the complexity of a photoreceptor cell (LAUGHLIN et al., 1975).

I. Review of Photoreceptor Structure

Photoreceptors are specialized cells evolved for high sensitivity to light. The light-absorbing molecule is a dipole embedded in a protein molecule. This chromophore-protein complex, the rhodopsin molecule, is part of the cell membrane, where it is free to undergo lateral and rotational diffusion. The high quantum-capture property of highly evolved photoreceptors is the result of several molecular, fine and gross structural mechanisms: 1. The concentration of rhodopsin molecules within the membrane is extremely high. 2. The membranes holding the rhodopsin molecules are organized in closely packed stacks of discs (vertebrate photoreceptors) or dense packages of tubes (rhabdomeric invertebrate photoreceptors). 3. Light is contained within the photoreceptor structure as the result of the high optical density of these membrane stacks (light guide) (LAUGHLIN et al., 1975; LIEBMAN, 1975). Besides these facts, the quantum-capture property of the whole light-absorbing structure of a photoreceptor is very sensitive to the orientation of the dipole molecule relative to the light path. In general, the dipole must be perpendicular to the light path for highest absorption. This is indeed found in the membrane stacks of the vertebrate rod outer segment (ROS). However, the dipoles are in general not randomly orientated in the plane perpendicular to the light path for maximal absorption of unpolarized light (Sec. C.IV).

1. The Binding of Rhodopsin in Vertebrate Membrane

Direct microspectrophotometric (MSP) measurements show that rhodopsin and its associated photoproducts are localized within the outer segments of rods (LIEBMAN, 1972). Electron microscopy demonstrates that each outer segment is a stack of membrane discs. Each disc consists of a single contiguous membrane enclosing a broad flattened intracellular vacuole (Fig. 24). Rhodopsin is essentially a membrane lipoprotein (WALD, 1973); it can only be extracted using detergents and requires a proportion of bound lipids to show its normal activity of the ROS disc membrane; on bleaching, they withdraw into the hydrophobic phase almost completely. These findings have recently been confirmed by freeze-fracture and freeze-etching techniques, although there is still real doubt as to whether the rhodopsin is bound to the inside or the outside surface of the disc (MASON et al., 1974; cf. RAUBACH et al., 1974). Thus, all evidence points toward rhodopsin conforming to the Singer-Nicholson model of a membrane-bound lipoprotein. It appears to be an approximately spheric molecule of about 4 nm diameter bound to the fluid lipid phase of the disc membrane by strong hydrophobic forces. The diffusion kinetics of rhodopsin *in vivo* more than confirm this view (see below).

2. Chromophore Orientation in Vertebrate Membrane

The structure of the opsin molecule and in particular the distribution of external hydrophilic and hydrophobic groups must determine the orientation at which rhodopsin sits in the lipid matrix. It also determines the region of the molecule to which the dichroic chromophore, retinal, is bound. Thus, there should be a constant relationship between the position of the hydrophobic/hydrophilic

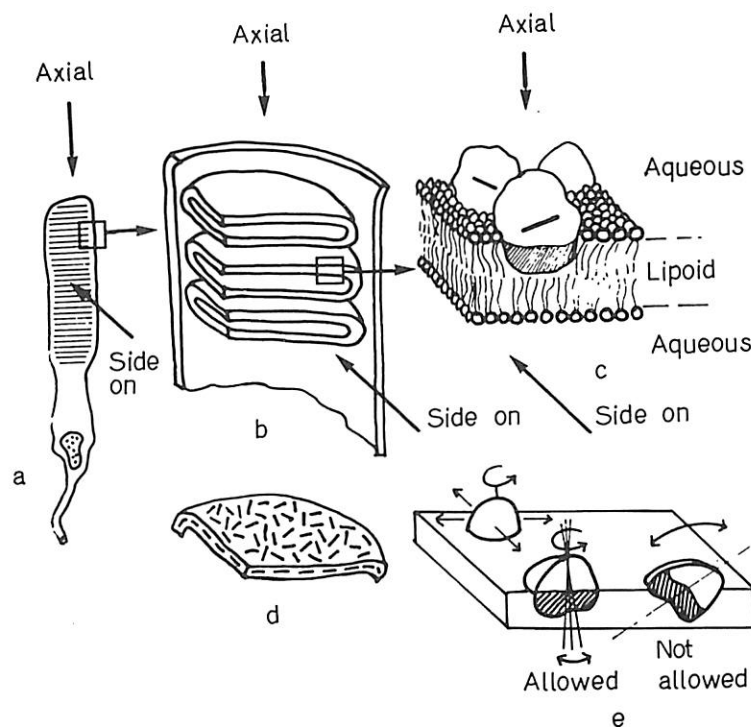


Fig. 24a-e. Structural and molecular organization of the photoreceptive membrane in rod outer segments. (a) A vertebrate rod photoreceptor. The arrows give the two important directions of light paths discussed in the text: axial light travels through the outer segment parallel to its long axis (under physiologic conditions, light reaches the outer segment from the inner segment); with *side-on* illumination, light travels along the short axis perpendicular to the long axis of the outer segment. (b) The disc membrane envelopes of the ROS. Axial light falls normally on the flat disc membrane; side-on light travels parallel to the disc membrane. (c) A fluid membrane model of the disc membrane. Rhodopsin molecules are globular proteins partly embedded in the lipid double layer. The hydrophilic part of the protein (light area) sticks out into the aqueous phase; the hydrophobic part (shadowed) dips into the membrane. The dipole chromophore (black line) is nearly parallel to the membrane surface. (d) A schematic illustration of the randomly oriented dipole molecules in the disc membrane. (e) Rhodopsin molecules are free to move laterally and rotationally within the fluid membrane. Wobbling, however, is strongly reduced by hydrophilic-hydrophobic forces

interface of the membrane as a whole and the position of the chromophore itself. In a wide, flat sea of membrane such as the disc surface, the chromophores should all have the same orientation relative to the plane of the membrane surface itself. This is indeed the case. When the stack of discs constituting the ROS is viewed from the side ("side-on"), the ROS is seen to be highly dichroic. When unbleached, light with an E vector parallel to the discs and thus perpendicular to the long axis of the rod is preferentially absorbed relative to light with the E vector parallel to the rod long axis (SCHMIDT, 1938). Comparison of the absorption spectrum for perpendicular and parallel polarized light shows that it is the chromophore of rhodopsin that is dichroic (LIEBMAN, 1962; HAROSI and MACNICHOL, 1974). Moreover, the photoproduct metarhodopsin II has the same direction of dichroism, but the free vitamin A molecule released from opsin at the close of bleaching has an orientation perpendicular to the membrane surface (DENTON, 1959; HAROSI and MACNICHOL, 1974). It seems that vitamin A dissolves in the lipid bilayer, the long hydrocarbon chain coming to lie parallel with the lipid chains. In this position, it is parallel to the direction of physiologically incident light and presumably has negligible physiologic absorption.

It is clear that when viewed from the side, the ROS membrane is a dichroic structure. However, the measured dichroism of this membrane is small compared with the measured arthropod polarization

sensitivity (PS) values. The most accurate determination of side-on dichroism gives a value of 4–5:1, but careful controls show that the measured value is underestimated as a consequence of scattering of the measuring beam (HAROSI and MACNICHOL, 1974). The magnitude of this error cannot be assessed. For this reason, the upper value of 5 is used for membrane dichroism throughout this work. Note that this value of 5 appears to be uncorrected for form dichroism (MOODY, 1964; see also below).

It is important to emphasize that the measured dichroism of the disc membrane is relatively small. One can postulate two principal reasons as to why dichroism might be reduced: 1. Although the chromophore is perfectly aligned with the membrane, it is not a perfect dipole. Thus, the measured dichroism in vertebrate rods represents the greatest possible dichroism that the retinal-opsin system can achieve. 2. The chromophore is an extremely effective dipole but is not perfectly aligned with the surface of the membrane; rather it is tilted. A slight tilt could arise from wobbling of the rhodopsin axes even though this type of rotation is opposed by the strong hydrophobic-hydrophilic bonding (Fig. 24). It is at present impossible to assess the relative importance of these two effects in reducing the measured dichroism. In particular, if the intrinsic dichroism of the chromophore were maximal, then it would be possible to calculate the tilt factor. Unfortunately, to our knowledge no such estimate of rhodopsin's intrinsic dichroism exists. The highest measured dichroism is 5:1, measured in sheared films (WRIGHT, 1973). In this situation, it cannot be assumed that the chromophore dipoles are perfectly orientated.

3. Motion of Rhodopsin Molecules in Vertebrate Membrane

The evidence given above suggests that the rhodopsin chromophore is aligned approximately parallel to the surface of the membrane. However, under normal physiologic illumination, the rod shows no dichroism with respect to light propagating along its optic (long) axis. It is now known that results from a random distribution of dipoles about the axis perpendicular to the membrane disc surface. This random distribution results from the ability of rhodopsin molecules to rotate within their lipid matrix.

When rods are illuminated along their long axis with linearly polarized light, it should be possible to selectively bleach those chromophores whose long axes run predominantly in the same direction as the **E** vector. The bleached photoreceptor should then be dichroic with an absorption maximum at right angles to that of the bleaching light. In practice it is extremely difficult to induce dichroism by this method in the intact cell. Extremely rapid flash photolysis experiments show that this is because the rhodopsin molecules are continually rotating in the membrane. The speed of rotation is so great that within 60 μ s the momentary dichroism induced by bleaching with linearly polarized light is totally randomized (CONE, 1972). When the same membrane is fixed with glutaraldehyde, the rhodopsin molecules are loosely bound together, rotation is prevented, and a high dichroism can easily be induced by selective bleaching (BROWN, 1972). From the kinetics and temperature dependence of the rotation effect together with estimates of the diameter of the rhodopsin molecule, it is possible to estimate that the lipid matrix within which rhodopsin is embedded has the viscosity of olive oil (CONE, 1972).

Two further series of elegant selective bleaching experiments show that rhodopsin is not just free to rotate in the lipid matrix; it can diffuse laterally across the matrix as well. When a large frog rod is viewed side-on and a thin longitudinal strip parallel to the optical axis is bleached, there is an initial large decrease in the absorbance measured at the peak wavelength of rhodopsin. This decrease is confined to the area bleached. However, within 40 s, the absorbance increases within the bleached strip which is accompanied by a decrease in absorbance in the surrounding unbleached region. Controls show that this effect is a redistribution of bleached and unbleached chromophores resulting from lateral diffusion of molecules in the membrane and that it is abolished by fixation in glutaraldehyde. Again it is possible to calculate the diffusion coefficient and from it derive the viscosity. Surprisingly, it is the same as the viscosity for rotational diffusion (Poo and CONE, 1974; LIEBMAN and ENTINE, 1974).

The studies of rhodopsin distribution across disc membrane, using the chromophore's known absorption properties as a "label", provide compelling evidence that the ROS disc membrane conforms to the Singer-Nicholson model of a fluid mosaic membrane. This evidence is supported by the X-ray diffraction data which show that the lipid matrix is a bilayer, the rhodopsin molecules float in this matrix, and that the rhodopsin molecules are not arranged across the surface of the membrane in a definite pattern, but rather seem to be distributed at random (WORTHINGTON, 1974).

VERTEBRATE PHOTORECEPTOR STRUCTURE

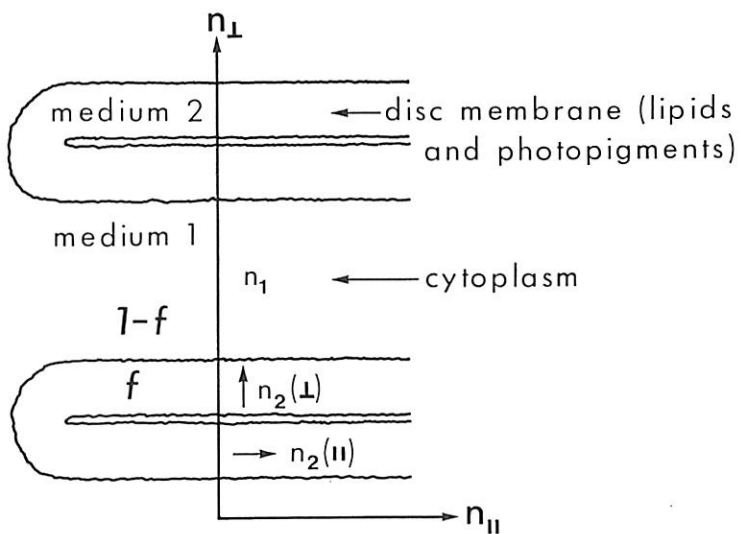


Fig. 25. Schematic vertebrate photoreceptor. The aqueous cytoplasm (medium 1) is isotropic, nonabsorbing, and of refractive index n_1 . The disc membrane (medium 2) is anisotropic with two intrinsic refractive index components $n_2(\parallel)$ parallel and $n_2(\perp)$ perpendicular to the discs and two intrinsic absorption coefficients $\alpha(\parallel)$ and $\alpha(\perp)$. The membrane volume fraction is f .

II. Dichroic Property of Photoreceptor Membrane

In this section, we analyze the dependence of absorption on the direction of the electric vector E of linearly polarized light. For comparison, we begin with vertebrate visual membrane. The analysis follows that given by SNYDER and LAUGHLIN (1975) and ISRAELACHVILI et al. (1976).

1. Vertebrate Disc Membrane Dichroism

In this section, we discuss the properties of a stack of absorbing slabs as a model for ROS membrane (Fig. 25). The amount of light absorbed when the polarization is parallel to the discs is generally found to be greater than when it is perpendicular to the discs.

The dichroic properties of the photoreceptor are related to the two absorption coefficients α_{\parallel} and α_{\perp} (Fig. 25) for light polarized parallel and perpendicular to the disc planes. The absorption coefficient α is defined as the fraction of light intensity absorbed per infinitesimal unit length of material; the fraction of light absorbed by a material of finite length l being proportional to $(1 - e^{-\alpha l})$. α is related to the molar extinction coefficient ϵ and concentration c by $\alpha = 2.3 \epsilon c$. The dichroic ratio $\alpha_{\parallel}/\alpha_{\perp}$ of a photoreceptor may be separated into an *intrinsic* and a *form* component. *Intrinsic dichroism* arises when the absorbing photopigments are anisotropically oriented in the disc membranes.

Form dichroism arises from the overall photoreceptor structure and the different refractive indices of the membrane and aqueous regions. This difference in the

refractive indices results in a different electric field intensity inside the disc membranes when the electric field polarization of the incoming light is parallel to the discs from that when the polarization is perpendicular to the discs. When the mean photoreceptor field \mathbf{E} is parallel to the discs, the internal fields are continuous across each boundary (Fig. 25) and therefore the same in both media 1 and 2 and equal to \mathbf{E} , so that $\mathbf{E}_2 = \mathbf{E}$. But when the mean field \mathbf{E} is perpendicular to the discs, the electric displacements \mathbf{D} are now continuous across each boundary and equal to $\mathbf{D} = \epsilon_{\perp} \mathbf{E}$, so that $\epsilon_2(\perp) \mathbf{E}_2 = \mathbf{D} = \epsilon_{\perp} \mathbf{E}$. Thus, the ratio of the fields in the absorbing medium 2 when \mathbf{E} is parallel so that it is perpendicular to the discs is $\epsilon_2(\perp)/\epsilon_{\perp} = (n_2(\perp)/n_{\perp})^2$.

Since the rate of absorption of light energy is proportional to the square of the electric field, the ratio of the absorption rates for light polarized parallel and perpendicular to the discs gives us an expression for the form dichroic ratio δ_F due only to the existence of absorbing *isotropic* plates (SNYDER and LAUGHLIN, 1975; ISRAELACHVILI et al., 1976).

$$\text{Form dichroism} = \delta_F \cong (n_2/n_1)^4, \quad (\text{F.1})$$

where n_2 is the refractive index of the disc membrane and n_1 of the surrounding cytoplasm. Thus, even when the chromophores are randomly oriented (in three dimensions) within the disc membrane, the dichroic ratio will always be greater than unity, since $n_2 > n_1$. The precise value for n_2/n_1 is uncertain, but ISRAELACHVILI et al. (1976) argue that its most likely value is 1.53/1.34 so that $\delta \cong 1.7$. They also point out that the actual absorbing part of the membrane is the retinal group or chromophore attached to the protein opsin; thus, it is not the refractive index of the membrane that should appear in Eq. (F.1) but that of the retinal. Since the refractive index around the retinal is likely to be close to that of the protein, the form dichroism could well be as high as $(1.60/1.34)^4 \approx 2.0$. Equation (F.1) is an approximation for $f \ll 1$ in Fig. 25. The exact expression is given by ISRAELACHVILI et al. (1976) and shown in Fig. 26.

The intrinsic dichroic ratio δ_I in Fig. 25 is given as $\alpha_{||}/\alpha_{\perp}$ so that the dichroic ratio δ of the total photoreceptor is

$$\text{Total dichroism} = \delta = \delta_F \delta_I \cong (n_2/n_1)^4 (\alpha_{||}/\alpha_{\perp}). \quad (\text{F.2})$$

In vertebrate rod outer segments, the form factor δ_F is probably greater than 1.5 and represents a purely structural amplification of the intrinsic dichroism. The most recent measurements of HAROSI and MACNICHOL (1974) show that the maximum $\delta \cong 5$ in frog rods. Correcting for form dichroism, this gives a maximum value of 3 for the intrinsic dichroism of the disc membrane.

2. Dichroism of Rhabdomeric Membrane

Our most sophisticated model for rhabdomeric photoreceptors is presented in Fig. 27, but it is both mathematically and intuitively easier to deal with the box model of the microvillus as introduced by SNYDER and LAUGHLIN (1975). There is

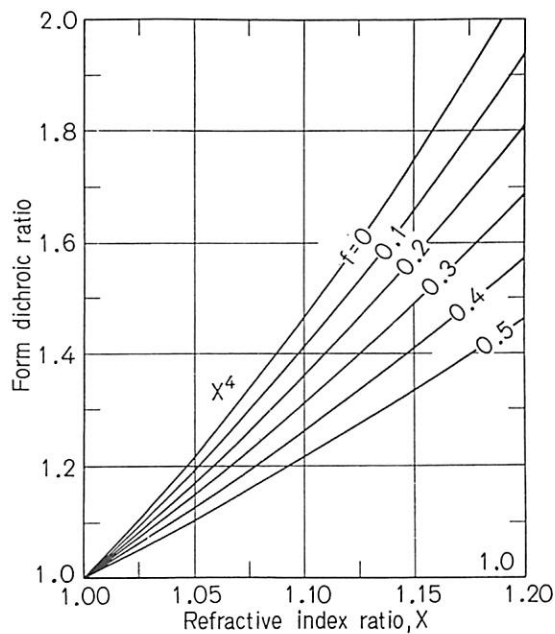


Fig. 26. Form dichroic ratio δ_F or relative absorption $\alpha_{\parallel}/\alpha_{\perp}$ of a vertebrate photoreceptor (Fig. 25) plotted for no intrinsic birefringence or dichroism. The total or net dichroic ratio is given by multiplying the plotted value by $\alpha_{\parallel}/\alpha_{\perp}$. The refractive index ratio $x = n_2/n_1$

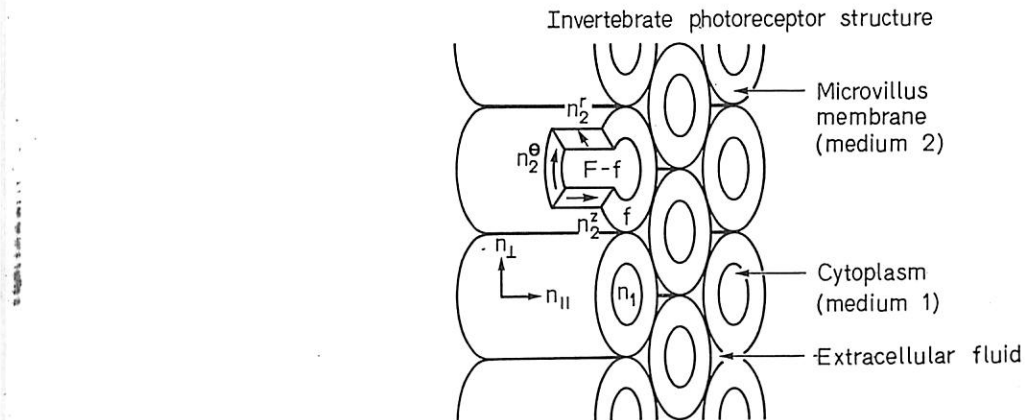


Fig. 27. Schematic rhabdomere-type invertebrate photoreceptor composed of microvilli tubules. The microvilli have a volume fraction F , and each is bounded by the photomembrane (medium 2) of volume fraction f , with three intrinsic refractive index components n_2^r , n_2^θ , and n_2^z , and intrinsic absorption coefficients α_r , α_θ , and α_z . The aqueous cytoplasm and extracellular fluid are assumed to have similar properties (medium 1), being isotropic and nonabsorbing. The bulk photoreceptor refractive indices are n_{\parallel} and n_{\perp} and the bulk absorption coefficients are α_{\parallel} and α_{\perp} . For close packed microvilli

$$F = \pi/2\sqrt{3} = 0.907$$

only about a 1% difference between the results based on either model (ISRAELACHVILI et al., 1976).

We found in Section I above that the disc structure of the vertebrate photoreceptor amplified any intrinsic dichroism. Thus, we would again anticipate some influence by the rhabdomeric structure of Fig. 27. However, it is clear from Fig. 28 that the effect of form dichroism δ_F is comparatively degraded or neutralized

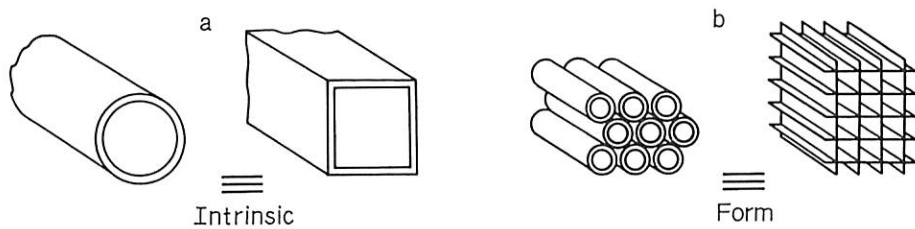


Fig. 28. (a) The individual microvillus as four vertebrate disc outer segments giving rise to the intrinsic component of dichroism. (b) Microvilli (rhabdomeric medium) as crossed sheets of disc membrane giving rise to the form component of dichroism. The fact that a vertebrate disc is formed from two membrane layers separated by an intradisc cytoplasmic phase does not alter the validity of our simple presentation

in rhabdoms because of the presence of crossed plates. The dichroic ratio $\delta = \alpha_{||}/\alpha_{\perp}$ of rhabdomeric membrane is then (SNYDER and LAUGHLIN, 1975)

$$\delta = \frac{2\alpha^z \delta_F}{\alpha^r + \alpha^\theta \delta_F}, \quad (\text{F.3})$$

$$\delta_F = n_2/n_1, \quad (\text{F.4})$$

where $\alpha^r, \alpha^z, \alpha^\theta$ are the absorption coefficients for E parallel to the radial, axial, and azimuthal directions of a microvillus. When the individual microvillus lacks intrinsic dichroism, $\alpha^r = \alpha^\theta = \alpha^z$, and $\delta = 2\delta_F/(1 + \delta_F)$ or $\delta \cong 1.2$ when $\delta_F = 1.5$. Thus, the rhabdomeric gross structure has a comparatively small effect on the dichroic ratio of rhabdomere membrane.

It is rather difficult to estimate the dichroic ratio of rhabdomeric material from Eq. (F.3) without making assumptions about the absorption coefficients $\alpha^z, \alpha^r, \alpha^\theta$, i.e., assumptions about the orientation of the chromophore. If, as did MOODY and PARRISS (1961), we assume ideal dipoles lying flat in the plane of the membrane, i.e., $\alpha^r = 0$ and $\alpha^z = \alpha^\theta$, we find from Eq. (F.3) that the dichroic ratio δ of rhabdomeric material is 2. This result is equivalent to assuming an infinite dichroic ratio (measured side-on) for vertebrate disc membrane because, if $\alpha^r = 0$ and the dipoles are ideal, $\alpha_{||}/\alpha_{\perp}$ is infinite. Thus, if the dipoles are random in the plane of the microvillus as they are in vertebrate discs, then the largest possible dichroic ratio is 2 for rhabdomeric membrane compared to infinity for vertebrate side-on dichroic measurements.

If we assume that the microvillus membrane is identical to rod disc membrane, we then have $\alpha^z = \alpha^\theta = \alpha_{||}$ and $\alpha^r = \alpha_{\perp}$ so that from Eq. (F.3)

$$\delta = \frac{2\delta_{\text{vert}}}{1 + \delta_{\text{vert}}}, \quad (\text{F.5})$$

where δ_{vert} is the dichroic ratio for disc membrane given by Eq. (F.2). Taking the maximum measured value of $\delta_{\text{vert}} = 5$, the value for the dichroic ratio of rhabdomeric material is 1.67. We note that the dichroic ratio of rhabdomeric membrane of *Musca* rhabdomeres 1–6 ranges from 1 to 2 (KIRSCHFELD and SNYDER, 1976).

Whenever the dichroic ratio of rhabdomeric material exceeds about 1.7, there must be some alignment of the dipoles with the microvillus axis. SNYDER and LAUGHLIN (1975), showed that a mean alignment of about 170° with the microvillus

axis gives a dichroic ratio of about 10, while perfect alignment gives about 20. This last value is not excessively greater than the largest dichroic ratio of 13 measured intracellularly in Crustacea by SHAW (1969b).

The *absolute sensitivity* of a photoreceptor to *unpolarized* light depends on the orientation of the dipoles within the membrane and also the gross structure of the photoreceptor. In both vertebrate discs and fly rhabdomeres 1–6, the optimum dipole orientation is a random alignment within the plane of the membrane, but in fused rhabdoms, characteristic of Crustacea, the absolute sensitivity is enhanced by high alignment of dipoles with the microvillus axis (SNYDER and LAUGHLIN, 1975). This is consistent with the measurements and supports the notion that dichroism is only a secondary consequence of the photoreceptor's primary objective-maximizing absolute sensitivity to unpolarized light. Animals that make use of polarization information could appear to do so with highly specialized modifications to the rhabdomeric structure, such as produced by tiered rhabdoms (WATERMAN, this volume, Part B). In fact, animals seem to counteract the effect of the dichroic material by twisting the rhabdom (MENZEL, 1975; SNYDER and MCINTYRE, 1975; WEHNER et al., 1975).

III. Birefringence of Photoreceptor Membrane

In this section, we analyze the dependence of the refractive index on the direction of the electric vector \mathbf{E} of linearly polarized light. For comparison, we again begin with vertebrate disc membrane. The development follows that presented by ISRAELACHVILI et al. (1976). We emphasize from the outset that sign conventions are *not* consistent throughout the literature. Parallel here is taken to mean parallel to the disc membrane or parallel to the microvillus axis.

1. Birefringence of Vertebrate Disc Membrane

We again refer to Fig. 25. The total birefringence of the vertebrate photoreceptor has a form component Δ_F and an intrinsic component Δ_I .

$$\frac{(n_{||} - n_{\perp})/n_1}{\text{total birefringence}} = \frac{\Delta_F}{\text{form birefringence}} + \frac{\Delta_I}{\text{intrinsic birefringence}} \quad (\text{F.6})$$

where we have normalized by dividing with n_1 and

$$\Delta_F \cong \frac{1}{2} f(1-f) \left(x - \frac{1}{x} \right)^2, \quad (\text{F.7a})$$

$$\Delta_I \cong -\frac{1}{2} f(1+f) \Delta, \quad (\text{F.7b})$$

$$\Delta = \{n_2(||) - n_2(\perp)\}/n_1, \quad (\text{F.7c})$$

$$X = n_2(\perp)/n_1, \quad (\text{F.7d})$$

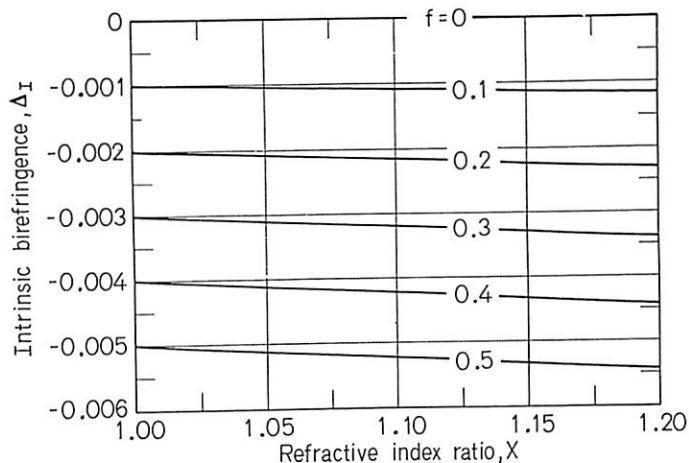


Fig. 29. Intrinsic birefringence Δ_I of vertebrate and invertebrate photoreceptors, plotted for $\Delta = +0.01$ for vertebrates (Fig. 25) and for $(2\delta - \Delta) = +0.02$, $F = \pi/2\sqrt{3}$, for invertebrates (Fig. 27) $x = m_2(\perp)/m_1$. The desired intrinsic birefringence Δ_I is obtained by linearly scaling the plotted value to the real value of Δ or $(2\delta - \Delta)$, i.e., by multiplying the plotted value by $\Delta/0.01$ or $(2\delta - \Delta)/0.02$. The curves are reliable to 1%. The total birefringence $(n_{||} - n_{\perp})/n_1$ of the photoreceptor is given by adding the intrinsic birefringence Δ_I to the form birefringence Δ_F as given by Fig. 30 (for vertebrates) and Fig. 31 (for invertebrates)

and f is the volume fraction of the disc membrane (Fig. 25). We differentiate between Δ_I , the intrinsic birefringence of the bulk structure, and Δ the intrinsic birefringence of the disc membrane.

Reasonable limits for the variables are:

$$1.08 < X < 1.2, \quad (\text{F.8a})$$

$$0.2 < f < 0.5, \quad (\text{F.8b})$$

$$-0.02 < \Delta < +0.02. \quad (\text{F.8c})$$

The variation of Δ_I with x at different values of f is shown in Fig. 29 plotted for $\Delta = +0.01$. Thus, for any value of Δ different from $\Delta = +0.01$, the value of Δ_I that goes into Eq. (F.6) is given by Δ_I as obtained from Fig. 29 multiplied by $\Delta/0.01$. For example, if $f = 0.3$, $x = 1.1$, and $\Delta = -0.005$, Δ_I is -0.0032 ($-0.005/0.01 = +0.0016$). Figure 30 is included as an example to show how the total birefringence varies with x for $f = 0.2$ and $f = 0.4$. The solid lines are for form birefringence only ($\Delta = 0$) while the dashed lines are for $\Delta = 0.005$.

Using our sign convention, LIEBMAN and ENTINE (1974) found that $n_{||} - n_{\perp} = +0.0010$ for the total birefringence of frog rods and estimated the form birefringence $n_1 \Delta_F = +0.0040$ and the intrinsic birefringence $n_1 \Delta_I = -0.0050$. Putting their values for $f = 0.37$ and $x = 1.475/1.365$ into our Eq. (F.7a) leads to $n_1 \Delta_F = +0.0039$ which is consistent with their estimation. From Eq. (F.7b) we obtain a value for the intrinsic membrane birefringence of frog rods of $n_1 \Delta = +0.013$. This last value indicates the degree of crystallinity for disc membrane.

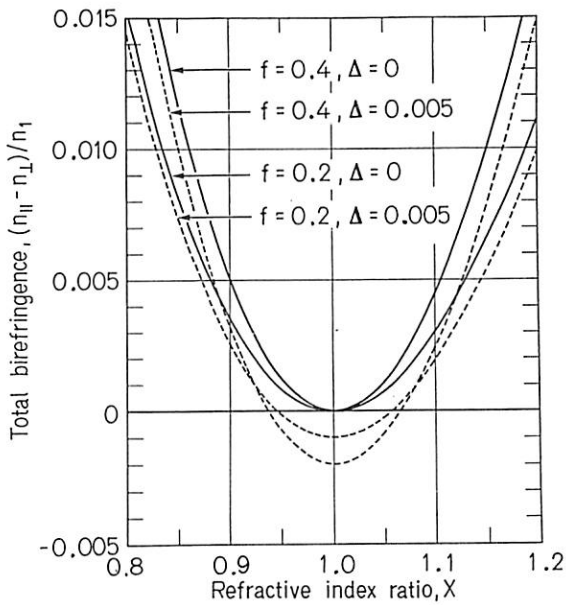


Fig. 30. Total or net birefringence of a vertebrate photoreceptor, illustrating its dependence on x , f , and Δ

2. Birefringence of Rhabdomeric Membrane

We now refer to Fig. 27. The microvillus core is filled with cytoplasm, whereas the external microvillus spaces are filled with extracellular fluid. The intracellular and extracellular regions will be assumed to have identical optical properties, characteristic of aqueous cytoplasm, i.e., isotropic and nonabsorbing and of refractive index n_1 . The membrane (medium 2) must now be assumed to be highly anisotropic with three refractive index components: n_2^r (for radial field direction), n_2^θ (for azimuthal field direction), and n_2^z (for axial field direction). We can again use Fig. 28 to gain intuition and derive a simple expression for birefringence of rhabdomeric membrane. For example, it is intuitive that the presence of crossed plates reduces the regularity of the membrane and we can anticipate a comparatively lower bulk form and intrinsic birefringence than for parallel plates. We again have Eq. (F.6) but with

$$\Delta_F \approx \frac{1}{4}f(1-f)\left(x - \frac{1}{x}\right)^2, \quad (\text{F.9a})$$

$$\Delta_I \approx -\frac{1}{4}f(1+x)(2k - \Delta), \quad (\text{F.9b})$$

$$x = n_2^r/n_1, \quad (\text{F.9c})$$

where the two intrinsic membrane birefringence components are

$$\Delta = (n_2^r - n_2^\theta)/n_1, \quad (\text{F.9d})$$

$$\bar{k} = (n_2^r - n_2^z)/n_1. \quad (\text{F.9e})$$

If the membrane is isotropic within its plane, $n_2^z = n_2^\theta$ and $\bar{k} = \Delta$. Then both form and intrinsic birefringence, and hence the total birefringence, are about half that of the vertebrate rod, assuming equal f , x , and Δ .

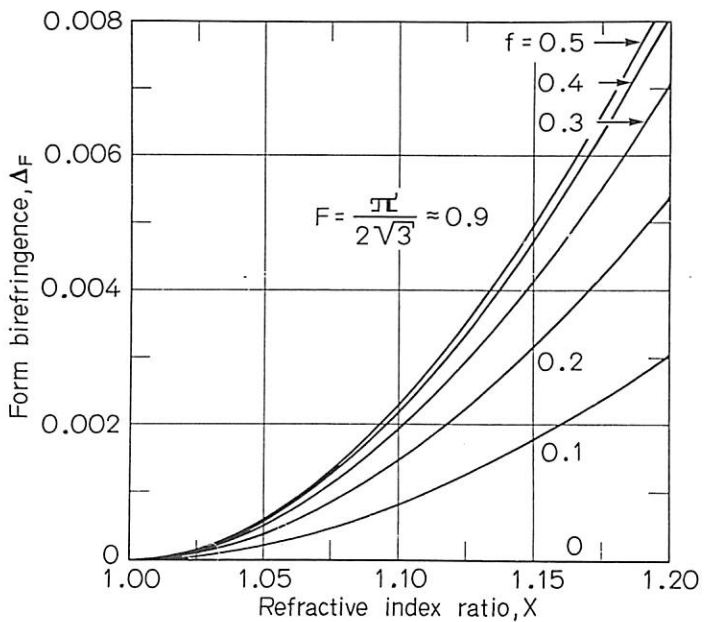


Fig. 31. Form birefringence $\Delta_F = (n_{||} - n_{\perp})/n_1$ of invertebrate photoreceptors, plotted for $F = \pi/2\sqrt{3}$ (i.e., closely packed microvilli) and no intrinsic membrane birefringence ($\bar{k} = \Delta = 0$). The intrinsic birefringence component Δ_I is given in Fig. 29

The microvilli tubules in invertebrate photoreceptors are usually closely packed (LASANSKY, 1970) so that $F \approx \pi/2\sqrt{3} \approx 0.9069$, although values for F as low as 0.6 are possible (TRUJILLO-CENÓZ, 1972). The membrane volume fraction f is related to F and to the ratio of the inner and outer microvilli radii (a/b) by

$$f = F \left(1 - \frac{a^2}{b^2} \right). \quad (\text{F.10})$$

Figure 31 shows the variation of the form component $\Delta_F \cos x$ at different values for $F = 0.9069$ and $\delta = \Delta = 0$. There is negligible difference between the birefringence for a hexagonal arrangement of microvilli ($F = \pi/2\sqrt{3}$) and a square array ($F = \pi/4$).

Recent measurements of birefringence on the rhabdomeric material of *Musca* (KIRSCHFELD and SNYDER, 1975) show that the large refractive index is obtained when \mathbf{E} is *perpendicular* to the microvilli of rhabdomeres 1–6 and a total birefringence $n_{||} - n_{\perp} = -(0.003 \text{ to } 0.005)$. By assuming that the density of rhabdomeric membrane is half that of rod disc membrane $f \cong 0.2$, and that the membrane refractive index ratio x is the same for both vertebrate and rhabdomeric material, KIRSCHFELD and SNYDER (1975) found the intrinsic component $n_1 \Delta_I = -(0.0046 \text{ to } 0.0066)$, i.e., about the same as measured by LIEBMAN et al. (1974) for disc membrane.

If we also assume $f = 0.2$ and $x \cong 1.08$ as for the vertebrate case, we find from Eq. (F.9b) that the intrinsic membrane birefringence $n(2\delta - \Delta) \cong 0.05$, i.e., about four times that of frog rods. We conclude, therefore, that microvillus membrane of *Musca* is significantly more crystalline (ordered) than frog outer segment disc membrane.

G. Waveguide Properties of Visual Photoreceptors

Many animals with highly evolved visual systems have long, narrow photoreceptive structures (outer segments or rhabdomeres) formed by a dense membrane packing with a greater refractive index than the surrounding medium (STOCKHAMMER, 1956; SIDMAN, 1957; SEITZ, 1968; STAVENGA, 1974; KIRSCHFELD and SNYDER, 1975). Consequently, these structures act as light guides, i.e. light is transmitted within them by the mechanism of total internal reflection. Light guides offer the potential for improved optical isolation from neighboring photoreceptors. However, their main advantage may be economy of photopigment for a given capture, because photon capture depends mainly on the length of the photoreceptor (outer segment) being rather insensitive to its diameter or shape (section C.II). This provides one explanation for why many animals have narrow or tapered outer segments. They would probably be even more narrow if it were not for the fact that below a certain diameter wave effects render the structure an inefficient absorber. Thus, the waveguide effects discussed below are most likely a by-product of nature's attempt to minimise the volume of photopigment per photon capture.

Light has been observed to propagate along outer segments as well as rhabdomere cross-sections in patterns known as waveguide modes (ENOCH, 1963; VARELA and WIITANEN, 1970; FRANCESCHINI and KIRSCHFELD, 1971a, b). The occurrence of these patterns is basically a consequence of the small diameter of these structures. The patterns formed by modes most probably have no role in vision, although in theory the fused rhabdom photoreceptors of some arthropods could distinguish between different modes (SNYDER and PASK, 1972; BERNARD, 1975). Nevertheless, the observation of modes serves to emphasize that the photoreceptor is a dielectric or optical waveguide (SNYDER and LOVE, 1980; SNYDER, 1975). Optical waveguides exhibit two properties that might also play a functionally significant role in vision or at least set the limiting performance of an photoreceptors:

1. Only a fraction of a mode's light energy is transmitted within the photoreceptor, the remainder travels along but outside of the photoreceptor. This phenomenon is related to the evanescent field associated with total internal reflection and is strongly wavelength dependent.

2. Because light energy travels outside of the photoreceptor, it is weakly coupled to neighboring photoreceptors and hence cross-talk is unavoidable.

As we shall show, it is necessary to understand the first property particularly when measuring refractive index or birefringence in intact animals.

Waveguide mode effects are specified when the parameter V is known, where (SNYDER, 1975; SNYDER and LOVE, 1980)

$$V = \frac{\pi d_{Rh}}{\lambda} (n_r^2 - n_s^2)^{1/2}, \quad (G.1)$$

where d_{Rh} is the diameter of the rhabdom, n_r and n_s are the refractive indexes of the rhabdom and its surround respectively, and λ is the wavelength in vacuum. For

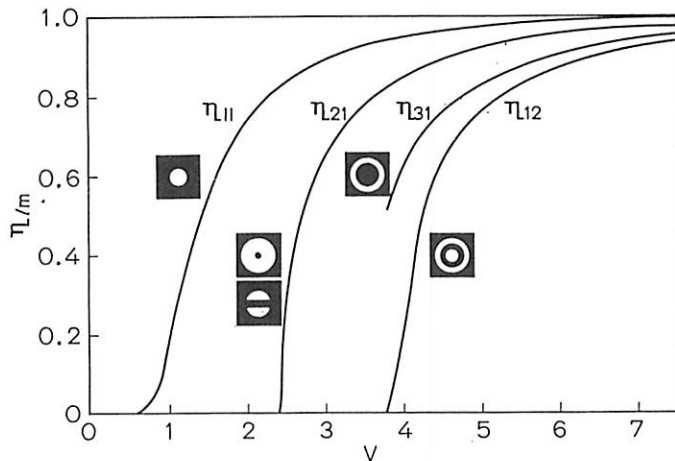


Fig. 32. The fraction η_{lm} of light power within a photoreceptor as a function of V for several low order modes designated by the lm notation (SNYDER, 1975). η for mode number 31 does not terminate abruptly as shown, but below $V=3.832$ η depends on the length of the rhabdom (SAMMUT and SNYDER, 1976)

example, the fraction η of light energy within the photoreceptor is shown as a function of V in Fig. 32. It is assumed here that the length of the rhabdom is greater than ten times its diameter, otherwise waveguide effects are decreased (SAMMUT and SNYDER, 1976).

It is nearly impossible to determine V using Eq. (G.1) because of the inability to obtain sufficiently accurate values of n_r and n_s representative of in situ conditions. Since $n_r \approx n_s$, small errors in a measurement of the refractive indices will lead to a larger error in $n_r^2 - n_s^2$ and hence in V . Nor is it possible to determine V from the "cut-off" properties of modes as suggested by ENOCH (1963) because we now know that modes do not exhibit a pronounced cut-off phenomenon (SNYDER, 1974; SAMMUT and SNYDER, 1976). KIRSCHFELD and SNYDER (1975, 1976) circumvented these difficulties by measuring the effect of waveguide modes on birefringence in nearly intact *Musca* rhabdomeres. It is of use to describe the technique of measurement here, since it demonstrates how an appreciation of waveguide mode effects can be used to advantage in obtaining the optical properties of rhabdomeres.

I. Determination of V for Fly Rhabdomeres

The rhabdomeres of *Musca*, shown in Fig. 33, are ideal for measuring waveguide effects. The central rhabdomere is about 1 μm in diameter and has been shown theoretically by SNYDER and MILLER (1972) and SNYDER and PASK (1973) to have pronounced waveguide effects compared to rhabdomeres 1–6, which have a diameter of 2 μm . Consequently, we have a "control" situation within one animal.

Unlike vertebrate photoreceptors, fly photoreceptors are birefringent to light propagating from the physiologic direction along the long axis of the receptor (STOCKHAMMER, 1956; SEITZ, 1969; KIRSCHFELD and SNYDER, 1975), i.e., their

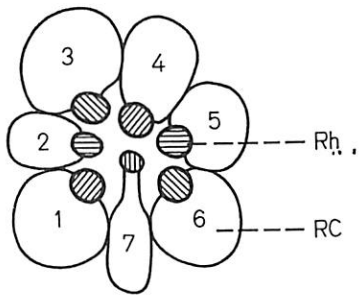


Fig. 33. Cross-section of the photoreceptor cells RC (Nos. 1-7) of the ommatidium of a fly. Rh: rhabdomeres, hatching indicates the direction of the microvilli. Rhabdomeres of cells 1-6 are approximately 2 μm in diameter at the distal end while cell 7 is approximately 1 μm in diameter

refractive index depends on the orientation of the \mathbf{E} vector of the light. Furthermore, it is possible to accurately measure the birefringence of fly rhabdomeres in nearly undisturbed physiologic conditions.

It is easy to see that the measured (effective or waveguide) birefringence $\langle \Delta n \rangle$ of the rhabdomeres must change with the wavelength of light and their diameter as well, if there are significant waveguide effects. This follows from the fact that only a fraction η of the total energy of a mode is transmitted within the photoreceptor, the remainder $1 - \eta$ travels along but outside the structure (SNYDER, 1975). η is highly dependent on V and therefore on the diameter of the structure and on the wavelength of light whenever waveguide effects are significant. Since the measured refractive index is smaller than the actual refractive index of the material for $\eta < 1$, the measured birefringence must also depend on η . If $\eta \approx 1$, the measured birefringence $\langle \Delta n \rangle$ is approximately that of the photoreceptor material Δn , since all the light travels inside the lightguide. When $\eta < 1$, a portion of the light travels outside the receptor and $\langle \Delta n \rangle$ is smaller than Δn , since the two characteristic refractive indices of the rhabdomeres approach n_s for $\eta \rightarrow 0$ (SNYDER, 1975).

It is implicit from the above discussion that the measured birefringence $\langle \Delta n \rangle$, which includes waveguide effects, equals the birefringence Δn of the photoreceptor material in the absence of waveguide effects multiplied by the fraction η of a mode's light power within the photoreceptor. Thus,

$$\langle \Delta n \rangle = \eta \Delta n, \quad (\text{G.2})$$

where $\langle \Delta n \rangle$ and Δn refer to birefringence due to light from the physiologic direction. This intuitive expression can be derived rigorously from two different theoretic methods (Appendix C). The important point is that the greater the wavelength, the smaller η and hence the smaller the *measured* birefringence. Thus, by measuring birefringence with light *from the physiologic direction*, we obtain information about η and Δn and can by use of Fig. 32 calculate V . The procedure is now described (KIRSCHFELD and SNYDER, 1976).

In order to measure the birefringence, portions of compound eyes of living flies (females of white eye mutant of *Musca*) were cut away and mounted on coverslips in a wet chamber in such a way that the cross-section of the rhabdomeres could be observed by means of a polarization microscope.

Undisturbed sections (rhabdomere lengths 30–50 μm) which are essential for the measurement may be obtained by using a loudspeaker-driven oscillating razor blade for sectioning (frequency 700 Hz, amplitude 50 μm ; KIRSCHFELD, 1967). The measurements were performed on white eye mutants of *Musca*, which lack all screening pigments since in the wild type fly pigment granules within the receptor cells move due to illumination of the receptors and change the refractive index of the medium surrounding the rhabdomere (KIRSCHFELD and FRANCESCHINI, 1969). The wavelengths used were $\lambda = 589$ and 656 nm. To our knowledge, the visual pigment in the rhabdomeres at these wavelengths is almost completely photoisomerized into rhodopsin, which by itself shows only negligible absorption at 589 and 656 nm (HAMDORF and ROSNER, 1973; STAVENGA, 1974). Hence, any interference of the visual pigment absorption with the measurements can be avoided. A second reason for selecting these long wavelengths of light is the fact that waveguide effects which are the topic of the investigation are expected to be more prominent and hence more easily detectable in the long wavelength part of the spectrum according to Eq. (G.1); the larger λ , the smaller V and the smaller η (see Fig. 32).

Between crossed polarizers, the birefringent rhabdomeres appear bright if their optical axes (the direction of the microvilli) are 45° to the analyzer orientation. Observed in white light, the rhabdomeres of large diameter (Nos. 1–6 in Fig. 33) appear white, whereas the small rhabdomeres (No. 7 in Fig. 33) appear green. This color is not due to absorption of light; it disappears if analyzer or polarizer are eliminated from the beam path. The effect, however, is exactly what we expect from waveguide theory. The rhabdomeres are more birefringent (and hence appear brighter) at short wavelengths where η is greater and less in the long wavelength part of the spectrum, as can be shown directly by measurements using monochromatic light.

If we know the birefringence Δn of the rhabdomere material in the absence of waveguide effects, we are able to determine η from the measured effective birefringence $\langle \Delta n \rangle$ [Eq. (G.2)]. Since we know η theoretically as a function of V (Fig. 32), we know as well the waveguide parameter of the rhabdomeres. Δn cannot be measured directly, however, since no rhabdomeres of a sufficiently large diameter (allowing a measurement without any waveguide influence) are available in the fly's eye. Nevertheless, we are able to determine V , if we measure the effective birefringence of the rhabdomeres at not one but at two different values of V . This allows us to eliminate Δn from Eq. (G.2). The two different V values necessary can be chosen arbitrarily by either using two different wavelengths of light (measuring at one and the same rhabdomere) or by measuring two rhabdomeres of different diameter in one and the same ommatidium (e.g., rhabdomeres 1 and 7, cf. Fig. 33) keeping the wavelength fixed. In the first case, we assume that Δn is constant within the spectral range used. This seems reasonable since the dispersion of n is the same as that of water with an additional constant (KIRSCHFELD and SNYDER, 1975). In the second case, we assume that Δn is the same for rhabdomeres 1–6 and 7. With these assumptions, the ratio of the two V numbers which we will use for the calculation is known from Eq. (G.1), since the ratios of the wavelength's respective diameters of the rhabdomeres are known.

Using Eq. (G.2), we can then form the ratio of the two measurements

$$\frac{\langle \Delta n_a \rangle}{\langle \Delta n_b \rangle} = \frac{\eta_a}{\eta_b}, \quad (\text{G.3})$$

where a and b indicate numbers for the two different V values. For the known ratio of two V numbers, we are able to calculate the ratio of η_a/η_b as a function of V_a and V_b and we can, therefore, determine V_a and V_b from our measured data and Eq. (G.1).

The ratio of the effective birefringence of five No. 7 rhabdomeres, measured at the wavelengths 656 and 589 nm, was 0.55 ± 0.05 (SDM). We then calculate V at 656 nm for No. 7 rhabdomeres with the method described above (open circle in Fig. 34) as well as for other wavelengths according to Eq. (G.1) (curve intersecting open circle).

Assuming that the birefringence of rhabdomeric material is the same in each photoreceptor, we can determine V for rhabdomeres 1–6 by knowing that their diameter is twice that of rhabdomere 7 (BOSCHEK, 1971). The results are shown in Fig. 34 by the curve intersecting the oblique cross. The ratio of the effective

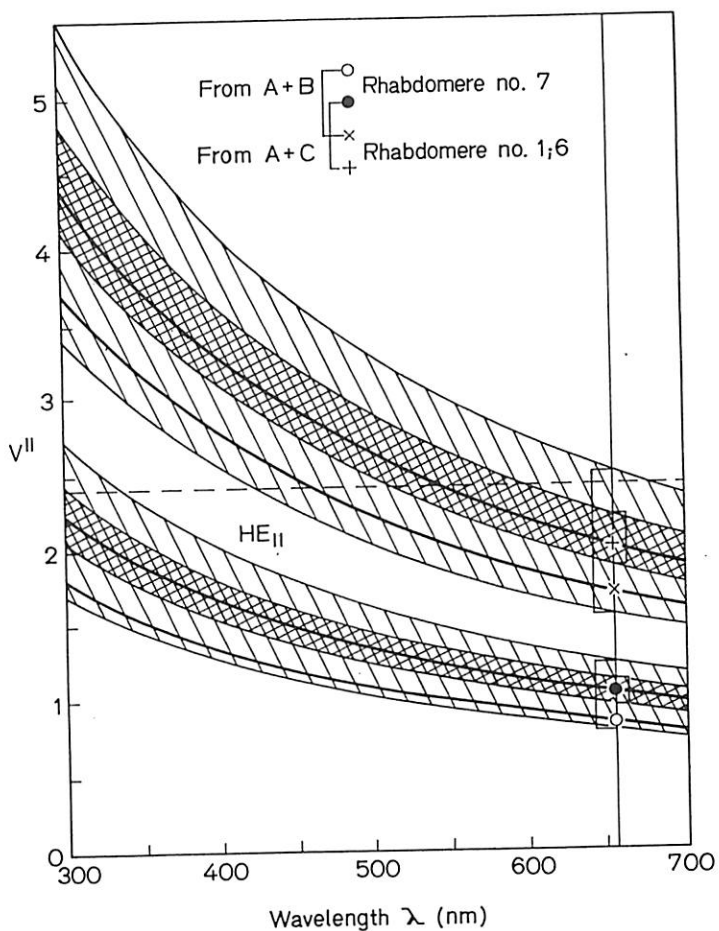


Fig. 34. The optical waveguide parameter V for fly photoreceptors as determined from the effective birefringence. For $V < 2.4$, only the first mode HE_{11} may exist. The upper set of curves is for rhabdomeres 1–6 while the lower is for rhabdomere 7. The hatched areas indicate the possible deviation in measured values. Further explanation of the symbols is in the text

birefringence for Nos. 7 and 1 rhabdomeres of five ommatidia was 0.24 ± 0.07 ($\lambda = 656$ nm). From this ratio, we obtain a second determination of V for No. 7 rhabdomeres (dot in Fig. 34 and intersecting curve) and No. 1 rhabdomeres (vertical cross and intersecting curve). There is sufficient coincidence between the results determined from the two sets of data. Hatched regions represent possible deviation in values. Below the horizontal broken curve at $V = 2.4$, only one mode can propagate.

Comparison of the curves shown in Fig. 34 with that for η given by Fig. 32 allows us to make some interesting observations for fly photoreceptors. First, only mode 1 can propagate on No. 7 rhabdomeres except perhaps for $\lambda < 340$ nm, consistent with direct observation of mode patterns in rhabdomere cross-sections. Waveguide effects are definitely significant for $\lambda > 350$ nm where η varies rapidly with the wavelength. On rhabdomeres 1–6, two mode families can propagate throughout most of the range of λ , also consistent with direct mode pattern observation. η for the first mode is nearly constant in rhabdomeres 1–6. The

determinations of V show that the waveguide properties of No. 7 rhabdomeres are alone sufficient to explain differences in the spectral sensitivity of rhabdomeres 1–6 and 7, as theoretically predicted by SNYDER and MILLER (1972) and SNYDER and PASK (1973). Nevertheless, there is increasing evidence for the view that differences in spectral sensitivities between receptors 1–6 and 7 and/or 8 cannot be explained by waveguide effects *alone*. This is supported by ERG measurements with spectral adaptation in *Drosophila* (STARK, 1975; MINKE et al., 1975; COSENS and WRIGHT, 1975), by analysis of *Drosophila* mutants lacking rhabdomeres in receptors 1–6 or 7 (STARK et al., 1975), by evaluation of an inhibitory influence of receptors 7 and/or 8 onto receptors 1–6 by means of single rhabdomere stimulation in *Musca* (KIRSCHFELD and LUTZ, unpublished), and by microspectrophotometry on individual No. 7 rhabdomeres (KIRSCHFELD and FRANCESCHINI, unpublished) in *Musca* and *Drosophila*.

To summarize our findings, waveguide effects are pronounced when the parameter V is less than 2. Assuming that all rhabdomeric membrane is similar to that of *Musca*, significant waveguide effects occur when the rhabdom diameter is less than or equal to 1 μm . One important fact emerges from this study. Waveguide effects are present in rhabdomeres principally because of the relatively low refractive index, $n_r \approx 1.39$. If n_r were 20% larger, waveguide effects would be insignificant, i.e., $\eta \approx 1$. Since the refractive index of a photoreceptor as well as its photoabsorption depend on the density of the membrane, it is quite probable that rhabdomeric membrane is as densely packed as physically possible.

II. Influence of Waveguide Effects on the Optical Properties of the Rhabdom

If the optical properties of a rhabdom are determined by passing light on-axis through it, then waveguide effects will influence the measurement. The absorption coefficient α then becomes $\alpha\eta$, where η is the fraction of light within the photoreceptor as given by Fig. 32. But, when taking ratios such as dichroic ratios $\alpha_{||}/\alpha_{\perp}$, the η values cancel. We have already shown that the birefringence becomes $\eta\Delta n$ in the presence of waveguide effects. STAVENGA (1974) has shown that the measurement of refractive index is also modified by waveguide effects but not simply with a multiplication by η . Instead, the measured refractive index $\langle n_r \rangle$ of the rhabdomere is

$$\langle n_r \rangle = kn_r + (1 - k)n_s, \quad (\text{G.4})$$

where $k = 1 - (U/V)^2$ and U is a waveguide parameter (SNYDER, 1969). Figure 35 shows k vs. V . We emphasize that waveguide effects distort measurements only when light is passed on-axis through a narrow photoreceptor and not when it is passed side-on.

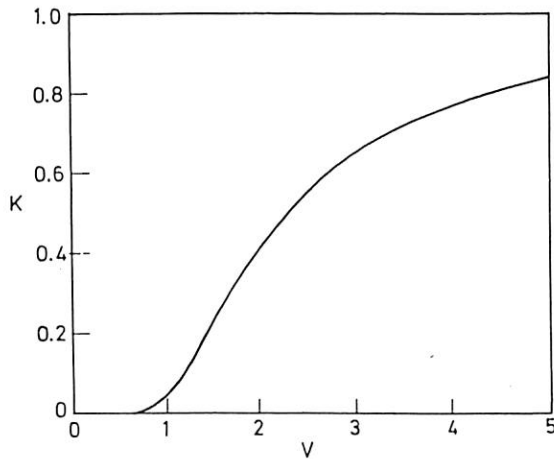


Fig. 35. The waveguide parameter k as a function of V for the first (HE_{11} mode)

Appendix A.

Influence of Waveguide Effects on Acceptance Angle $\Delta\varrho$

In Section B.I we derived an expression for the acceptance angle $\Delta\varrho$ of a retinula cell given by Eq. (3.7) as

$$(\Delta\varrho)^2 = (\Delta\varrho_l)^2 + (\Delta\varrho_r)^2, \quad (A.1)$$

where the symbols are defined by Fig. 4 and Table 1. Our derivation ignored the possible influence of waveguide mode effects which were described in Section G. Here, we derive $\Delta\varrho$ for a photoreceptor with pronounced waveguide mode effects. As an example, we consider retinula cell 8 in *Musca*.

In the presence of pronounced waveguide mode effects, i.e., when the parameter V of Section G is less than 2, a photon striking the center of the rhabdomere's cross-section is more likely to be accepted than if it is incident near the periphery. Furthermore, there is a finite probability that a photon will be accepted even if it misses the rhabdomere cross-section altogether (Fig. 36) (SNYDER, 1975). This is to be contrasted to the classic or top hat profile expected from simple geometric considerations. The position r_0 in Fig. 36 is $d_{Rh}/2$. Now, we next explain how to obtain the rhabdomere acceptance profile in Fig. 36.

The probability of observing a photon at a position r in the cross-section of a photoreceptor is proportional to the intensity of the electromagnetic field at that position. The intensity profile A_r is given as (SNYDER, 1969)

$$A_r = J_0^2(Ur/r_0); r \leq r_0, \quad (A.2)$$

where J_0 is a Bessel function of order zero and U is a waveguide parameter which is approximated by (SNYDER, 1969)

$$U \cong 2.4 e^{-1/V}. \quad (A.3)$$

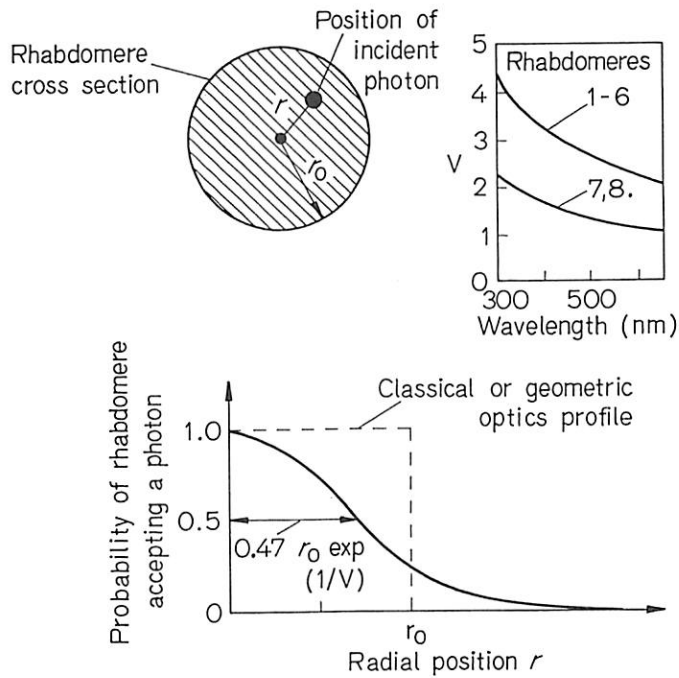


Fig. 36. Probability of rhabdomeres 7 and 8 accepting a photon at position r in its cross-section. The probability profile is proportional to the electromagnetic field intensity of a circular dielectric cylinder. The profile shown is applicable only for $V \geq 2.4$, where V is a characteristic waveguide parameter determined from direct measurements on *Musca* (KIRSCHFELD and SNYDER, 1975). The diameter of the rhabdomere $d_{Rh} = 2r_0$

Now it is a fact that the function J_0^2 is fit well by a Gaussian function of the form

$$A_r \cong e^{-2.77(r/f\Delta\varrho_r)^2}, \quad (A4)$$

where f is the focal length and $\Delta\varrho_r$ is the angular width of the acceptance profile at 50% sensitivity. Since, at 50% sensitivity, $J_0^2(x) = 0.5$, $x = Uf\Delta\varrho_r/d_{Rh} = 1.12$, we have that

$$\Delta\varrho_r \cong 1.12(d_{Rh}/f)/U. \quad (A5)$$

This expression is valid only when $V < 2$, otherwise more modes are present and $\Delta\varrho_r \rightarrow d_{Rh}/f$ the larger V . In other words, we are only considering the situation of strong waveguide effects. Thus, the problem is reduced to solving Eq. (A1) for $\Delta\varrho$. The parameter V has been measured by KIRSCHFELD and SNYDER (1976) (see Sec. G) for rhabdomeres 7 and 8 and is shown in the insert of Fig. 36. We take $\Delta\varrho_1 = \lambda/D$ so that

$$\Delta\varrho = \frac{\lambda}{D} \left\{ 1 + 0.22 \left(\frac{d_{Rh}}{\lambda F} \right)^2 e^{2/V} \right\}^{1/2}, \quad (A6)$$

where $F = f/D$. STAVENGA (1975) has found that $F \cong 1.9$ in most ommatidia of *Musca* where $d_{Rh} \cong 1 \mu\text{m}$ in rhabdomeres 7 and 8. The most extreme waveguide effects occur in rhabdomere 8, presumed to be a blue-sensitive cell ($\lambda \cong 0.47 \mu\text{m}$) (HARRIS et al., 1976). For $\lambda \cong 0.47 \mu\text{m}$, $V \cong 1.4$, so that $\Delta\varrho \cong 1.61 \lambda/D$ rather than

$1.65 \lambda/D$ had we used the classic profile (taking $\Delta\varrho_r = d_{Rh}/f$). Thus, the presence of pronounced waveguide effects does not significantly alter the acceptance angle $\Delta\varrho$ from that given by Eq. (B.7). However, the shape of the acceptance function should be more Gaussian shaped than cells 1–6 and the shorter cell 7. The reason is that the larger diameter of rhabdomeres 1–6 decrease the waveguide effect as does the short length of rhabdomere 7 (SAMMUT and SNYDER, 1976).

Appendix B.

Criteria to be a Point or Extended Source

If we ignore diffraction and aberrations, then it is intuitive that, as far as a rhabdom is concerned, an extended source is one in which the angular diameter $\Delta\varrho_r$ of the rhabdomere is less than the angular diameter $\Delta\psi$ of the source, i.e., $\Delta\psi > \Delta\varrho_r$. Similarly, a point source obeys $\Delta\psi \ll \Delta\varrho_r$. We now modify these conclusions by accounting for the imperfect optics as expressed by the angular sensitivity function A of the retinula cell.

The number $n(\phi)$ of photons absorbed by a retinula cell during the integration time of the eye (due to a distant point source, inclined at angle ϕ to the axis of the ommatidium) is

$$n(\phi) = n(0) A(\phi) = n(0) e^{-2.77(\phi/\Delta\varrho)^2}. \quad (\text{B1})$$

We have assumed a Gaussian acceptance function A , where $\Delta\varrho$ is the half width acceptance angle (Fig. 1). The number of photons absorbed N in one integration time, due to a uniform source of angular diameter $\Delta\psi$, is

$$N = 2\pi \int_0^{\Delta\psi/2} n(\phi) \sin \phi \, d\phi \quad (\text{B2a})$$

$$\cong 2\pi \int_0^{\Delta\psi/2} \phi n(\phi) \, d\phi \quad (\text{B2b})$$

$$= (\pi/2.77)(\Delta\varrho)^2 n(0) \{1 - e^{-0.69(\Delta\psi/\Delta\varrho)^2}\} \quad (\text{B2c})$$

assuming the source is centered on the axis of the ommatidium.

Now it is intuitive that $n(0)$ is proportional to Q times the pupil area $\pi D^2/4$, where Q is the fraction of photons entering the rhabdom

$$Q = \frac{\int_0^\infty \phi A_r \, d\phi}{\int_0^\infty \phi A \, d\phi} = \left(\frac{\Delta\varrho_r}{\Delta\varrho} \right)^2. \quad (\text{B3})$$

This result is also an excellent approximation for the case when A_r is a step function and A_1 the diffraction intensity pattern.

f
Q
d
e
t

It is possible to obtain $n(0)$ by the convolution process given in Fig. 4 when the heights of the functions are properly normalized. The A_r is correct, but A_l must be properly normalized so that the volume under A_l is proportional to the pupil area. Convolution of A_l with A_r will then give Q for $\phi=0$.

From Eqs. (B1), (B2), and (B3) and the logic of Section I.D, we have an expression for the number of photons absorbed by a uniform source of angular diameter $\Delta\psi$

$$N = \hat{I}D^2(\Delta\varrho_r)^2 \{1 - e^{-0.69(\Delta\psi/\Delta\varrho)^2}\} \quad (\text{B4a})$$

$$= \bar{N} \{1 - e^{-0.69(\Delta\psi/\Delta\varrho)^2}\}, \quad (\text{B4b})$$

where \hat{I} is defined in Table 1.

When $\Delta\psi = 1.8\Delta\varrho$, to an accuracy of 90 %, we can replace the bracketed portion of Eq. (B2b) by unity resulting in the expression for an infinite uniform source. When $\Delta\psi = 0.4\Delta\varrho$, to an accuracy of 90 %, we can replace the bracketed portion of Eq. (B4) by $0.69(\Delta\psi/\Delta\varrho)^2$ so that $N = 0.69(D\Delta\psi)^2(\Delta\varrho_r/\Delta\varrho)^2$, i.e., the same dependence on D , $\Delta\varrho_r$, and $\Delta\varrho$ of a distant point source.

In conclusion, as far as the light gathering of a rhabdom is concerned, *when the angular diameter $\Delta\psi$ of the source obeys $\Delta\psi > 1.8\Delta\varrho$, the source appears infinite in extent to a rhabdom of an ommatidium centered beneath it. When $\Delta\psi < 0.4\Delta\varrho$, the source has the behavior of a distant point.*

Appendix C.

Influence of Waveguide Effects on Birefringence of a Rhabdomere

In Section G we stated that the birefringence $\langle\Delta n\rangle$ of a rhabdomere, when measured along its long axis, is given by

$$\langle\Delta n\rangle = \eta\Delta n, \quad (\text{C1})$$

where η is the fraction of light power within the rhabdomere and Δn is the birefringence of the rhabdomeric material. Here we provide two different derivations of Eq. (C1). They both have in common the assumption that the birefringence is small, i.e., $\Delta n \ll 1$.

Birefringence is the difference in the refractive index due to light polarized in one direction and that polarized in a perpendicular direction. The refractive index of a material is the ratio of the speed of light in vacuum to its speed in the material. If mode effects are significant, some of the light travels in the medium external to the photoreceptor. Thus, the speed of light traveling along the receptor represents some average of the speed in the photoreceptor and the surrounding medium.

1. Solution by Coupled Mode Theory

The easiest way to derive Eq. (C1) is by appealing to the philosophy of coupled mode theory (SNYDER, 1972). Here we begin with a photoreceptor of refractive index $n_{||}$ and ask what happens if it changes slightly to n_{\perp} , i.e., a change of amount Δn . The modal propagation constant $\beta_{||}$,

$$\beta_{||} = 2\pi \langle n_{||} \rangle / \lambda, \quad (C2)$$

where $\langle n_{||} \rangle$ is the effective refractive index in the presence of mode effect, changes from $\beta_{||}$ to β_{\perp}

$$\beta_{\perp} = 2\pi \frac{\langle n_{||} \rangle}{\lambda} \left(1 + \frac{\eta \Delta n}{n_{||}} \right). \quad (C3)$$

This last result is found from Eq. (14) in SNYDER (1974), i.e., from the perturbed propagation constant. We can then calculate $\langle \Delta n \rangle$ as follows:

$$\langle \Delta n \rangle = \left(\frac{\lambda}{2\pi} \right) (\beta_{||} - \beta_{\perp}) \quad (C4a)$$

$$= \eta \Delta n \quad (C4b)$$

assuming $\langle n_{||} \rangle \approx n_{||}$, which is true because the refractive index of the rhabdomeric material is only slightly greater than the surrounding medium.

2. Solution by Effective Refractive Index

STAVENGA (1974) has shown that the measured or effective refractive index $\langle n_r \rangle$ of a rhabdomere is

$$\langle n_r \rangle = k n_r + (1 - k) n_s, \quad (C5)$$

where n_r and n_s are the refractive indices of the rhabdomere and surround respectively and

$$k = 1 - (U/V)^2, \quad (C6)$$

where U is a waveguide parameter and V is defined in Section G. Now by expressing Eq. (C5) for parallel and perpendicular components of \mathbf{E} and then subtracting the two expressions we find that

$$\langle \Delta n \rangle = \Delta n + \left(\frac{U^{||}}{V^{||}} \right)^2 (m_r^{||} - n_s) - \left(\frac{U^{\perp}}{V^{\perp}} \right)^2 (n_r^{\perp} - n_s), \quad (C7)$$

where $\langle \Delta n \rangle = \left\langle n \frac{1}{r} \right\rangle - \langle n_s^{\parallel} \rangle$. Assuming that $\Delta n \ll 1$, we can then express all quantities involving perpendicular components in terms of parallel components by using a Taylor series expansion. For example

$$V^{\perp} \cong V^{\parallel}(1 + \varepsilon), \quad (\text{C8a})$$

$$\varepsilon = \Delta n / 2 (n_r^{\parallel} - n_s), \quad (\text{C8b})$$

and also

$$\begin{aligned} U^{\perp} &= U(V^{\parallel} + \varepsilon V^{\parallel}) \\ &\cong U(V^{\parallel}) + \varepsilon V^{\parallel} \left(\frac{dU}{dV} \right)_{V^{\parallel}}. \end{aligned} \quad (\text{C9})$$

Using the relationships

$$\frac{dU}{dV} = \frac{U}{V} \left(1 - \frac{1}{\xi} \right), \quad (\text{C10})$$

$$\eta = \left(\frac{U}{V} \right)^2 \left\{ \frac{V^2 - U^2}{U^2} + \frac{1}{\xi} \right\} \quad (\text{C11})$$

both taken from SNYDER (1969) where ξ is a waveguide parameter, we can then show, after tedious algebra, that Eq. (C1) is correct.

Appendix D.

Two-Point Resolution

In this section, we consider two-point resolution. We know from Appendix B that the number of photons $n(\phi)$ absorbed by a rhabdom due to a distant point source is given as

$$n(\phi) = n(0) A(\phi), \quad (\text{D1})$$

where $n(0)$ is proportional to $(D \Delta \varrho_r / \Delta \varrho)^2$ (see Table 1 for definitions) and

$$A(\phi) = e^{-2.77(\phi/\Delta \varrho)^2}. \quad (\text{D2})$$

Now suppose there are two-point sources separated by angle ϕ . In order to resolve them, there must be one relatively unilluminated ommatidium between the two directly illuminated ones. Thus, the point sources are separated by an angle $\phi = 2\Delta\phi$. The rhabdom of the central relatively unilluminated ommatidium absorbs n_0 photons, where

$$n_0 = 2n(\Delta\phi) = 2n(0) A(\Delta\phi). \quad (\text{D3})$$

The two directly illuminated rhabdoms each absorb n_+ photons, where

$$n_+ = n(0) + n(2\Delta\phi) \quad (\text{D4a})$$

$$= n(0) \{1 + A(2\Delta\phi)\} \cong n(0). \quad (\text{D4b})$$

We can now define a signal amplitude σ_{sig} in analogy with that due to the sinusoidal grating discussed in Section A.4.

$$\sigma_{\text{sig}} = (n_+ - n_0)/2 \quad (\text{D5a})$$

$$\cong \{n(0)/2\} \{1 - 2A(\Delta\phi) + A(2\Delta\phi)\} \quad (\text{D5b})$$

while the noise amplitude σ_{noise} is given by

$$\sigma_{\text{noise}} = \left\{ \frac{n_0 + n_+}{2} \right\}^{1/2} \quad (\text{D6a})$$

$$= \left\{ \frac{n(0)}{2} \right\}^{1/2} \{1 + 2A(\Delta\phi) + A(2\Delta\phi)\}^{1/2}. \quad (\text{D6b})$$

Thus, the signal to noise ratio SNR is

$$\text{SNR} = \left\{ \frac{n(0)}{2} \right\}^{1/2} \frac{\{1 - 2A(\Delta\phi) + A(2\Delta\phi)\}}{\{1 + 2A(\Delta\phi) + A(2\Delta\phi)\}^{1/2}}. \quad (\text{D7})$$

The eye design that optimizes the resolution of two points is found by determining the value of $\Delta\varrho_r$ that maximizes Eq. (D7). The optimum value of $\Delta\phi$ is that which gives threshold resolution ($\text{SNR} = 1$) at each given intensity. Unlike the acuity task of sinusoidal gratings or a white noise pattern, it is not advantageous to increase $\Delta\phi$ indefinitely as intensity decreases.

Appendix E.

Arbitrary Lattice of Ommatidia

In this section, we consider ommatidia with an arbitrary (but periodic) lattice of visual axes. The pupil is assumed to be circular and to have the same area for each arrangement. The highest angular spatial frequency v_s that can be sampled by an array of photoreceptors is

$$v_s = 1/2\phi_{\text{sd}}, \quad (\text{E1})$$

where ϕ_{sd} is the angular distance between the centers of neighboring *sampling* photoreceptors. For example, from Fig. 2, $\phi_{\text{sd}} = \Delta\phi$ for square lattice and $\phi_{\text{sd}} = \sqrt{3}\Delta\phi/2$ for an hexagonal lattice.

Now, using Eq. (E1), we repeat the steps of Section D leading to Eqs. (B.21) and (B.22) with $\Delta\phi$ replaced by ϕ_{sd} , so that p becomes $D\phi_{sd}$. Thus, all of the results in this paper for p of a square lattice of ommatidia apply equally to $D\phi_{sd}$ for an arbitrary lattice. The diffraction-limited case $v_s = v_{co} = D/\lambda$ from Eq. (E1) gives $D\phi_{sd} = \lambda/2$ as in the square lattice. Thus, *the intensity necessary for a diffraction-limited eye to be the optimum design is the same for all packing geometries*. However, the highest anatomic resolving power v_s results from hexagonal packing.

The *minimum* number of photons \bar{N} and intensity parameter \hat{I} necessary for a diffraction-limited eye to be the optimum design is found from Eqs. (B.15) and (B.16) setting $v = v_{co} = D/\lambda$ with $\Delta\varrho_r = 0.75\phi_{sd}$ (with $D\phi_{sd} = \lambda/2$) leading to

$$\log \tilde{m}^2 \bar{N} = 3.53, \quad (\text{E2})$$

$$\log \tilde{m}^2 \hat{I} = 4.38 - \log \lambda^2, \quad (\text{E3})$$

with λ in μm , e.g., $\log \tilde{m}^2 \hat{I} = 4.98$ when $\lambda = 0.5 \mu\text{m}$. *Note that the longer the wavelength, the greater the intensity must be.*

Appendix F.

Consequences of Parameter p Constant in all Regions of the Eye

In this section, we consider the consequences of having the parameter $p = D\Delta\phi$ [see Eq. (B.2)] constant in all regions of an eye. We assume the eye is designed at optimum for the light-adapted state discussed in Section II.C so that $\Delta\varrho_r = 0.75\Delta\phi$ and $\bar{N} = 0.56\hat{I}(D\Delta\phi)^2$. *Thus, when $D\Delta\phi$ is constant over the eye, every ommatidium has the same light-gathering capacity for extended uniform sources.*

The number N of photons captured by a rhabdom due to a distant point source is proportional to the facet diameter squared D^2 times a fraction Q that depends only on the ratio $\Delta\varrho_r/\Delta\varrho_l$, i.e., to within a constant $N = D^2 Q(\Delta\varrho_r/\Delta\varrho_l)$, (see Appendix B). For a light-adapted eye with a diffraction-limited lens pupil, the ratio of the two acceptance angles (see Table 1) is

$$\frac{\Delta\varrho_l}{\Delta\varrho_r} = \frac{\lambda/D}{0.75\Delta\phi} = \frac{1.33\lambda}{D\Delta\phi}. \quad (\text{F1})$$

Thus, when $D\Delta\phi$ is constant over all regions of the eye, each ommatidium receives the same fraction of the total light entering the facet due to a distant point source.

Appendix G.

Polarization Sensitivity of Individual Retinula Cells of a Twisted Fused Rhabdom

In this section, we derive an expression for the polarization sensitivity of individual rhabdomeres of a fused rhabdom, twisted uniformly along its length. The analysis follows from the theory of SNYDER (1973) and SNYDER and MCINTYRE

(1975). The rhabdom is assumed to have the property that the total number of photons absorbed is independent of the direction of \mathbf{E} . This condition is approximated by many fused rhabdoms, e.g., rhabdoms like that of Fig. 21 with eight rhabdomeres of equal cross-sectional area, equal dichroism, and equal absorption coefficients. Although we use this symmetric rhabdom for our following example, the results apply to any rhabdom that is *macroscopically* isotropic.

When considering the total number of photons absorbed by the entire rhabdom, we can assume that the rhabdom is isotropic with an absorption coefficient $(\alpha_{||} + \alpha_{\perp})/2$, where $\alpha_{||}$ and α_{\perp} are the absorption coefficients of rhabdomeric membrane when \mathbf{E} is parallel and perpendicular to the axis of the microvilli membrane. Thus, the total number of photons $\tilde{n}(z)$, in the cross-section, at any position z along the length of the rhabdom is

$$\tilde{n}(z) = \tilde{n}(0) e^{-(\alpha_{||} + \alpha_{\perp})z/2} \quad (G.1)$$

independent of the direction of \mathbf{E} . Now the number of photons $d\tilde{n}$ absorbed in a differential length of *rhabdomere* dz is proportional to $\tilde{n}(z)$ as well as the fractional cross-sectional area of the rhabdomere (taken here to be one-eighth because all eight rhabdomeres are assumed to have equal area) multiplied by the absorption coefficient of the rhabdomere. However, we must distinguish two cases. When \mathbf{E} is parallel to the microvilli of the rhabdomere

$$(d\tilde{n})_{||} = \frac{1}{8} \alpha_{||} \tilde{n}(z) dz \quad (G2)$$

and when \mathbf{E} is perpendicular to the microvilli of the rhabdomere

$$(d\tilde{n})_{\perp} = \frac{1}{8} \alpha_{\perp} \tilde{n}(z) dz \quad (G3)$$

so that when \mathbf{E} is at angle ψ with the microvillus axis,

$$d\tilde{n} = (d\tilde{n})_{||} \cos^2 \psi + (d\tilde{n})_{\perp} \sin^2 \psi \quad (G4a)$$

$$= \frac{dz}{8} \tilde{n}(0) e^{-(\alpha_{||} + \alpha_{\perp})z/2} \{ \alpha_{||} \cos^2 \psi + \alpha_{\perp} \sin^2 \psi \}. \quad (G4b)$$

When the rhabdom is twisted, angle ψ is a function of position z along the length of the rhabdom so that the number of photons absorbed N by a rhabdomere of a twisted rhabdom is found by integrating Eq. (G4b) throughout the total length L of the rhabdom.

$$N \{ \psi(0) \} = \frac{n(0)}{8} \int_0^L e^{-(\alpha_{||} + \alpha_{\perp})z/2} \{ \alpha_{||} \cos^2 \psi + \alpha_{\perp} \sin^2 \psi \}, \quad (G5)$$

where ψ is given as $\psi(z) = \psi(0) - \Omega(z)$ and $\Omega(z)$ is the amount of twist at position z . Assuming a uniform twist rate gives $\Omega(z) = z\Omega(L)/L$. The integrals are easily

evaluated in closed form by integration by parts. The polarization sensitivity ratio PS of a retinula cell is defined as

$$PS = \frac{N\{\psi_{\max}(0)\}}{N\{\psi_{\max}(0) + 90^\circ\}}, \quad (G6)$$

where $\psi_{\max}(0)$ is the inclination of \mathbf{E} to the microvilli axis that gives maximum N . Although only elementary algebra is necessary for solving these equations, the expressions are long and therefore only the results (Fig. 23) are presented.

References

- Autrum, H., Wiedemann, I.: Versuche über den Strahlengang im Insektenauge. Z. Naturforsch. **17b**, 480—482 (1962).
- Barlow, H.B.: The size of ommatidia in apposition eyes. J. Exp. Biol. **29**, 667—674 (1952).
- Barlow, H.B.: Physical limits of visual discrimination. In: Photophysiology (ed. A.C. Giese), Vol. II, pp. 163—202. New York: Academic Press 1964.
- Barros-Pita, J.C., Maldonado, H.: A fovea in the praying mantis eye. II. Some morphological characteristics. Z. Vergl. Physiol. **67**, 79—92 (1970).
- Beersma, D.G.M., Stavenga, D.G., Kuiper, J.W.: Optical organization of the eye of the fly *Musca domestica* and behavioural consequences. J. comp. Physiol. **102**, 305—320 (1975).
- Bernard, G.: Physiological optics of the fused rhabdom. In: Photoreceptor optics (eds. A.W. Snyder, R. Menzel). Berlin-Heidelberg-New York: Springer 1975.
- Blakemore, C., Muncey, J.P.J., Ridley, R.M.: Stimulus specificity in the human visual system. Vision Res. **13**, 1915—1931 (1973).
- Born, M., Wolf, E.: Principles of optics, p. 367. New York: Pergamon Press 1970.
- Boscheck, C.B.: On the fine structure of the peripheral retina and lamina ganglionaris of the fly, *Musca domestica*. Z. Zellforsch. **118**, 369—409 (1971).
- Bracewell, R.: The Fourier transform and its applications. New York: McGraw-Hill 1965.
- Brown, P.K.: Rhodopsin rotates in the visual receptor membrane. Nature (Lond.) New Biol. **236**, 35—38 (1972).
- Campbell, F.W., Gubisch, R.W.: Optical quality of the human eye. J. Physiol. (Lond.) **186**, 558—578 (1966).
- Campbell, F.W., Robson, J.G.: Application of Fourier analysis to the visibility of gratings. J. Physiol. (Lond.) **197**, 551—566 (1968).
- Carlson, A.B.: Communication systems, p. 337. New York: McGraw Hill 1968.
- Collett, T.S., Land, M.F.: Visual control of flight behaviour in the hoverfly, *Syritta pipiens* L. J. comp. Physiol. **99**, 1—66 (1975).
- Cone, R.A.: Rotational diffusion of rhodopsin in the visual receptor membrane. Nature (Lond.) New Biol. **236**, 39—43 (1972).
- Cosens, D., Wright, R.: Light elicited isolation of the complementary visual input systems in white-eye *Drosophila*. J. Insect Physiol. **21**, 1111—1120 (1975).
- Crawford, B.H.: The dependence of pupil size upon external light stimuli under static and variable conditions. Proc. roy. Soc. Lond. B**121**, 376—395 (1936).
- Denton, E.J.: The contribution of the oriented photosensitive and other molecules to the absorption of whole retina. Proc. roy. Soc. Lond. B**150**, 78—89 (1959).
- Døving, K.B., Miller, W.H.: Function of insect compound eyes containing crystalline tracts. J. gen. Physiol. **54**, 250—267 (1969).
- Dvorak, D., Snyder, A.W.: The relationship between visual acuity and illumination in the fly, *Lucilia sericata*. Z. Naturforsch. **33c**, (1978).

- Enoch, J. M.: Optical properties of the retinal receptors. *J. opt. Soc. Amer.* **53**, 71—85 (1963).
- Fermi, G., Reichardt, W.: Optomotor reactions of the housefly *Musca domestica*. *Kybernetik* **2**, 15—28 (1963).
- Fox, R., Lehmkuhle, S., Westendorf, D. H.: Falcon visual acuity. *Science* **192**, 263—265 (1976).
- Franceschini, N.: Sampling of the visual environment by the compound eye of the fly: fundamentals and applications. In: *Photoreceptor optics*. (eds. A. W. Snyder, R. Menzel). Berlin-Heidelberg-New York: Springer 1975.
- Franceschini, N., Kirschfeld, K.: Etude optique *in vivo* des éléments photorécepteurs dans l'oeil composé de *Drosophila*. *Kybernetik* **8**, 1—13 (1971a).
- Franceschini, N., Kirschfeld, K.: Les phénomènes de pseudopupille dans l'oeil composé de *Drosophila*. *Kybernetik* **9**, 159—182 (1971b).
- French, A. S., Snyder, A. W., Stavenga, D. G.: Image degradation by an irregular retinal mosaic. *Biol. Cybernetics* **27**, 229—233 (1977).
- Georgeson, M. A., Sullivan, G. D.: Contrast constancy: deblurring in human vision by spatial frequency channels. *J. Physiol. (Lond.)* **252**, 627—656 (1975).
- Goetz, K. G.: Die optischen Übertragungseigenschaften der Komplexaugen von *Drosophila*. *Kybernetik* **2**, 215—221 (1965).
- Goldman, S.: Information theory. New York: Prentice Hall 1953.
- Goldsmith, T. H.: The polarization sensitivity—dichroic absorption paradox in arthropod photoreceptors. In: *Photoreceptor optics* (eds. A. W. Snyder, R. Menzel), pp. 392—409. Berlin-Heidelberg-New York: Springer 1975.
- Goldsmith, T. H., Bernard, G. D.: The visual system of insects. In: *The physiology of insecta*, Vol. II, 2nd ed. New York: Academic Press 1974.
- Goodman, J. W.: Introduction to Fourier optics. New York: McGraw Hill 1968.
- Gribakin, F. G., Govardovskii, V. I.: The role of the photoreceptor membrane in photoreceptor optics. In: *Photoreceptor optics* (eds. A. W. Snyder, R. Menzel), pp. 215—236. Berlin-Heidelberg-New York: Springer 1975.
- Hamdorf, K., Rosner, G.: Adaptation und Photoregeneration im Fliegenauge. *J. comp. Physiol.* **86**, 281—292 (1973).
- Harosi, R. E., MacNichol, E. F., Jr.: Dichroic microspectrophotometer: a computer assisted, rapid, wavelength-scanning photometer for measuring the linear dichroism of single cells. *J. opt. Soc. Amer.* **64**, 903—918 (1974).
- Harris, W. A., Stark, W. S., Walker, J. A.: Genetic dissection of the photoreceptor system in compound eye of *Drosophila melanogaster*. *J. Physiol. (Lond.)* **256**, 415—439 (1976).
- Horridge, G. A.: Optical mechanism of clear zone eyes. In: *The compound eye and vision of insects*, (ed. G. A. Horridge). Oxford: Clarendon Press 1975.
- Horridge, G. A.: The compound eyes of insects. *Sci. Am.* **237**, 108—120 (1977).
- Horridge, G. A., Giddings, C., Stange, G.: The superposition eye of skipper butterflies. *Proc. roy. Soc. Lond.* **B182**, 457—495 (1972).
- Horridge, G. A., Mimura, K., Hardie, R. C.: Fly photoreceptors. III. Angular sensitivity as a function of wave length and the limits of resolution. *Proc. roy. Soc. Lond.* **B194**, 151—177 (1976).
- Israelachvili, J., Sammut, R., Snyder, A. W.: Birefringence and dichroism in invertebrate photoreceptors. *J. Opt. Soc. Amer.* **65**, 221—222 (1976).
- Kirschfeld, K.: Die Projektion der optischen Umwelt auf das Raster der Rhabdomere im Komplexauge von *Musca*. *Exp. Brain Res.* **3**, 248—270 (1967).
- Kirschfeld, K.: The absolute sensitivity of lens and compound eyes. *Z. Naturforsch.* **29c**, 592—596 (1974).
- Kirschfeld, K.: The resolution of lens and compound eyes. In: *Neural processing in visual systems* (eds. F. Zettler, R. Weiler). Berlin-Heidelberg-New York: Springer 1976.
- Kirschfeld, K., Franceschini, N.: Optische Eigenschaften der Ommatidien im Komplexauge von *Musca*. *Kybernetik* **5**, 47—52 (1968).
- Kirschfeld, K., Franceschini, N.: Ein Mechanismus zur Steuerung des Lichtflusses in den Rhabdomeren des Komplexauges von *Musca*. *Kybernetik* **6**, 13—22 (1969).
- Kirschfeld, K., Franceschini, N.: The possible role of photostable pigments within the membrane of photoreceptors. In: *Biophysics of structure and mechanism*. Contribution presented at EMBO Workshop October, 1976.

- Kirschfeld, K., Snyder, A.W.: Waveguide mode effects, birefringence, and dichroism in fly photoreceptors. In: Photoreceptor optics (eds. A.W.Snyder, R.Menzel). Berlin-Heidelberg-New York: Springer 1975.
- Kirschfeld, K., Snyder, A.W.: Measurement of a photoreceptor's characteristic waveguide parameter. *Vision Res.* **16**, 775—778 (1976).
- Kirschfeld, K., Wenk, P.: Dorsal eye of simuliid flies. *Z. Naturforsch.* **31c**, 764—765 (1976).
- Kuiper, J.W.: On the image formation in a single ommatidium of the compound eye in diptera. In: The functional organization of the compound eye (ed. C.G.Bernhard), pp. 35—50. Oxford: Pergamon Press 1966.
- Kuiper, J.W., Leutscher-Hazelhoff, J.T.: Linear and nonlinear responses from the compound eye of *Calliphora erythrocephala*. In: Cold Spring Harbor Symp. Quant. Biol. **30**, 419—428 (1965).
- Land, M.F., Collett, T.S.: Chasing behaviour of houseflies (*Fannia canicularis*). *J. comp. Physiol.* **89**, 331—357 (1974).
- Lasansky, A.: Ultrastructural features of and extra-cellular ionic pathways in the *Limulus* ommatidium. *Neurosci. Res. Program Bull.* **8**, 467—469 (1970).
- Laughlin, S.B.: Receptor function in the apposition eye. An electrophysiological approach. In: Photoreceptor optics (eds. A.W.Snyder, R.Menzel) pp. 479—498. Berlin-Heidelberg-New York: Springer 1975.
- Laughlin, S.B., Menzel, R., Snyder, A.W.: Dichroism, absorption, and the polarisation sensitivity of photoreceptors. In: Photoreceptor optics (eds. A.W.Snyder, R.Menzel). Berlin-Heidelberg-New York: Springer 1975.
- Le Grand, Y.: Light, colour, and vision, p. 84. London: Chapman and Hall, 2nd ed. 1968.
- Liebman, P.A.: *In situ* microspectrophotometric studies on the pigments of single retinal rods. *Biophys. J.* **2**, 161—178 (1962).
- Liebman, P.A.: Microspectrophotometry of photoreceptors. In: Handbook of sensory physiology (ed. H.J.A.Dartnall), Vol. VII/1. Berlin-Heidelberg-New York: Springer 1972.
- Liebman, P.A.: Birefringence, dichroism, and rod outer segment structure. In: Photoreceptor optics (eds. A.W.Snyder, R.Menzel). Berlin-Heidelberg-New York: Springer 1975.
- Liebman, P.A., Entine, G.: Lateral diffusion of visual pigment in photoreceptor disc membrane. *Science* **185**, 457—459 (1974).
- Liebman, P.A., Jagger, W.S., Kaplan, M.W., Borgoont, F.G.: Membrane structure changes in rod outer segments associated with rhodopsin bleaching. *Nature (Lond.)* **251**, 31—36 (1974).
- Lillywhite, P.G., Laughlin, S.B.: Transducer noise in a photoreceptor. *Nature (Lond.)* (submitted) (1977).
- Mallock, A.: Proc. roy. Soc. Lond. **B55**, 85 (1894).
- Mallock, A.: Divided composite eyes. *Nature (Lond.)* **110**, 770—771 (1922).
- Mason, W.T., Fager, R.S., Abrahamson, E.W.: Structural response of vertebrate photoreceptor membranes to light. *Nature (Lond.)* **247**, 188—191 (1974).
- Mazokhin-Porshnyakov, G.A.: Insect vision. New York: Plenum Press 1969.
- McIntyre, P., Kirschfeld, K.: Chromatic aberration of a Dipteran Corneal Lens (in preparation) (1978).
- Melamed, J., Trujillo-Cenoz, O.: The fine structure of the central cells in the ommatidia of dipterans. *J. Ultrastruct. Res.* **21**, 313—334 (1968).
- Menzel, R.: Polarization sensitivity in insect eyes with fused rhabdoms. In: Photoreceptor optics (eds. A.W.Snyder, R.Menzel). Berlin-Heidelberg-New York: Springer 1975.
- Menzel, R., Blakers, M.: Colour receptors in bee eye: morphology and spectral sensitivity. *J. comp. Physiol.* **108**, 11—33 (1976).
- Menzel, R., Snyder, A.W.: Polarized light detection in the bee, *Apis mellifera*. *J. comp. Physiol.* **88**, 247—270 (1974).
- Minke, B., Wu, C.F., Pak, W.L.: Isolation of light induced response of the central retinula cells from the electroretinogram of *Drosophila*. *J. comp. Physiol.* **98**, 345—355 (1975).
- Moody, M.F.: Photoreceptor organelles in animals. *Biol. Rev.* **39**, 43—86 (1964).
- Moody, M.F., Parriss, J.R.: The discrimination of polarised light by *Octopus*: a behavioural and morphological study. *Z. vergl. Physiol.* **44**, 268—291 (1961).
- Mote, M.I.: Polarization sensitivity. A phenomenon independent of stimulus intensity or state of adaptation in the retinula cells of the crabs *Carcinus* and *Callinectes*. *J. comp. Physiol.* **90**, 389—403 (1974).
- O'Neill, E.L.: Introduction to statistical optics. Reading, Massachusetts: Addison-Wesley 1963.

- Petersen, D.P., Middleton, D.: Sampling and reconstruction of wave number limited functions in N-dimensional euclidean spaces. *Information and Control.* **5**, 279—293 (1962).
- Pierce, J.R.: Symbols, signals, and noise. New York: Harper and Row 1961.
- Poo, M., Cone, R.A.: Lateral diffusion of rhodopsin in the photoreceptor membrane. *Nature (Lond.)* **247**, 438—441 (1974).
- Portillo, J. del: Beziehungen zwischen den Öffnungswinkeln der Ommatidien, Krümmung und Gestalt der Insektenaugen und ihrer funktionellen Aufgabe. *Z. vergl. Physiol.* **23**, 100—145 (1936).
- Raubach, R.A., Nemes, P.P., Dratz, E.A.: Molecular organisation of rod disc membrane. *Exp. Eye Res.* **18**, 1—19 (1974).
- Robson, J.G.: Receptive fields. In: *Handbook of perception*. New York: Academic Press 1976.
- Rodieck, R.W.: The vertebrate retina, principles of structure and function. San Francisco: W.H. Freeman and Co. 1973.
- Rose, A.: Vision, human, and electronic. New York-London: Plenum Press 1973.
- Sammut, R., Snyder, A.W.: Ambiguity in determination of waveguide parameter V from mode cutoffs. *Vision Res.* **16**, 881—882 (1976).
- Schmidt, W.J.: Polarisationsoptische Analyse eines Eiweiß-Lipoid-Systems, erläutert am Außenglied der Sehzellen. *Kolloid-Z.* **85**, 137—148 (1938).
- Seitz, G.: Der Strahlengang im Appositionsauge von *Calliphora erythrocephala* (Meig.). *Z. vergl. Physiol.* **59**, 205—231 (1968).
- Seitz, G.: Polarisationsoptische Untersuchungen am Auge von *Calliphora erythrocephala* (Meig.). *Z. Zellforsch.* **93**, 525—529 (1969).
- Shaw, S.R.: Interreceptor coupling in ommatidia of drone honey bee and locust compound eyes. *Vision Res.* **9**, 999—1029 (1969a).
- Shaw, S.R.: Sense cell structure and interspecies comparisons of polarized light absorption in arthropod compound eyes. *Vision Res.* **9**, 1031—1041 (1969b).
- Sherk, T.E.: Development of the compound eyes of dragonflies (Odonata). III. Adult compound eyes. *J. exp. Zool.* **203**, 61—80 (1978).
- Sidman, R.L.: The structure and concentration of solids in photoreceptor cells studied by refractometry and interference microscopy. *J. Biophys. Cytol.* **3**, 15—29 (1957).
- Snyder, A.W.: Asymptotic expressions for eigenfunctions and eigenvalues of dielectric or optical waveguides. *IEEE Transactions on Microwave Theory and Techniques* **17**, 1130—1138 (1969).
- Snyder, A.W.: Coupled mode theory for optical fibers. *J. opt. Soc. Amer.* **62**, 1267—1277 (1972).
- Snyder, A.W.: Polarization sensitivity of individual retinula cells. *J. comp. Physiol.* **83**, 331—360 (1973).
- Snyder, A.W.: Leaky ray theory of optical waveguides of circular cross section. *Appl. Phys.* **4**, 273—298 (1974).
- Snyder, A.W.: Photoreceptor optics—theoretical principles. In: *Photoreceptor optics* (eds. A.W. Snyder, R. Menzel). Berlin-Heidelberg-New York: Springer 1975a.
- Snyder, A.W.: Acuity of compound eyes: physical limitations and design. *J. comp. Physiol.* **116**, 161—182 (1977).
- Snyder, A.W., Laughlin, S.B.: Dichroism and absorption by photoreceptors. *J. comp. Physiol.* **100**, 101—106 (1975).
- Snyder, A.W., Laughlin, S.B., Stavenga, D.G.: Information capacity of eyes. *Vision Res.* **17**, 1163—1175 (1977a).
- Snyder, A.W., Love, J.D.: Optical Waveguide Theory, Chapman and Halls; Wiley 1980.
- Snyder, A.W., McIntyre, P.D.: Polarization sensitivity of twisted fused rhabdoms. In: *Photoreceptor optics* (eds. A.W. Snyder, R. Menzel). Berlin-Heidelberg-New York: Springer 1975.
- Snyder, A.W., Menzel, R., Laughlin, S.B.: Structure and function of the fused rhabdom. *J. comp. Physiol.* **87**, 99—135 (1973).
- Snyder, A.W., Miller, W.H.: Fly colour vision. *Vision Res.* **12**, 1389—1396 (1972).
- Snyder, A.W., Miller, W.H.: Photoreceptor diameter and spacing for highest resolving power. *J. opt. Soc. Amer.* **67**, 696—698 (1977).
- Snyder, A.W., Miller, W.H.: Telephoto lens system of falciform eyes. *Nature* **275**, 128, 129 (1978).
- Snyder, A.W., Pask, C.: Light absorption in the bee photoreceptor. *J. opt. Soc. Amer.* **62**, 998—1008 (1972).
- Snyder, A.W., Pask, C.: Spectral sensitivity of dipteran retinula cells. *J. comp. Physiol.* **84**, 59—76 (1973).

- imited functions in N-
).
- brane. *Nature* (Lond.)
- rümmung und Gestalt
00—145 (1936).
- mbrane. *Exp. Eye Res.*
- emic Press 1976.
tion. San Francisco:
73.
- V from mode cutoffs.
- äutert am Außenglied
- hala (Meig.). *Z. vergl.*
- throcephala (Meig.). *Z.*
- compound eyes. *Vision*
- light absorption in
- Adult compound eyes.
- cells studied by re-
7).
- f dielectric or optical
1130—1138 (1969).
- 267—1277 (1972).
- ol. 83, 331—360 (1973).
- pppl. Phys. 4, 273—298
- eceptor optics (eds.
- J. comp. Physiol. 116,
- J. comp. Physiol. 100,
- on Res. 17, 1163—1175
- iley 1980.
- ms. In: Photoreceptor
r 1975.
- d rhabdom. *J. comp.*
- 2).
- solving power. *J. opt.*
- 275, 128, 129 (1978).
- . Amer. 62, 998—1008
- . Physiol. 84, 59—76
- Snyder, A.W., Sammut, R.: Direction of *E* for maximum response of a retinula cell. *J. comp. Physiol.* 85, 37—45 (1973).
- Snyder, A.W., Sammut, R.: Contribution of unbound modes to light absorption in visual photoreceptors. *J. opt. Soc. Amer.* 64, 1711—1714 (1974).
- Snyder, A.W., Srinivasan, M.V.: Human psychophysics: functional interpretation for contrast sensitivity vs spatial frequency curve. *Biological Cybernetics* (in press) (1978).
- Snyder, A.W., Stavenga, D.G., Laughlin, S.B.: Spatial information capacity of compound eyes. *J. comp. Physiol.* 116, 183—207 (1977b).
- Srinivasan, M.V., Bernard, G.D.: The effect of motion on visual acuity of the compound eye: a theoretical analysis. *Vision Res.* 15, 515—525 (1975).
- Stark, W.A.: Spectral selectivity of visual response alterations mediated in interconversions of native and intermediate photopigments in *Drosophila*. *J. comp. Physiol.* 96, 343—356 (1975).
- Stark, W.A., Harris, W., Walker, J.: Genetic isolation of three receptor spectral sensitivities with different photopigment conversions in *Drosophila*. Abstract of paper presented at Spring, 1975, meeting of the Association for Research in Vision and Ophthalmology, Sarasota, Fla. (1975).
- Stavenga, D.G.: Visual receptor optics, rhodopsin, and pupil in fly retinula cells. Thesis, Rijks-universiteit Groningen, Groningen, The Netherlands (1974).
- Stavenga, D.G.: Optical qualities of the fly eye. An approach from the side of geometrical, physical, and waveguide optics. In: *Photoreceptor optics* (eds. A.W.Snyder, R.Menzel), pp. 126—144. Berlin-Heidelberg-New York: Springer 1975.
- Stockhammer, K.: Zur Wahrnehmung der Schwingungsrichtung linear polarisierten Lichtes bei Insekten. *Z. vergl. Physiol.* 38, 30—83 (1956).
- Täuber, U.: Photokinetics and dichroism of visual pigments in the photoreceptors of *Eledone (Ozoena) moschata*. In: *Photoreceptor optics* (eds. A.W.Snyder, R.Menzel). Berlin-Heidelberg-New York: Springer 1975.
- Trujillo-Cenóz, O.: The structural organization of the compound eye in insects. In: *Handbook of sensory physiology* (ed. M.G.F.Fuortes), Vol. VII/2, pp. 5—62. Berlin-Heidelberg-New York: Springer 1972.
- Tunstall, J., Horridge, G.A.: Electrophysiological investigation of the optics of the locust retina. *Z. vergl. Physiol.* 55, 167—182 (1967).
- Varela, G., Viitanen, W.: The optics of the compound eye of the honeybee (*Apis mellifera*). *J. gen. Physiol.* 55, 336—358 (1970).
- Vries, H. de: Physical aspects of the sense organs. *Prog. Biophys.* 6, 208—264 (1956).
- Wald, G.: Visual pigment and photoreceptor physiology. In: *Biochemistry and physiology of visual pigments* (ed. H. Langer), pp. 1—16. Berlin-Heidelberg-New York: Springer 1973.
- Walcott, B.: Anatomical changes during light adaptation in insect eyes. In: *The compound eyes and vision of insects* (ed. G.A.Horridge). London: Oxford Press 1975.
- Watanabe, A., Mori, T., Nagata, S., Hiwatashi, K.: Spatial sinewave responses of the human visual system. *Vision Res.* 8, 1245—1263 (1968).
- Wehner, R.: Pattern recognition. In: *The compound eye and vision of insects* (ed. G.A.Horridge), pp. 75—113. Oxford: Clarendon Press 1975.
- Wehner, R.: Polarized light navigation by insects. *Sci. Amer.* 235, No. 1, 106—115 (1976).
- Wehner, R., Bernard, G.D., Geiger, E.: Twisted and non-twisted rhabdoms and their significance for polarization detection in the bee. *J. comp. Physiol.* 104, 225—245 (1975).
- Worthington, C.R.: Structure of photoreceptor membranes. *Ann. Rev. Biophys. Bioeng.* 3, 53—109 (1974).
- Wright, W.E.: Orientation of intermediates in the bleaching of sheer-oriented rhodopsin. *J. gen. Physiol.* 62, 509—523 (1973).
- Wyszecki, G., Stiles, W.S.: *Color science: concepts and methods, quantitative data, and formulae*. New York: John Wiley 1967.